Journal of the National Academy of Forensic Engineers®

http://www.nafe.org

ISSN: 2379-3252

DOI: 10.51501/jotnafe.v38i2

Vol. 38 No. 2 December 2021

National Academy of Forensic Engineers®

Journal Staff

Technical Review Process

The Technical Review Committee Chair chooses the reviewers for each Journal manuscript from amongst the members and affiliates of the NAFE according to their competence and the subject of the paper, and then arbitrates (as necessary) during the review process. External reviewers may also be utilized when necessary. This confidential process concludes with the acceptance of the finished paper for publication or its rejection/withdrawal. The name(s) of authors are included with their published works. However, unpublished drafts together with the names and comments of reviewers are entirely confidential during the review process and are excised upon publication of the finished paper.

National Academy of Forensic Engineers®

Board of Directors

President
Liberty Janson, PE, DFE
Senior Member

President-Elect
Samuel Sudler, PE, DFE
Senior Member

Senior Vice President
Joseph Leane, PE, DFE
Fellow

Vice President
Steven Pietropaolo, PE, DFE
Senior Member

Treasurer
Bruce Wiers, PE, DFE
Senior Member

Secretary
Richard Rice, PE, DFE
Fellow

Past Presidents
James Petersen, PE, DFE
Fellow

John Certuse, PE, DFE
Fellow

Martin Gordon, PE, DFE
Fellow

Directors at Large
Daniel Couture, PEng, DFE
Member

Robert Peruzzi, PhD, PE, DFE
Member

Executive Director
Rebecca Bowman, PE, Esq.

Journal of the National Academy of Forensic Engineers®

Editorial Board

Submitting Proposed Papers to NAFE for Consideration

Please visit the Journal's author page at
http://journal.nafe.org/ojs/index.php/nafe/information/authors for submission details.

We are looking for NAFE members who are interested in giving presentations on technical topics that will further the advancement and understanding of forensic engineering at one of the academy's biannual meetings and then developing those presentations into written manuscripts/papers, which will go through a single-blind peer review process before publication. Only papers presented at a NAFE regular technical seminar and have received oral critique at the seminar will be accepted for review and publication. We recommend that you review the About the Journal page for the journal's section policies as well as the Author Guidelines listed on the Submissions page. Authors need to register with the journal prior to submitting or, if already registered, can simply log in and begin the process. The first step is for potential authors to submit a 100- to 150-word maximum abstract for consideration at an upcoming conference into the online journal management system.

Copies of the Journal

The Journal of the National Academy of Forensic Engineers® contains papers that have been accepted by NAFE. Members and Affiliates receive a PDF download of the Journal as part of their annual dues. All Journal papers may be individually downloaded from the NAFE website. There is no charge to NAFE Members & Affiliates. A limited supply of Volume 33 and earlier hardcopy Journals (black & white) are available. The costs are as follows: $15.00 for NAFE Members and Affiliates; $30.00 for members of the NSPE not included in NAFE membership; $45.00 for all others. Requests should be sent to Mary Ann Cannon, NAFE, 1420 King St., Alexandria, VA 22314-2794.

Comments by Readers

Comments by readers are invited, and, if deemed appropriate, will be published. Send to: Ellen Parson, Journal Managing Editor, 3780 SW Boulder Dr, Lee's Summit, MO 64082. Comments can also be sent via email to journal@nafe.org.

Material published in this Journal, including all interpretations and conclusions contained in papers, articles, and presentations, are those of the specific author or authors and do not necessarily represent the view of the National Academy of Forensic Engineers® (NAFE) or its members.

 ISSN: 2379-3252

Table of Contents

* Paper presented at the NAFE seminar held in July 2018 in Buffalo.

+ Paper presented at the NAFE seminar held in January 2019 in Orlando.

† Paper presented at the NAFE seminar held in July 2019 in Denver.

§ Paper presented at the NAFE seminar held in January 2020 in San Diego.

‡ Paper presented at the NAFE seminar held in July 2021 in Providence.

Forensic Engineering Investigation and Analysis of Crack Formation in Acetal Resin Nuts Used for Water Supply Lines

By Edward S. George, PE (NAFE 621M), Donald J. Fournier, Jr., PE (NAFE 626S), Paul Eason, PhD, PE, and Charles R. King

Abstract

Non-destructive and destructive techniques were used to document and model crack formation in acetal resin nuts used for household toilet water supply lines. The morphologies of creep rupture and overload failure were documented using optical microscopy and scanning electron microscopy (SEM). The forensic investigation stemmed from litigation between a homeowner, plumbing contractor, and parts supplier related to a failure at a single residence. Fortuitously, 447 fittings in service for approximately two years under similar conditions were available for examination. In many properly installed fittings, cracks had initiated at the notch created by the sharp thread root radius, as predicted by engineering mechanics and finite element analysis. This study found that the cracks had propagated via plastic creep.

Keywords

Acetal resin nut, plastic nut, threaded nut, stress concentrations, creep rupture, scanning electron microscopy (SEM), liquid dye penetrant, fracture morphology

Introduction

A plumbing contractor was sued by a homeowner related to the failure of an acetal resin nut that was part of a water supply line to the toilet tank (**Figure 1**). The plumbing contractor subsequently filed a third-party lawsuit against the supplier of the water line, alleging negligent design and manufacture of the acetal resin nut.

The subject nut failed at the base of the thread. This type of failure has occurred in similar water supply lines from other suppliers and has been the subject of previous litigation and debate among experts, mainly focused on diverging opinions of installation error versus design defect[1,2]. Very often, the nuts are embossed with lettering on the end cap, advising to "hand tighten" only. In previous lawsuits (and in the subject lawsuit), the defendant suppliers — and experts retained by their attorneys — took the position that the nuts failed because they were overtightened by installation with a tool[3]. The opposing view expressed by plaintiffs — and experts retained by their attorneys — was that the nuts failed due to creep rupture of the plastic material caused by a combination of design and manufacturing defects related to the thread and the material used to make the nuts[4].

In the subject investigation, the authors were provided with 447 water supply lines with a common use history. Installation involved connecting the lines to residential toilets. The installation was within new home construction in a single neighborhood in South Florida. They were removed by the plumbing contractor after three identical supply line nut failures occurred within two years of installation.

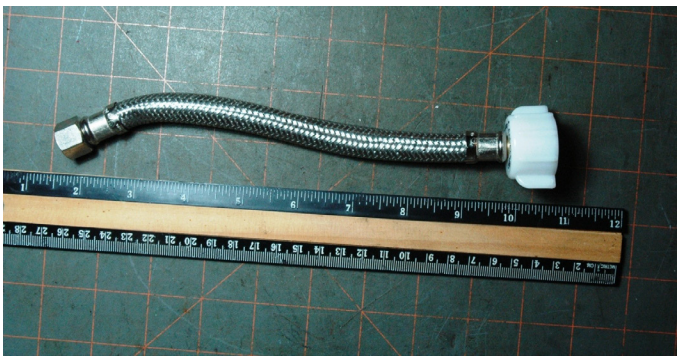

Figure 1
As-received photo of toilet supply line.

Edward S. George, PE, 124 Calle de Leon, St. Augustine, FL 32086, (904) 826-1431, eandsconsultinginc@gmail.com

Non-destructive and destructive techniques were used to detect cracks. Nuts with cracks were then inspected using optical microscopy and SEM. The stress concentrations in the threaded connection where the cracks originated were the relative stress concentrations in the threaded connection that was qualitatively modeled using Finite Element Analysis (FEA) to determine regions of high stress.

Fourier-transform infrared spectroscopy (FTIR) was performed on the subject nut to identify the polymer. It was determined that the material was polyoxymethylene (acetal).

Scope of Work

The following tasks were performed:

- Examination of plastic nuts that had been in service for approximately two years.
- Optical microscopic examination of the nuts to determine the presence of tool marks.
- Excluding nuts with any surface marks.
- Application of liquid dye penetrant to the interior of the nuts that had no tool marks.
- Cutting some of the dyed nuts in cross-section.
- Applying a torque to some of the dyed nuts to cause overload failure.
- Examination of the fracture surfaces of the failed nuts using an optical microscope.
- Examination of the fracture surfaces of a subset of nuts with cracks using SEM.
- 3D modeling and qualitative FEA.

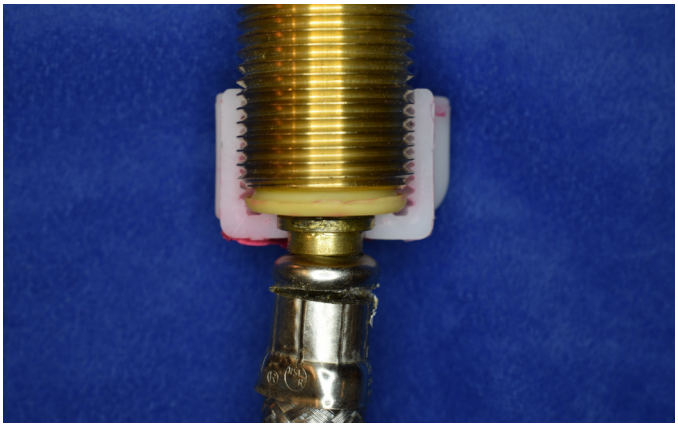

Figure 2
Cross-section showing connection to male-threaded fitting at base of toilet tank.

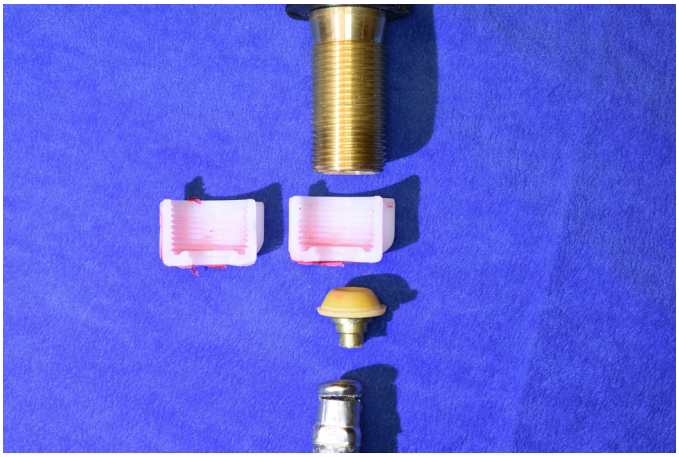

Figure 3
Exploded view of cross-section of connector components.

Observations

In use, the toilet connector threads onto a male pipe at the bottom of the toilet tank, compressing a rubber gasket between the interior surface of the connector and the end of the male pipe to prevent water leakage (**Figures 2** and **3**). The contact between the end of the male pipe and the connector creates an outward-directed longitudinal force on the interior surface of the connector. This force creates a shear stress and bending moment within the wall of the connector, with the highest stress located at the interior surface at the bottom of the wall (as shown in **Figure 4**). In addition, the threaded wall of the cap is subjected to a

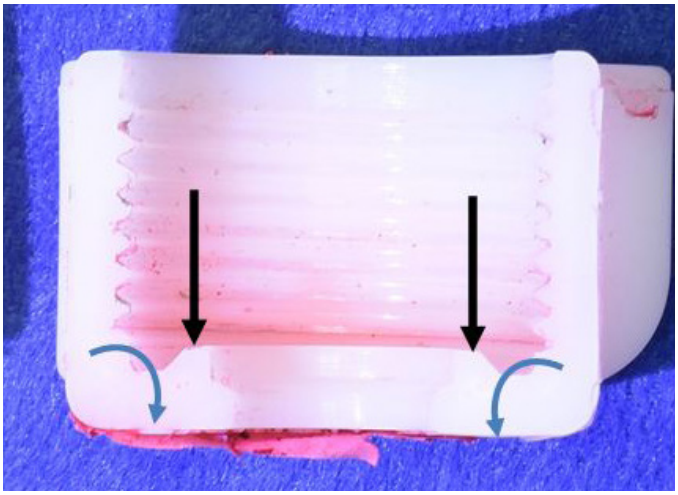

Figure 4
Cross-section of nut with crack, showing force and bending moment at end-cap.

combination of shear and radial stresses from the threaded connection.

The interior thread extends to the base of the cap. The sharp-edged roots of threads are known as stress risers, which lead to local stress concentrations many times greater than the stress that would be present without the stress riser[5]. **Figures 5** and **6** show a cross-section of a nut examined during this investigation that revealed the presence of a crack that formed at the root of the base thread, as predicted by static analysis of the applied forces and illustrated in the output of FEA performed during this investigation (shown in **Figure 7**).

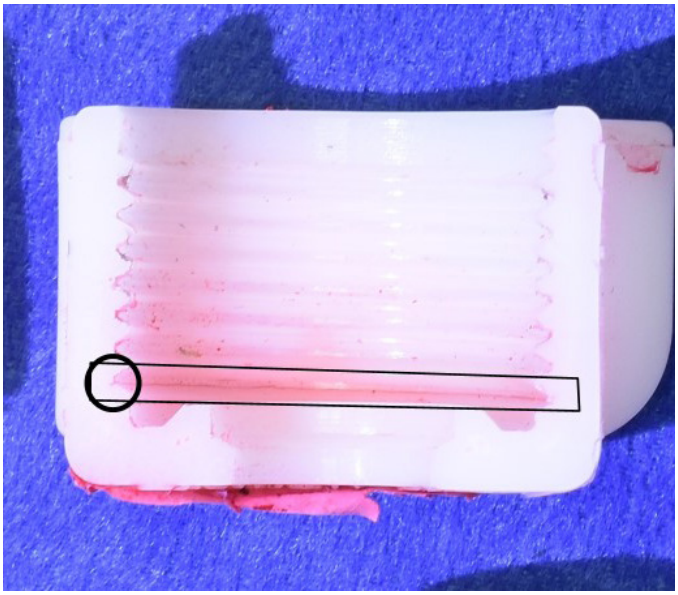

Figure 5
Cross-section of nut, showing crack at root of base thread.

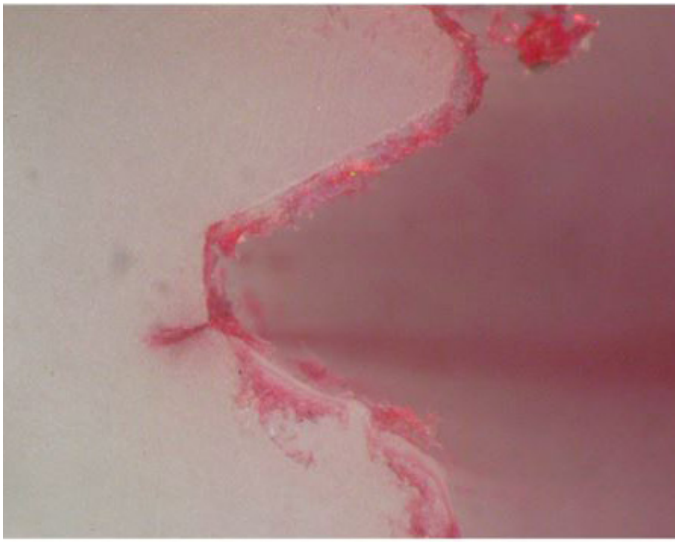

Figure 6
Close-up of crack in cross-section.

FEA was conducted to provide qualitative predictions of stress risers and their locations relative to the internal thread profile. Several sample nuts were cross-sectioned on various planes to facilitate detailed measurements and the internal geometry of the nut. These measurements were used to create a three-dimensional mesh model of the plastic nut.

FEA analysis was performed using a standard simulation software. The geometry of the fitting was based on measurements of a cross-section. Material properties were obtained from material datasheets. A tensile force was applied to the base of the fitting. The goal was not to determine stress values but to identify the most probable location for stress risers in this type of loading. The static simulation performed on the resulting model revealed a stress riser in the root of the base thread of the nut (**Figure 7**), consistent with both the physical findings and predictions based on engineering mechanics.

Since these nuts are made of an acetal resin plastic, they are susceptible to creep — the mechanism by which

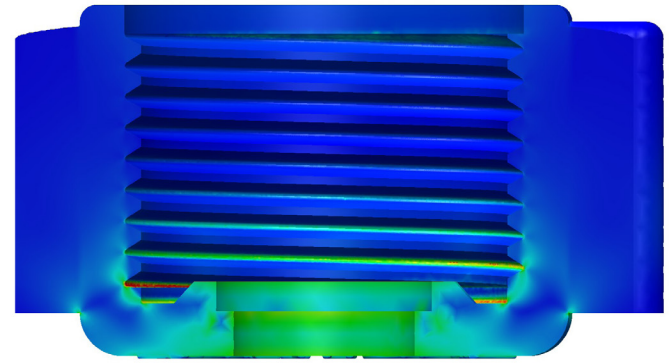

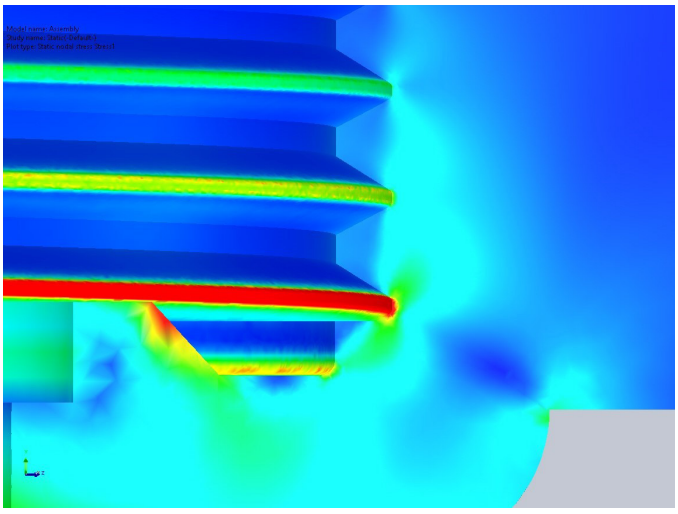

Figure 7
Qualitative FEA image, showing peak stress at root of base thread in red.

Figure 8
End of nut embossed with instruction to "hand tighten only," which has been colored for this photograph.

a plastic material will deform over time when subjected to a continuously applied load[6,7].

The subject nut in the original case appeared to have tool marks on the outer surface. Experts opined that the nut had been over-torqued, causing creep to occur and leading to the failure. Raised lettering on the end of the nut cap stated "HAND TIGHTEN ONLY" (**Figure 8**). However, this is not a reliable or accurate torque specification. Several studies have identified many factors that determine torque when hand tightening a nut[3,4], including age, gender, strength of the individual doing the tightening, and the location of the nut being tightened. Arguably, this means there is no torque specification for these nuts.

Figure 9
Composite photograph of cross-section of subject nut; interior thread ends at a notch in the upper left of image.

Investigation

The subject nut was examined by experts retained by the parties involved. The joint examination included visual examination under optical microscope and SEM. **Figure 9** is a composite photograph of the fracture surface of the subject nut. Failure initiated at the notched end of the interior thread at the base of the fitting, consistent with the location of the highest stress as shown by FEA.

Fortunately, the number of fittings that had been installed in the previous two years by the plumbing company involved were removed from service. As part of the forensic investigation, the supply lines were sent to the laboratory for inspection. A non-destructive technique called Liquid Dye Penetrant (LDP) testing was used to determine if any of the previously installed nuts possessed cracks[10].

This technique uses dye applied to the interior threads of the nuts. If a crack exists, the dye will migrate into the crack surface by capillary action and then can be detected visually or with a microscope. Post Emulsifiable Red Dye Penetrant was sprayed on the interior surfaces of the sample nuts, according to the directions of the manufacturer. After a 30-minute dwell time (to allow the dye to penetrate any small cracks in the sample), the dye was removed using soft cotton swabs followed by a small cotton tip to ensure there was no dye remaining on the internal threaded surfaces. Each nut was numbered and documented.

During the first phase of the investigation, 43 fittings were cut in cross-section. Incipient cracks were present at the root of the base thread in 11 of these, as seen in the sample shown in **Figures 5** and **6**. The onset of cracks in 25 percent of the samples with no evidence of tool marks, along with the three prior known failures of the same parts associated with this installation, provided strong evidence of a design or manufacturing defect specific to this lot of fittings. At this point in the study, deposition testimony was provided by experts for the various parties, and the suits were settled.

After the resolution of the legal cases, the authors decided to continue the investigation. The initial approach was modified by developing a method to expose the fracture surface. To do so, a hole in the shape of the nut was machined into a block of wood, and the male thread from a toilet fixture was attached to the socket of a torque wrench with epoxy. Using a calibrated torque meter, 0 to 600 inch-pounds, each nut was torqued to failure,

Figure 10
Torque wrench and nut in wood block.

Figure 11
Before torque to failure — no tool marks.

Figure 12
Torqued to failure.

and the load required to do so was recorded (**Figures 10** through **12**). The required torque to cause the part to fracture ranged from 14 to 22 nanometers (nm) 125 to 200 inch-pounds, consistent with data reported by Timpanaro, Shcerzer, Keifer and Eason[4], who reported torque values of 16.9 to 26.8 nm (150 to 237 inch-pounds).

The thread base of an additional 100 supply line nuts was then examined microscopically to determine if any cracks had started over the two-year in-service period. These nuts had no signs of tool marks. As shown in **Figures 13** and **14**, Sample #17 had red dye penetrant on the inside of the fracture surface, indicating the presence of a crack. Of the 100 parts examined in this phase, 10 were found with cracks at the base of the last thread, corresponding to a crack formation rate of 10 percent.

The fracture surface of Sample #17 was examined by means of Scanning Electron Microscopy, using an

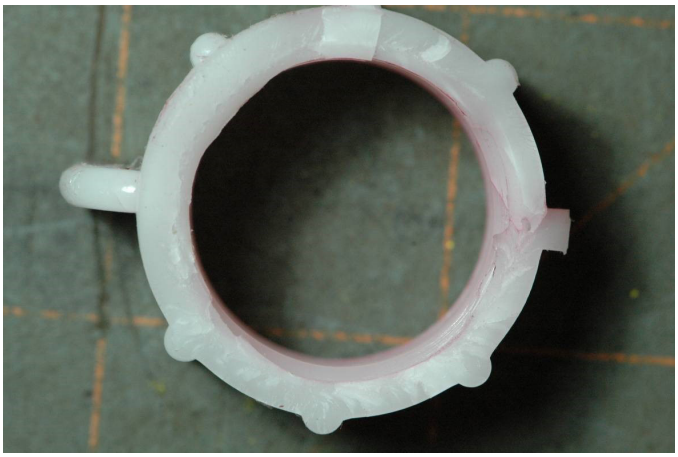

Figure 13
Fracture surface of Sample #17.

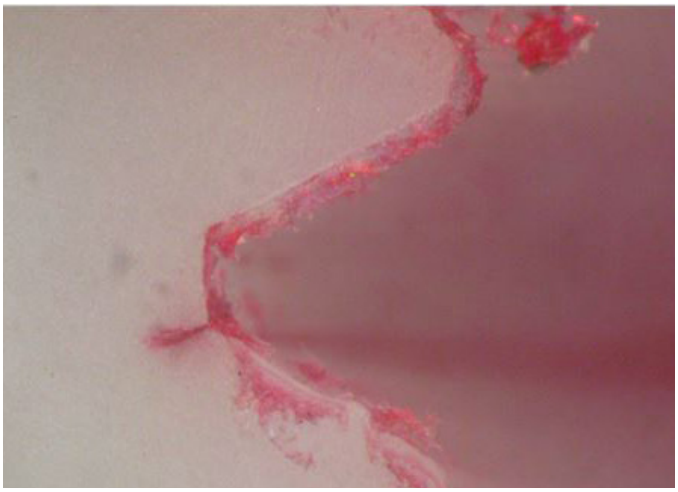

Figure 14
Red dye penetrant in crack on the fracture surface of Sample #17.

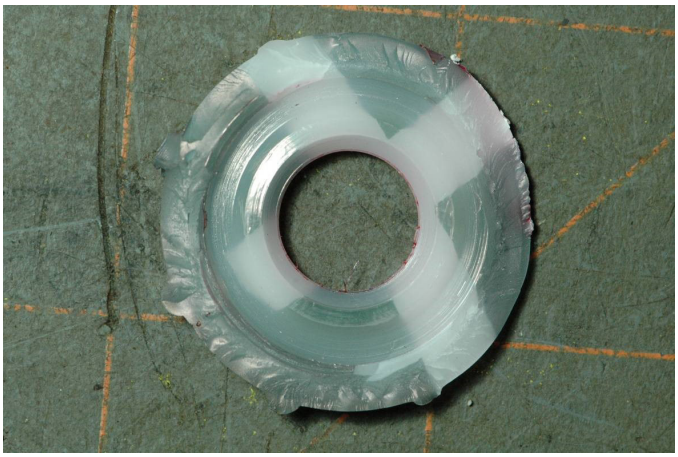

Figure 15
Sample #17, sputter coated.

analytical SEM. The fracture surface was imaged in an uncoated state, using a 5kV accelerating voltage, and spot size of between 96 and 117 nm with the average spot size of 100 nm with a resulting absorption current of 0.58 pascals, to avoid sample charging. After imaging the fracture surface at multiple magnifications, the sample was removed and coated with gold, using a vacuum sputtering system (**Figure 15**). The sample was placed back in the analytical SEM, and the series of fractographs was replicated with respect to location and magnification, at 5kV accelerating voltage, and slightly higher absorption current to illustrate the ability of gold coating to permit higher quality imaging (without changing the features and morphology of the fracture surface). Note that at 20,000 times magnification, the gold coating is invisible to the viewer, as its thickness of approximately 50 angstroms falls below the resolution of the microscope.

The SEM images after gold coating clearly show two different types of fracture morphologies present in the surface of the same sample. One has plate-like fracture zones corresponding to a fast overload fracture achieved with the torque wrench, while the other (crack that visually showed as red in color) has a tufted appearance associated with sustained loading over time, resulting in creep rupture morphology. See **Figures 16** through **20**. Under sustained

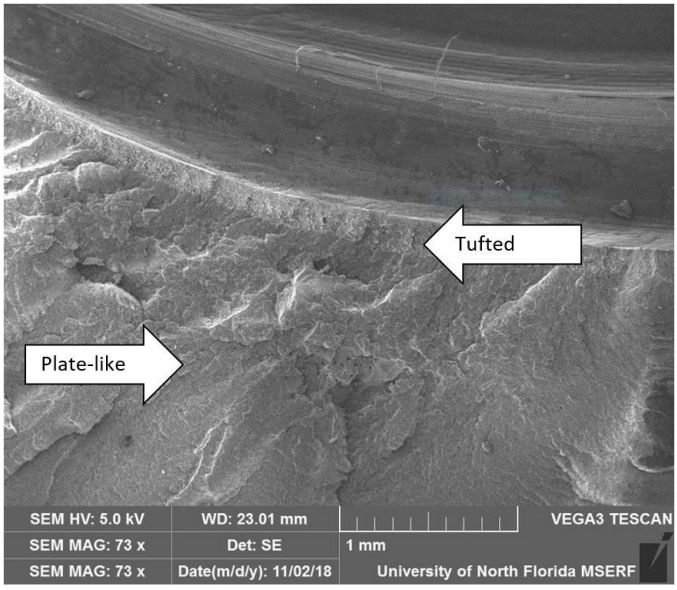

Figure 17
Medium magnification, Sample #17,
gold coated showing fracture morphologies.

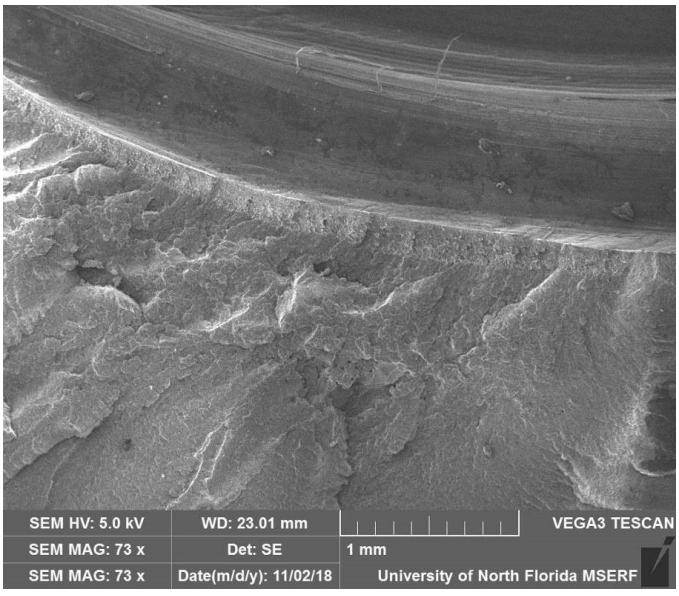

Figure 16
Medium magnification, Sample #17.

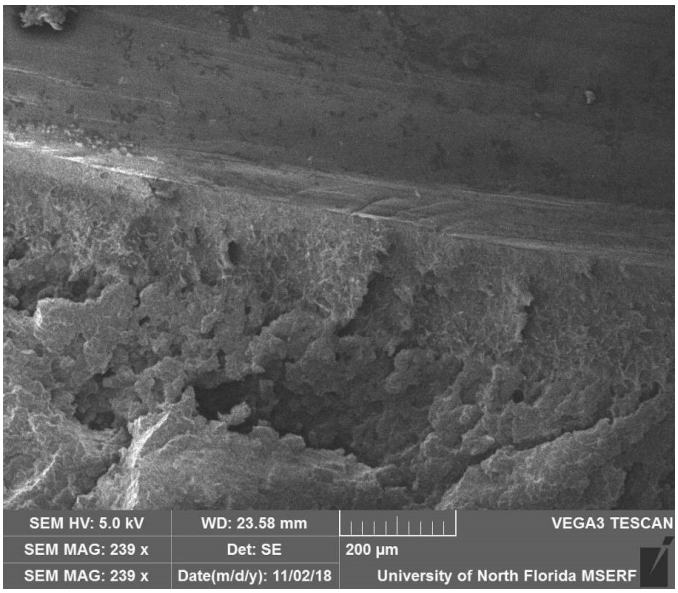

Figure 18
Higher magnification, Sample #17.

loading, this material undergoes slow, stable crack extension, resulting in the development of a tufted fracture surface appearance. These tufts represent fibril extension and subsequent rupture in various polymers[9].

SEM was also performed on two more cracked parts, Sample #9 and Sample #27, which were picked at random from the 10 parts with visible cracks. The SEM photographs for these two samples reveal the same two types of fracture morphology (plate-like and tufted), as described above and shown in **Figures 21** through **24**.

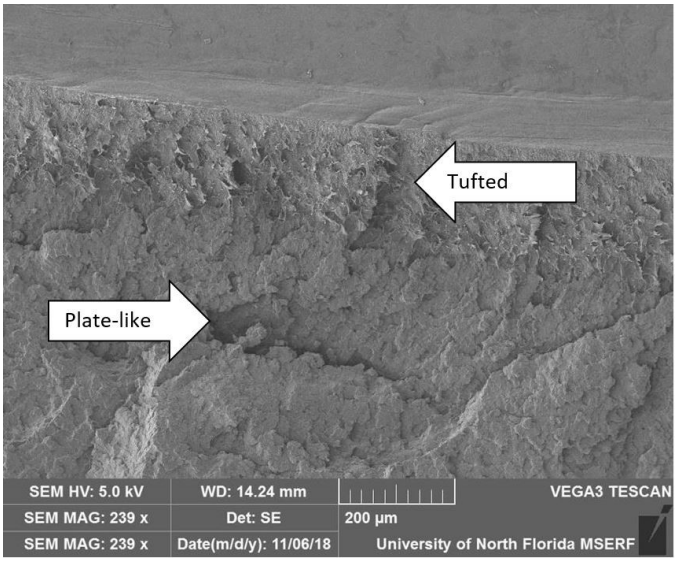

Figure 19
Higher magnification, Sample #17,
gold coated showing fracture morphologies.

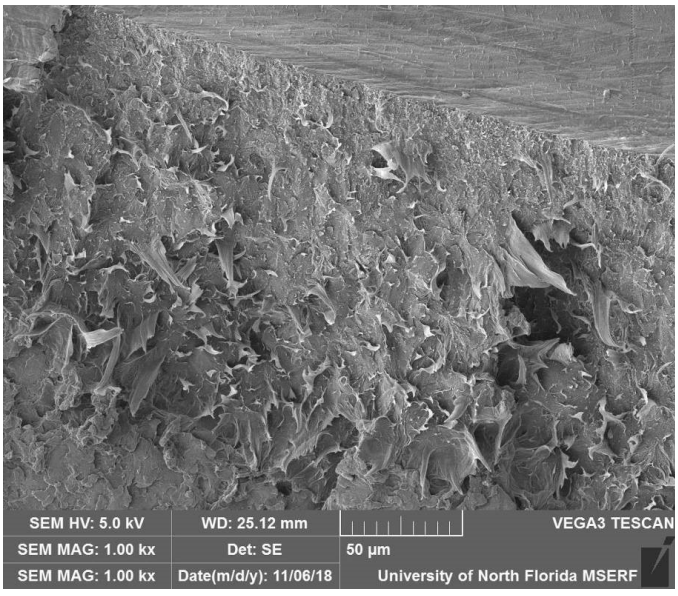

Figure 20
Even higher magnification, Sample #17,
gold coated showing tufted appearance of fracture surface.

The authors also attempted to quantify the meaning of "hand tighten" as applied to the installation of these nuts. The torque recorded during the hand tightening tests was within the range of 2.0 to 3.4 nm (18 to 30 inch-pounds), consistent with data reported by Timpanaro, Shcerzer, Keifer, and Eason[4], who reported torque values of 1.1 to 3.4 nm (10 to 30 inch-pounds). When compared to the torque to cause overload failure, the values are approximately seven times the values achieved by hand tightening.

Conclusion

This study provided a unique opportunity to examine

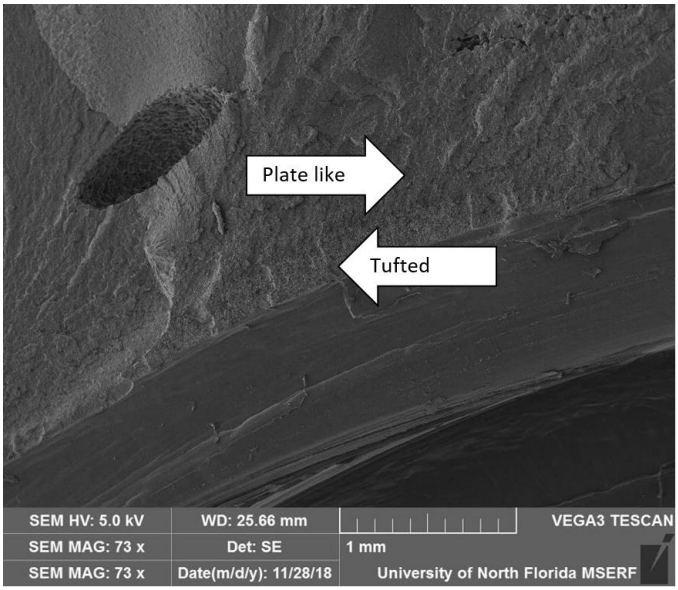

Figure 21
Sample #9, medium magnification.

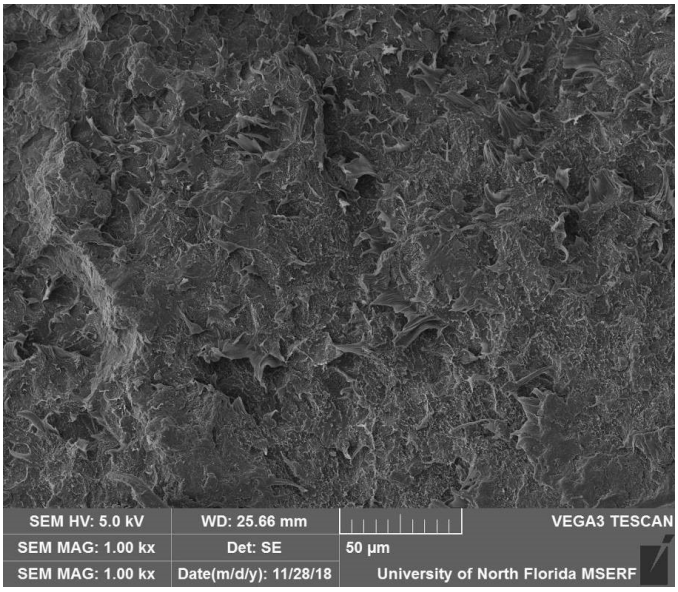

Figure 22
Sample #9, higher magnification of tufted area.

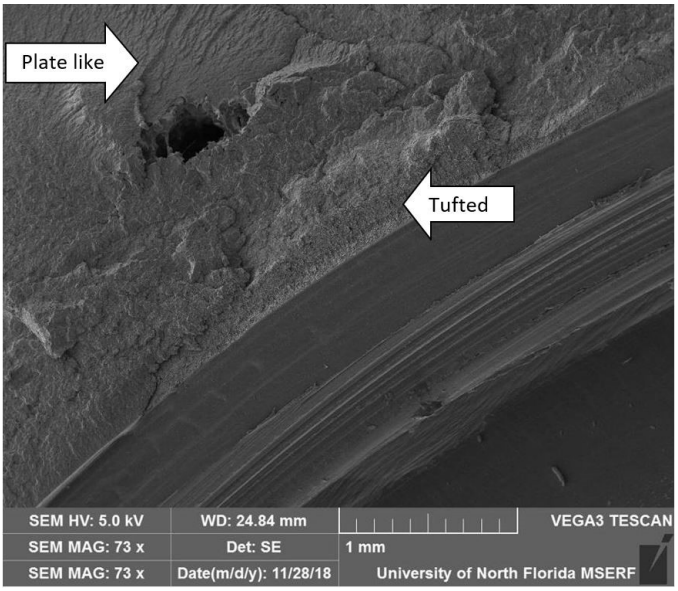

Figure 23
Sample #56 with two fracture morphologies.

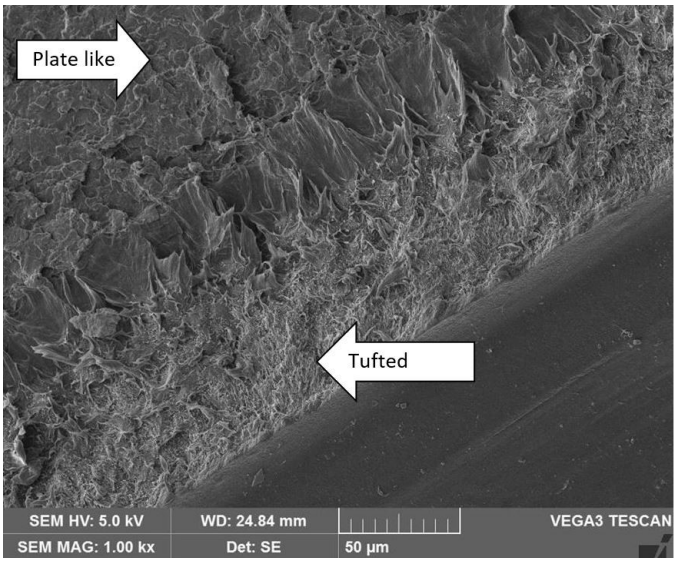

Figure 24
Sample #56 at higher magnification.

a statistically relevant sample size of acetal resin toilet nuts that had been subjected to remarkably similar installation and in-service conditions. They were installed by the same plumbing contractor, in the same newly constructed neighborhood, and had the same water supply. Additionally, they were all removed at the same time after approximately two years of service.

In this investigation, 143 fittings with no evidence of external tool marks were examined after the application of liquid dye penetrant to the interior threads. Of these, 43 were cut in cross-section, and cracks were observed in the base thread in 11 samples, corresponding to a rate of crack formation of ~25 percent. An additional 100 fittings were torqued to failure, exposing the entire fracture surface. Of these, 10 percent had cracks at the base thread. Thus, based on these two different studies, the rate of crack formation in these plastic nuts was concluded to be in the range of 10 to 25 percent (**Figure 25**). In addition, there were three known failures of nuts during the two-year period these fittings were in use.

Method	Number Examined	Crack Frequency
Cross Section Cut	43	25%
Torque to Failure	100	10%

Figure 25
Number of samples and crack frequency.

The torque achieved by hand tightening was approximately seven times less than the torque required to cause the nut to fracture in overload. Of the nuts examined in which there was no evidence of tool marks, the high rate of crack formation indicates that cracks formed even when the nut was hand-tightened — and that crack formation did not require installation with a tool.

Although this is well known in the industry, it bears repeating in this study. SEM was performed on cracked areas. It was observed that gold coating presents clear advantages in fracture surface imaging and causes no deleterious effects on the surface morphology. The 10-nm layer of conductive material protected the polymer sample from the highly energetic beam during its interaction with the sample.

The SEM study revealed the presence of a tufted surface morphology, which is associated with slow stable crack extension due to sustained loading over time defined as plastic creep[8,9].

This study confirms that these acetal resin plastic toilet nuts were prone to crack formation by creep deformation with no evidence of over-tightening. All cracks formed at the root of the base thread, which served as a stress riser at the location of the greatest stress in the part. This failure mode is recognized and warned against by manufacturers of acetal resin plastic. Consequently, it is the opinion of the authors that the crack formation in these nuts was the result of a defective design of the thread geometry and the inappropriate use of acetal resin plastic for the material of construction. Notably, this part is no longer available in the United States.

References

1. Anderson P, McCormick DF. Parties for Steven Rensel v. Fluidmaster, Inc., 8:14-cv-00648. CourtListener. 2014 Apr 14 [accessed 2020 Oct 21]. https://www.courtlistener.com/docket/4151307/parties/steven-rensel-v-fluidmaster-inc/.

2. Integrated Database. Docket for Trabakoolas v. Watts Water Technologies, Inc., 3:12-cv-01172. CourtListener. 2012 Mar 8 [accessed 2020 Oct 21]. https://www.courtlistener.com/docket/4179096/trabakoolas-v-watts-water-technologies-inc/.

3. Jones JW. Forensic Engineering Analysis of Toilet Connector Failures in a Class-Action Lawsuit. Journal of the National Academy of Forensic Engineers. 2015 Jan 1 [accessed 2020 Oct 21]. https://journal.nafe.org/ojs/index.php/nafe/article/view/18.

4. Timpanaroa A, Scherzer R, Keifer OP, Eason PD. Case Studies in Engineering Failure Analysis; Analysis of acetal toilet fill valve supply line nut failure. Jacksonville, FL: Elsevier Ltd; 2017.

5. Shigley JE, Budynas RG, Mischke CR. Mechanical engineering design. Boston, ny: McGraw-Hill Higher Education; 2004.

6. General Electric Company. GE Plastics. Processing. GE Engineering Thermoplastics Injection Molding Processing Guide. Guide. Injection Molding. PDF Free Download. 1999 Jan 1 [accessed 2020 Oct 21]. https://docplayer.net/15046049-Ge-plastics-processing-ge-engineering-thermoplastics-injection-molding-processing-guide-guide-injection-molding.html.

7. DuPont Delrin. acetal resin PRODUCT AND PROPERTY GUIDE. PDF Free Download. 2006 [accessed 2020 Oct 21]. http://docplayer.net/46172037-Dupont-delrin-acetal-resin-product-and-property-guide.html.

8. Masters JE, Gilbertson LN. Fractography of modern engineering materials. menards.club. 1993 Jan 1 [accessed 2020 Oct 21]. https://rujefewabapuni.menards.club/fractography-of-modern-engineering-materials-book-27013my.php.

9. Fractography of Modern Engineering Materials. Composites and Metals. Copyright by American Society for Testing and Materials 1987, STP 948.

10. ASTM E1417/E1417M-16 Standard Practice for Liquid Penetrant Testing.

Forensic Engineering Analysis of a Crash Caused by Swingout of an Articulated Booster on a Semi-Trailer

By Shawn Ray, PE (NAFE 970S), Donald J. Fournier, Jr., PE (NAFE 626S), Reza Vaghar, PhD, PE (NAFE 979S), and Steven Mitchell, PhD, PE

Abstract

An unloaded lowboy trailer with an articulated booster axle was traversing a curved exit ramp when the trailer tires lost traction, and the booster axle redirected the rear of the trailer into oncoming traffic. The reconstruction used a detailed analysis of roadway geometry, truck geometry, and suspension characteristics to determine the cause of the trailer swingout. A comprehensive topographical map was created from 3D laser scans. The interaction of each tire with the pavement surface was used to determine the individual wheel loads. Dynamic analysis of the curved path quantified the speed required to cause loss of traction and subsequent swingout.

Keywords

Truck-tractor, lowboy semi-trailer, swingout, booster axle, dolly, rolling lateral friction, cross over collision, forensic engineering

Background

In early afternoon in February, a truck-tractor towing an empty lowboy semi-trailer with a booster axle was exiting a major turnpike proceeding toward the highway on a bi-directional entrance-exit ramp with a single lane in each direction when the truck's trailer drifted into the opposing lane of traffic. Meanwhile, a pickup on the same ramp approached from the opposite direction and collided with the rear of the trailer. After the first collision, a passenger car collided with the rear of the pickup, which had stopped abruptly due to the collision with the trailer.

Witnesses described the rear of the lowboy trailer as having rapidly rotated across the centerline median, swinging into the oncoming lane. Later, it was determined that the rear tires of the trailer lost traction, causing the trailer to drift clockwise into the opposing lane, colliding with the pickup. The road surface was wet due to light rain. It was daylight but overcast, and the ramp advisory posted speed was 35 mph.

Motivation

The truck-tractor and empty lowboy semi-trailer were on the inside of the curve, and a pickup, car, and other traffic were on the outside of the curve. Traffic was moderately heavy, and witnesses were consistent in their description. No pre-impact physical evidence, such as tire marks, was documented. The witnesses, area of impact, and reconstruction indicated that the rear of the semi-trailer suddenly swung into the outside of the curved path (crossing over the centerline) before colliding with the oncoming pickup.

The initial task was to collect evidence, orient the vehicles at impact and final rest, and determine how the collision occurred. Then stepping back in time to the moments just prior to collision, the positions of the vehicle were plotted on scaled diagrams.

Based on site evidence and witness statements, the rear of the trailer suddenly departed the curved path of the tractor-trailer and crossed over the centerline median without warning to its driver. The quick lateral movement without any tire marks indicated the articulated booster axle was causing the redirection of the rear of the trailer. The empty lowboy semi-trailer was longer than most truck-tractor-trailer combinations so that it could carry large, heavy cargo.

The theory was proposed that the length of the trailer and the articulated booster axle enabled a bridging effect

Shawn Ray, PE, 5410 NW 33rd, Suite 100, Fort Lauderdale, FL 33309, (954) 777 4790, shawnray1@gmail.com

on the compound roadway curves that caused the articulated booster axle to lift the rear wheels of the trailer. This loss of normal force reduced the lateral tire friction, which created an instability. This, in turn, caused the articulated booster axle and the rear of the trailer to follow a line tangent to the curve rather than the intended roadway curve.

The next phase of the collision reconstruction was to evaluate this theory and to determine if the theory was consistent with the evidence.

Due to the specific set of circumstances and the bridging effect created by the long truck-trailer combination on this ramp, traditional planar accident reconstruction techniques and crash simulation software proved insufficient to reconstruct the incident. Advanced three-dimensional (3D) graphics and geometric techniques (together with specific physics-based kinematic equations) were used to reconstruct this accident and explain the unusual combination of factors that led to the loss of traction at the rear of the trailer.

The accident investigation included a detailed analysis of the physical evidence, roadway geometry, truck geometry, and suspension effects using high-definition (HD) 3D laser scanning, electronic total station survey data, and unmanned aerial vehicle (UAV) aerial imagery.

The reconstruction included a customized kinematic model of the truck-tractor, semi-trailer, and booster axle, which was created by the authors to evaluate the vehicle-specific dynamics. Multiple graphics and scale models were used to demonstrate the findings of the accident reconstruction and illustrate the specific combination of truck-trailer and roadway factors that led to this event.

Forensic Engineering Analysis and Collision Evaluation

The collision evaluation included a review of the following material:

1. Police traffic crash report and police investigation material.

2. Scene photographs.

3. Witness statements and depositions.

4. Service records for the tractor trailer, vehicle specifications, records, and history for each vehicle.

The investigation tasks included:

1. Documenting the site with photographs and video at ground level and from the air.

2. Documenting the path and speed of traffic with aerial video.

3. Documenting the roadway with HD 3D laser scans and electronic total station measurements.

4. Examining, photographing, and measuring the truck and trailer.

5. Documenting the truck and trailer with HD 3D laser scans.

6. Inspecting the brakes of the truck and trailer.

7. Conducting an axle-by-axle measurement of weight with varying booster axle pressures.

8. Imaging the crash data from the pickup's Airbag Control Module (ACM).

9. Performing drag factor tests at the site and similar surfaces in the surrounding area with a towed full-size trailer tire.

Accident Site

The accident site was a two-lane, bi-directional entrance-exit ramp with one lane of traffic in each direction. The opposing lanes were separated by a small, raised median and solid yellow painted centerlines approximately 1 foot from the centerline median curb. **Figure 1** shows

Figure 1
Accident site location and roadway configuration.

an aerial photograph of the accident site. For orientation purposes, north is to the bottom of the figure; the turnpike is the north-south highway on the left of the figure.

The ramp interchange was originally constructed between 1963 and 1967 as part of the turnpike and state route construction projects. Multiple overlays and maintenance projects have occurred during the 50-plus-year life of the roadway. Changes to the surface included reduction in the elevation difference between the road surface and the center raised median curb and surface slopes — it was not in compliance with current roadway standards[1]. This ramp has since been reconstructed to bring it up to current standards as part of a previously planned construction project.

The ramp was comprised of two 15-foot lanes with paved shoulders on the outside of each side. The roadway combined three changing geometries simultaneously: a horizontal curve, a vertical curve, and superelevation.

A detailed set of 3D scans and total station measurements (in combination with aerial drone photography) were used to document the accident site, roadway geometry, alignment, superelevation, and pavement elevations. These characteristics were then analyzed as part of a detailed reconstruction.

In the area of the collision, there was a 2-foot paved shoulder along the outside radius for southbound traffic and a 5-foot shoulder along the inside radius for northbound traffic. In the area of the collision, the radius of the center of the median was 250 feet. Vehicles heading along the inside lane (in a northerly direction) were proceeding downhill; vehicles in the outside lane (in a southerly direction) were proceeding uphill. The downhill slope in the area of the collision decreased from 4.5% to 1% as vehicles proceeded down the ramp.

There was a superelevation associated with the curve that increased from 8% to 12%. Along the ramp, each of the variables (radius, grade, and superelevation) changed with respect to location — and the rate of change was not constant. **Figure 2** shows the tractor driver's approach to the area of the cross-over event.

Traffic was described as moderate-to-heavy, and witnesses each reported traveling at or slightly below the advisory speed of 35 mph. **Figure 3** shows the post-impact locations and condition of the pickup.

Figure 2
Truck driver view approaching the area of the crash event.

Figure 3
Collision scene photo taken by investigating officer.

The pickup was in the outside lane on an uphill grade. The truck was heading downhill in the inside lane.

The interrelationship between the changing roadway geometry and the truck/trailer dimensions created a bridge, lifting the trailer tires as the truck entered the bowl created by the geometry of the exit ramp. The trailer weight was transferred to the articulated booster axle, which steered along a constant elevation curved path nearly tangent to the roadway centerline median.

Truck-Tractor and Semi-Trailer

The first vehicle was a 2007 Class 8 conventional cab 6x4 tractor chassis. The engine's event data recorder was set with the "Quick Stop" record "off" consistent with the factory default position and did not record sudden deceleration data. The tractor was pulling a lowboy trailer with a booster axle. **Figure 4** shows photographs of the combination. **Figure 5** and **Figure 6** show the articulated booster axle. The large and heavy loads transported by this tractor-trailer combination often require an articulated rear booster axle. The booster axle is attached to the trailer with

Figure 4
Truck-tractor and semi-trailer with booster axle.

Figure 5
Trailer with booster axle.

a pin and can articulate as necessary to navigate turns.

The overall length of the truck and trailer combination was 84 feet. The driver dropped off a large crane earlier in the day and was returning to the equipment yard on a road that had been driven many times prior by this rig.

Pickup Truck

The second vehicle was a 2008 four-door extended cab 4x2 pickup truck. The curb weight was 4,794 lb. The pickup was powered by a 4.7-liter V8 gasoline engine. It was equipped with an airbag control module (ACM) that stores crash data during an impact. Data was downloaded and analyzed showing that the speed at impact was 28 mph. The delta-v recorded by the pickup's ACM was 14.2 mph. The pickup truck was towing an open trailer with landscape equipment. The two occupants in the front seats of the pickup were both seriously injured in the crash.

Passenger Car

The third vehicle was a 2005 passenger car, which collided with the rear of the trailer being pulled by the pickup. This impact did not cause or contribute to the initial collision between the truck and the pickup. Since there was no substantive effect of this collision, the car's involvement will not be included in this discussion.

Analytical Method

The forensic engineering evaluation of the pre-collision events utilized custom mathematical, Computer

Figure 6
Trailer with booster axle.

Aided Drawing and Design (CADD), and physical models. The graphical, geometric, and analytical methods that were applied in the analysis included the following:

1. Created 3D CADD models based on the photographs, measurements, and laser scans of the truck and trailer to evaluate its shape and geometry in three dimensions.

2. Created 3D CADD models of the site based on measurements, total station survey data, laser scans, and mapping with aerial photos.

3. Determined tire positions of truck and trailer on the road along the travel path.

4. Determined the topography of the road surface

along the paths of the tractor and trailer tires.

5. Identified gaps between road surface and tire contact patches assuming no suspension droop. (See definition at end of section.)

6. Measured vertical loads at the contact point of trailer tires at different elevations of the tractor and booster wheels to measure suspension droop of trailer wheels, and to quantify unloading due to bridging effect of the road surface and vehicle geometries.

7. Created a detailed kinematic model of the truck-trailer configuration to determine the dynamic relationship between speed and friction for the subject trailer on the subject road.

8. Measured roadway friction with a truck tire test apparatus under wet and dry conditions. (See note at end of section.)

9. Determined speed at which trailer inertial force exceeded available traction force, causing trailer rotation.

Definition: The "gap" for the purpose of this document is the height difference between a datum established by the elevation of the booster and tractor tires on either end and the trailer tires in between.

Note: The truck tire test apparatus was a purpose-built mobile drag sled utilizing truck tires comparable to the tires on the subject trailer and was used to measure the roadway drag factor at the site and other similar roadway surfaces in the area. It was modeled after the device described in SAE J2505[2].

Evaluation of Topographic Factors

The changing roadway radius curve, the changing downhill slope, and the changing superelevation of the roadway had to be modeled accurately to determine the trailer and booster axle tire loading at specific locations along the ramp. The combined length of the truck, trailer, and booster axle created a bridge, lifting the trailer tires as the truck entered the bowl created by the exit ramp geometry. This bridging effect was exacerbated by a depression in the roadway surface at the beginning of the curve. This depression was due, in part, to the compound effect of the combined curves, as well as years of high traffic volumes and multiple maintenance and resurfacing operations.

As the trailer's weight was transferred to the articulated booster axle, the axle steered forward rather than following the curve of the exit ramp. The wet roadway enabled a loss of lateral traction at the trailer tires without complete lift or separation of the tires from the roadway.

Trailer Weighing

Wheel load measurements were conducted to study the effect of the roadway geometry on the loading of trailer axles and tires. To mimic the gap caused by the roadway geometry and trailer length, the complete rig (including tractor, trailer, and booster axle) was configured as it was on the day of the accident.

In order to quantify the wheel loading and weight transfer from axle to axle for the truck, trailer, and booster axle, the weights of each wheel load were measured on level ground and under a series of progressively increasing differential tractor/booster heights.

Scale platforms were placed under each pair of trailer and booster axle wheels on one side. Wheels on the other side and tractor wheels were supported by wood shims such that all the wheels were at the same level. The tractor and the booster wheels were lifted in ½-inch increments from an initial height of 1 inch up to a maximum of 4 inches. At each level, the loads on the trailer and booster wheels were measured with the scales and all data recorded. **Figure 7** shows the setup for the wheel load measurements.

The results showed that as the trailer gap increased, the loads on the trailer axles generally decreased —

Figure 7
Wheel load measurement.

and the load on the booster axle increased. **Figure 8** shows the wheel load of the trailer and booster axles as a function of raised height of the tractor-booster axle datum. Data from these measurements were used in the kinematic model for trailer slide-out.

Next the truck, trailer, and booster axle geometries were matched to a detailed model of the actual roadway geometry. **Figure 9** demonstrates the trailer wheel lift and gap analysis along the roadway in the area leading up to the collision event. The graph illustrates the difference in height between the asphalt and each of the trailer wheels, driver (D) and passenger (P), for each of the three axles (T1, T2, T3). The figure illustrates the tractor-trailer position when the trailer tires are in the area of maximum height difference and maximum horizontal curvature. This position correlates with the likely loss of traction and subsequent impact. Note that this analysis assumes no droop in the trailer suspension.

Figure 8
Wheel load as a function of raised height of tractor-booster axle datum.

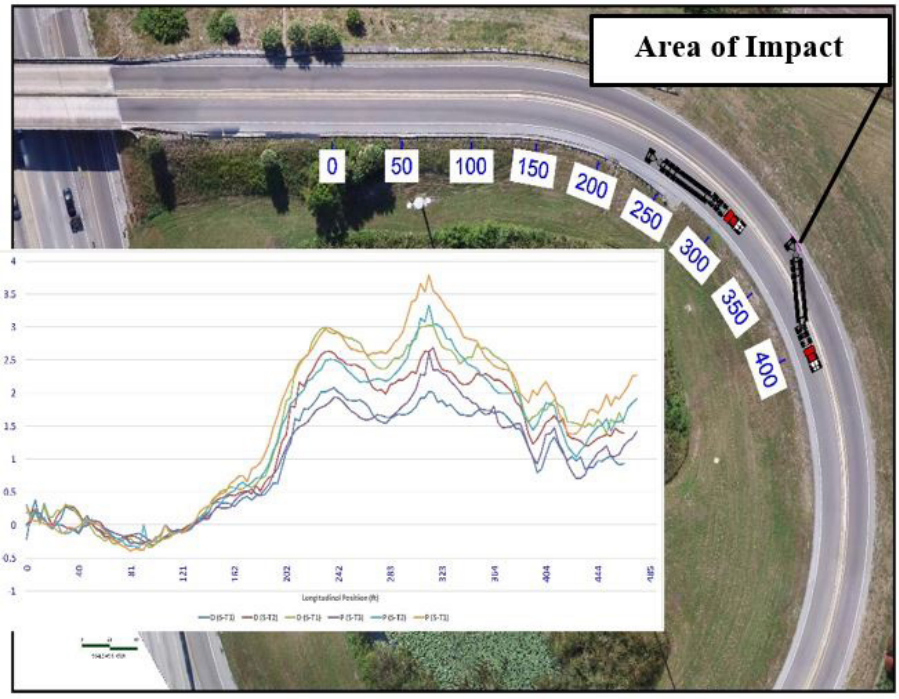

Figure 9
Elevation difference of trailer tires above roadway surface from the tractor-booster axle.

Figure 10 is a contour map of the road surface elevation and shows the tractor-trailer positions at the beginning of the wheel height difference and at the maximum height difference. **Figure 11** is a graphic representation of the trailer tire lift. **Figure 12** illustrates the bridging created by the idealized lift of the trailer due to booster axle loading. This illustration does not include suspension droop. In real-world conditions, the tires were significantly unloaded but did not lose complete contact with the road surface. Reduced normal force caused a reduction in lateral traction, which allowed the trailer to swing to the left in the right-hand curve.

The roadway surface was not significantly deteriorated. However, multiple overlays and repaving had occurred, and the center raised median was no longer functional to impede cross-over events due to the accumulation of asphalt that resulted in the increase in road surface height, as illustrated in **Figure 13**.

The vertical and horizontal components of the ramp slope and

curvature, along with the superelevation of the road surface combined to create a geometry conducive to unloading the trailer wheels for this tractor trailer. This relationship between slope and superelevation is shown in **Figure 14**.

Kinematic Model

The loss of lateral traction of the trailer tires, which permitted the booster axle to redirect the trailer into the opposing lane, was related to roadway friction, vertical loads, and location-specific roadway geometry. The configuration of this rig and the sensitivity of the wheel loading required a kinematic model specific to the facts of this event to evaluate the movement and rotational characteristics of the truck, trailer, and booster axle on this segment of roadway.

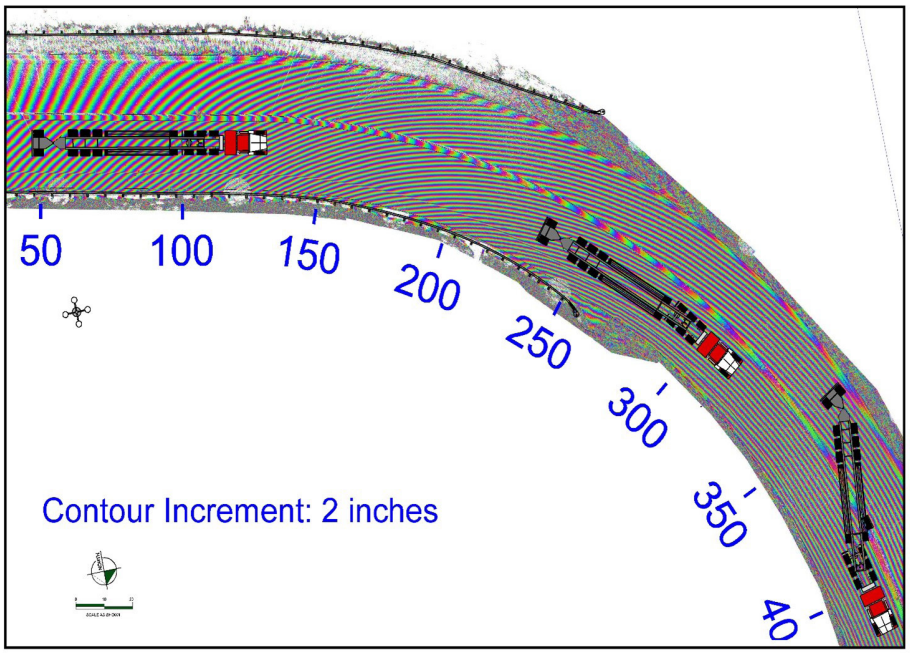

Figure 10
Truck semi-trailer position at wheel lift on road surface showing lines of constant elevation.

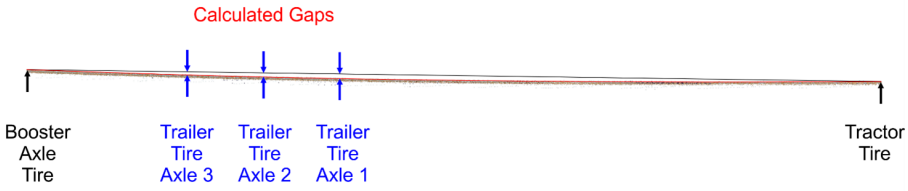

Figure 11
Gap analysis at area with loss of trailer tire friction.

Figure 12
Trailer wheel lift with booster axle loading before suspension droop.

Traditional methods to determine the critical speed of a vehicle on a curve require certain assumptions that were not applicable in this case due to the unusual geometry of this tractor trailer and the geometric configuration of the roadway[3]. Therefore, a kinematic model was created to determine the conditions necessary for the trailer to slide out during movement along this curved path by assuming that the moment about the kingpin created by the centrifugal force must exceed the resistance moment caused by the lateral friction forces of the trailer tires.

The center of mass of the trailer relative to the kingpin was calculated based on detailed measurements of the trailer using the 3D laser scan. The weights of the individual trailer components were determined through either direct measurements or from spec sheets. The center of mass of the trailer was calculated.

$$X_{cm} = \frac{1}{W_T}\sum W_i \bar{X}_i$$

Where X_{cm} is the center of mass of the trailer relative to the kingpin, W_T is the total weight of the trailer, W_i and X_i are respectively weight and relative center of mass location of individual trailer components.

The trailer wheel loads were determined based on direct measurements of individual tire loads. The resistance moment at the kingpin was calculated based on measured coefficient of friction of the wet road, trailer tire loading forces, and the moment arms from individual axles to the kingpin.

$$M_f = \sum \mu f_i X_i$$

Where M_f is the resistance

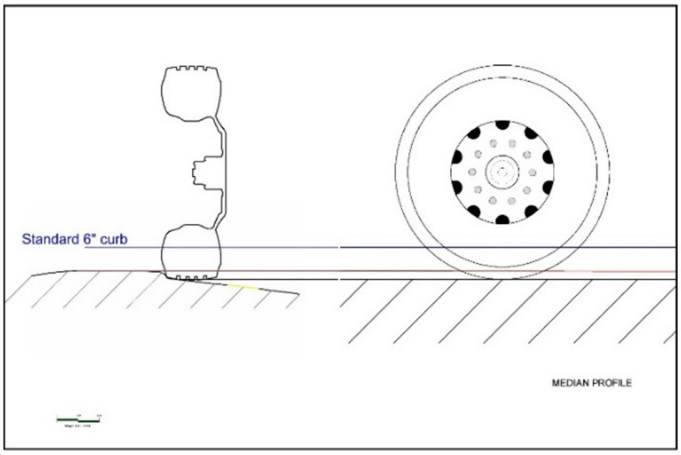

Figure 13
Center median height above road surface.

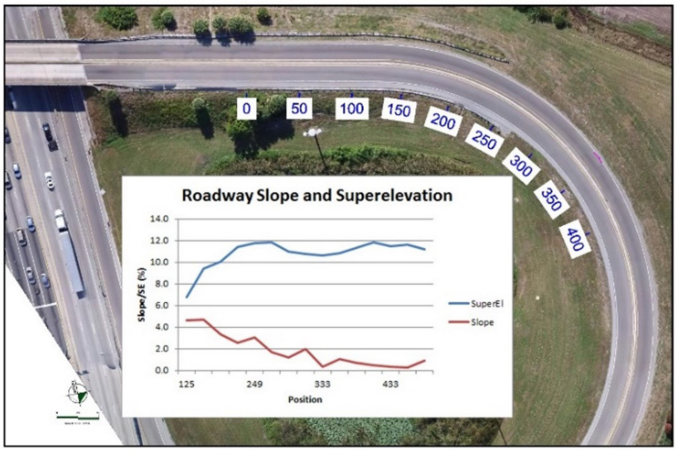

Figure 14
Superelevation road surface geometry.

moment, μ is wet road coefficient of friction that includes any roadway slope such as grade and superelevation, f_i are tire loading forces, and X_i are moment arms from individual axles to the kingpin.

The moment about the kingpin created by the centrifugal force was calculated based on the travel speed of the truck, radius of the curve, and the distance between the kingpin and the center of mass of the trailer.

$$M_C = \frac{W_T v^2}{rg} X_{cm}$$

Where M_C is the moment due to centrifugal force, v is the travel speed of the truck, r is the radius of the curve, X_{cm} is the center of mass of the trailer relative to the kingpin, and W_T is the total weight of the trailer.

When the centrifugal force moment exceeds the resistance moment the trailer will slide out. The angular acceleration of the trailer during slide-out was calculated based on equations of motion for angular momentum.

$$\sum M_{KP} = \bar{I}_{KP}\alpha$$

Where M_{KP} is the total moment about the kingpin, I_{KP} is the total moment of inertia relative to the kingpin, and α is the angular acceleration of the trailer.

The total moment of inertia relative to the kingpin was calculated using the parallel axis theorem and individual moments of inertia of the trailer components.

$$\bar{I}_{KP} = \sum[\bar{I}_i + m_i d_i^2]$$

Where I_{KP} is the total moment of inertia relative to the kingpin, I_i, m_i, and d_i respectively are moment of inertia, mass, and center of mass distances from the kingpin of individual trailer components.

The slide-out time to reach a specific slide angle at impact was calculated from angular acceleration.

$$t = \sqrt{2\theta/\alpha}$$

Where t is the slide-out time, θ is slide angle, and α is the angular acceleration of the trailer.

The maximum critical speed for the tractor-trailer at the onset of trailer slide-out as a function of roadway friction is shown in **Figure 15**. Two geometric scenarios are shown: the actual road geometry with varying slope

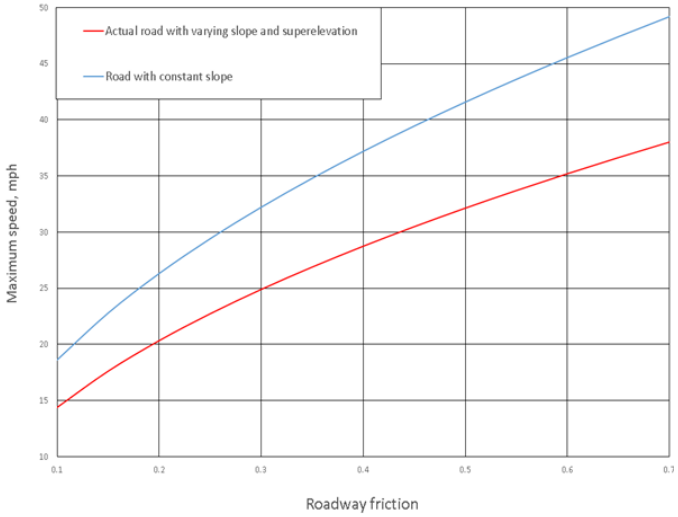

Figure 15
Maximum speed without trailer slide-out.

and superelevation, and a road with constant slope.

Conclusions

The detailed forensic engineering evaluation and reconstruction of this collision event allowed the following conclusions to be reached:

1. Changes in the roadway geometry along the path of the truck that allowed the trailer to "bridge" across lower elevation contours beginning over 250 feet before impact were quantified. The geometric characteristics were:

    a. Downslope changed from 4.5% to 1% in 142 feet (as show in **Figure 9**).

    b. Superelevation changed from 8% to 12% over 140 feet.

    c. Radius of curve continually decreased from a straight section of road to a curve with a radius of 230 feet.

2. The geometric characteristics, in combination with the long wheelbase of the trailer with booster axle, raised the height of the trailer relative to the roadway, thereby reducing the vertical load on the trailer wheels and the associated traction available to the tires needed to maintain lateral stability.

3. Rainwater acted as a lubricant to reduce the friction between the tires and the roadway. The wet friction value for a truck tire on this road surface was measured to be 0.35 (0.30 to 0.40, +/- one standard deviation). When dry, the friction value was 0.76 (0.68 to 0.85, +/- one standard deviation).

4. At the location where the trailer tires had less friction force available because of the dip and curve in the road, the curvature of the roadway created centrifugal force on the trailer. Typically, centrifugal force is resisted by the lateral traction of the tires. However, in this case, the moment about the kingpin created by the centrifugal force exceeded the lateral traction at the trailer tires at a speed of 27 mph, whereas the advisory speed was 35 mph.

5. The rotation of the trailer was caused by the combination of road surface geometry that created a bend and dip at the onset of the decreasing radius curve; the wet pavement; and the long wheelbase of the trailer with booster axle.

6. At the measured tire friction of 0.35 for the wet road, the geometry of the road surface and the geometry of this particular trailer reduced the safe travel speed for this tractor trailer from 35 to 27 mph.

As is often the case, this traffic accident arose from a combination of roadway, vehicle, operational, and environmental factors. The roadway was not in compliance with current AASHTO standards due to its age and resurfacing activities over the years — and was scheduled to be rebuilt. The tractor trailer was operated unloaded with a booster axle that interacted with the road surface to lift the trailer wheels as it passed over the wet roadway. Although the driver had reduced his speed, it was still too fast for this rig on this section of roadway when wet.

The forensic engineering analysis identified the influence of these factors on the reduction of lateral traction as a function of vehicle speed. The conclusion reached from this analysis was that, at the time of the accident, the safe travel speed for this tractor trailer was reduced from 35 mph to 27 mph, a speed below the posted advisory speed and that was consistent with the statement of the truck driver. The conclusions reached based on this detailed forensic analysis were helpful to the parties in the resolution of claims arising from this unfortunate traffic accident.

References

1. A Policy on Geometric Design of Highways & Streets AASHTO, 6th Edition, 2011.

2. Measurement of Vehicle-Roadway Frictional Drag, SAE J2505, 2010.

3. Use of the Critical Speed Formula, SAE J2969, International, Society of Automotive Engineers, Jan 2017.

Forensic Engineering Investigation of Electrical and Electronic Causes of an Industrial Equipment Failure

By Robert O. Peruzzi, PhD, PE, DFE (NAFE 954M)

Abstract

This case involved industrial equipment whose repeated, seemingly random failures resulted in the buyer of that equipment suing the seller. The failures had been isolated to a group of several transistors within electro-mechanical modules within the equipment, but the root cause of those transistors failing had not been determined. The equipment seller had more than 1,000 units in the field with no similar failures. And the electro-mechanical module manufacturer had more than 20,000 units in the field with no similar failures. Electrical contractors hired by the buyer had measured power quality, and reported no faults found in the three-phase power at the equipment terminals. This paper presents circuit analyses of the failing electro-mechanical module, basics of electrostatic discharge damage and protection, and the root cause of these failures — an electrical code-violating extraneous neutral-to-ground bond in a secondary power cabinet.

Keywords

Forensic engineering, electrical engineering, electronic engineering, troubleshooting, investigating, National Electrical Code, NEC, industrial equipment, power routing, grounding, neutral, bonding

Introduction

The industrial equipment investigated in this paper can be classified as medium-duty (1 to 10 tons), fully automated, electric motor-operated, consumer product packaging equipment (hereinafter referred to as "the equipment")[1]. Featuring robotic functionality, including optical sensing, product handling, material handling, and basic quality control, the equipment automatically generates reports of operating and production status at regular intervals and issues alarms, triggering immediately when warranted.

Human operators load the somewhat fragile products onto a conveyor belt to be packaged as individual units. The equipment repositions the units on the conveyor belt with a higher degree of precision and spacing. Compressed air removes any dust from the units. The units are placed within packages, and then the packages are wrapped in plastic film. Hot air shrinks the plastic film. Printed labels are applied to the packages. The final packages, now much less fragile, are stacked onto pallets. Forklift operators move the pallets to loading docks or into the warehouse storage area.

The equipment's optical sensing uses infrared, optical and UV light sources with corresponding photodetectors. Temperature sensors control the shrink-wrapping hot air blower, and there are physical position sensors, angle sensors, and rotation counters as well. Sensing is done at multiple points and times during the process. The sensors make the process observable to a control system microprocesser within the equipment. The microprocessor controls mechanical manipulators and tools, heaters, and blowers. The combination of observability and controllability results in a stable control system[2].

Three-phase 480VAC power enters the factory from a transformer mounted on a nearby utility pole and is distributed through a main panel and two sub-panels. The equipment has its own transformer, rectifiers, and power conditioners, delivering AC and DC of various voltages throughout the system.

Background

The seller manufactures and services the equipment. The buyer purchased and deployed a set of the equipment. The equipment control system first failed within two months of deployment. The seller repaired and returned it to the buyer's facility. It failed again within two months.

Robert O. Peruzzi, PhD, PE, DFE, 719 Fourth Ave., Bethlehem, PA 18018, (610) 462-3939; peruzzi@rperuzzi.com

Except for frequent failures, the buyer was satisfied with the operation of the equipment. The buyer purchased and deployed a second unit within nine months of purchasing the first unit.

Failures continued to occur in both units every few months, and more frequently during the cold months — the heating season. Specifically, it was the physical position sensors, angle sensors, and rotation counters that failed (seemingly randomly). The seller replaced the various sensors eight separate times in less than a year. Each time, the equipment was out of service for days or weeks.

The seller claimed that the failures were caused by transient voltage fluctuations (a rapid voltage change in fundamental frequency voltages over several cycles) at the buyer's premises. The buyer's electrician tested for electrical abnormalities and reported normal readings that should not cause problems with the equipment.

After two years, the buyer was frustrated and purchased a set of similar packaging equipment from the seller's competitor. The buyer demanded a full refund for the two sets of the seller's equipment plus compensation for what the buyer had spent for ongoing repairs and lost revenue due to system downtime.

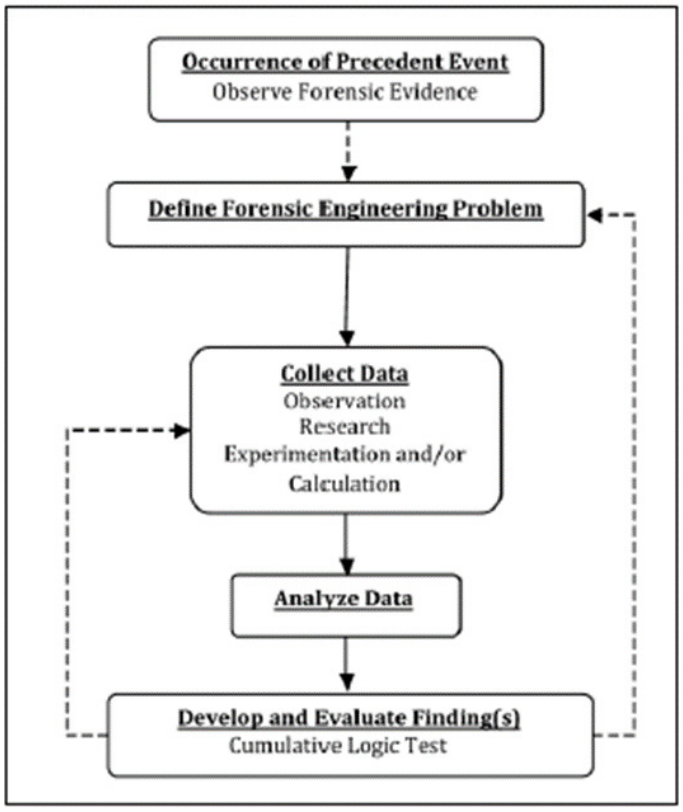

Figure 1
Flowchart illustrating forensic engineering method presented in "Forensic Engineering and the Scientific Method" by Liptai and Cecil.

Research and Hypotheses

For a complete description of the scientific method as it applies to forensic engineers, see "Forensic Engineering and the Scientific Method"[3]. From that article is **Figure 1**, a flowchart illustrating the forensic engineering method utilized in applied science or technology, which is an adaptation of the most general scientific method.

Three competing hypotheses (shown in **Figure 2**) were developed after reviewing the available documents. The hypotheses and their elements are discussed below:

1. *First hypothesis*: Although the buyer's electrician tested and reported normal readings that should not cause problems with equipment, the author's first hypothesis was that equipment failure was due to a fault in the three-phase power distribution. **Figure 3** on page 24 shows amplitude versus time plots of voltages and currents of the three phases. Plots of voltage and current on the neutral wire, referred to as ground, are not included. (Power quality testers, including three phases plus neutral, were available in March of 2019.) The current plots show current spikes of more than 5.6 kA and voltage excursions down to about 192.5V from 210V. That's less than 10%, and was considered acceptable by the electrician and the buyer. Plus, it was within the range required by the seller.

Within the buyer's factory, the circuit powering the equipment also powers two chargers for lithium-ion battery powered forklifts. The current spikes occur when the battery is plugged in to the charger.

Presenting a balanced load to the three-phase source is not a system requirement. The current and voltage fluctuations do not exceed specified limits required by the seller.

Notice that there is no plot of the voltage and current of the neutral wire. With proper power distribution, if neutral voltage and current were plotted, the unbalanced current would appear in that plot — and a voltage plot would show only a few volts excursion. A high-impedance return path on the

neutral wire could be problematic, causing higher voltage excursions. The author suspected a fault with the routing of neutral wires, which serves as the core of the first hypothesis.

2. *Second hypothesis*: Electrostatic discharge (ESD) was damaging the transistors. Provided documents isolated the failure to the output stage of the position sensors within the equipment. This push-pull output stage drives a digital signal through wire from the sensor to the microprocessor. A representative push-pull output stage is shown in **Figure 4** on page 24.

   The output stage is a complementary metal oxide semiconductor (CMOS) inverter. It consists of a P-type metal oxide field effect transistor (MOSFET), abbreviated as a PFET, and an N-type MOSFET (NFET). The input signal is connected to both the PFET and the NFET. Both MOSFETS connect to the output. The "load" connected to the output symbolizes several meters of shielded cable connected to the input of a microprossesor within the equipment.

   VDD is a DC voltage derived from one phase from the equipment's three-phase power. VSS is derived from the neutral wire of the three-phase power. The sensor's housing is connected to safety ground. The push-pull function is to drive a representative of signal "input" from the position sensor through a length of wire to the microprocessor.

   When the input voltage is below the threshold, the NFET "turns off" and does not conduct. The

	Hypothesis	Basis	Tests
1	Faulty three-phase power distribution	Although the buyer's electrician tested and reported normal readings that should not cause problems with equipment, this hypothesis is that equipment failure was due to a fault in the three-phase power distribution	1. Inspect 3-phase power from the transformer, through the main and sub-panels to the equipment, looking for proper configuration of three hot phases, neutral return, and ground connections
			2. If no faults found by visual inspection, perform a multi-day power quality measurement, including measuring of voltage and current on the neutral return line
2	Electro-Static Discharge damaged the output stage of the position sensors	Unwinding plastic film from a roll is a well-known generator of static build-up. Failures occurred more frequently during the winter months, when static build-up is more of a problem	1. Review the equipment design documentation to determine how ESD is intended to be mitigated
			2. Inspect the equipment for damaged shielded connectors and functionality of ESD mitigation subsystems
			3. Use a hand-held static-voltage meter to measure static voltage inside the equipment during operation
3	Radio Frequency Emission damaged the output stage of the position sensors	Microprocessors and electronic components operating at high switching frequencies emit electro-magnetic waves at radio frequencies. Metal surfaces and metal products being packaged and wrapped may reflect such waves. It's possible for non-linear elements within the equipment systems to amplify and shift the frequency, and be picked up and conducted into wires of the position sensors	1. Review the equipment design documentation to determine the specified grounding and shielding requirements
			2. Visually inspect the equipment for proper grounding, shielding, and any damage to grounding and shielding
			3. Use a hand-held static-voltage meter to measure electric field strength inside the equipment during operation

Figure 2
Hypothesis table.

PFET "turns on" and pushes current from the positive power supply "VDD," through the PFET, through the output, and through cable to microprocessor input — indicated as "load."

When the input voltage is above the threshold, the PFET "turns off" and does not conduct. The NFET "turns on" and pulls current back from the microprocessor input and cable, through the output, through the NFET, and to the negative power supply "VSS."

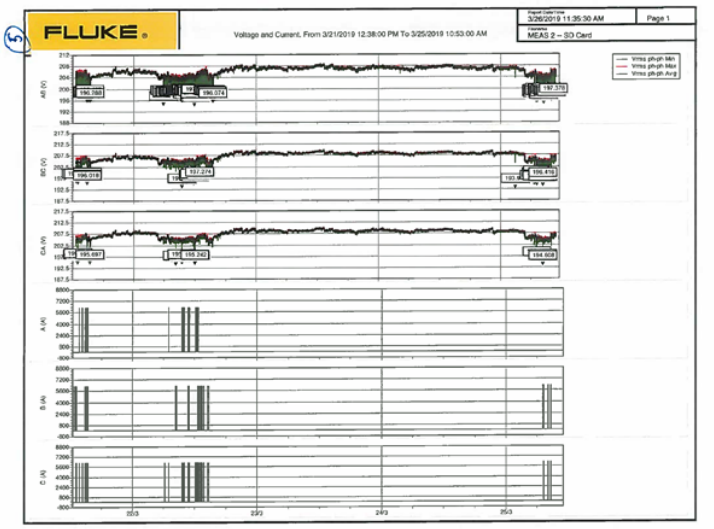

Figure 3
No problems with three hot-phase voltages appear in this voltage power quality plot.

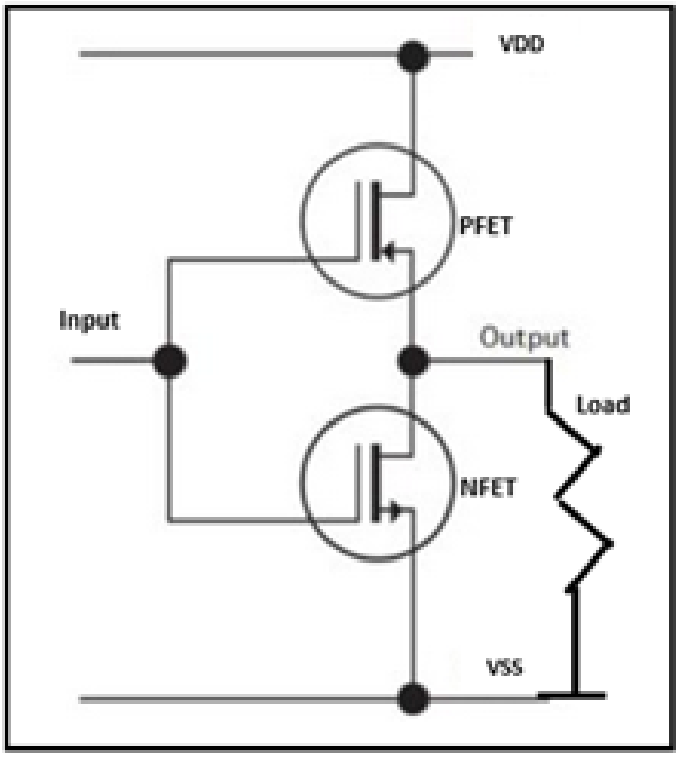

Figure 4
Typical CMOS push-pull output stage.

The microprocessor interprets the pattern of voltages developed at its input as digital logic signals and uses them in its control algorithm for the system.

The push-pull output stage is robust when there is proper connectivity to VDD, VSS, and safety ground at all points. However, if for some reason VSS even momentarily reaches a significantly higher voltage than the output, current from VSS can overpower the normal operation of the NFET, burst through its electronic "barrier," and flow upward from VSS to the output. If VSS reaches a voltage significantly higher than VDD, current from VSS can overpower the normal operation of both the NFET and the PFET and flow through both up to VDD.

Either event can generate enough heat to damage the semiconductor junctions of one or both MOSFETs. Even after VSS voltage returns to normal, the damaged MOSFETs can allow current to leak from VDD through the PFET and NFET to VSS — no matter the state of the input. The leakage current generates heat, which further increases the leakage current and generates more heat. This is known as thermal runaway, and eventually melts the active areas of the MOSFETs. One cause of such a catastrophic failure is ESD.

Static electricity is called static because it does not move through wires; however, if enough builds up, it will jump from one object to another[4]. The hypothesis to be investigated is that static charge built up somewhere in the equipment and jumped to VSS in **Figure 4**, resulting in high enough voltage between VSS and the output or between VSS and VDD to damage the NFET, the PFET, or both.

Components such as the position sensors that failed are designed for self protection from ESD during manufacture, test, and installation. Protection from ESD in operation is the responsibility of the equipment designer (that is, the seller). It is the buyer's responsibility to repair any damage to the equipment that compromises protection, such

as loose grounding wires or straps. To be investigated was whether or not the ESD protection of the equipment was adequate.

A typical static electrical charge buildup in electrical equipment occurs when plastic material (such as plastic shrink wrap) is unwound from a roll. Multiple solutions can be used to mitigate this tribological effect[5].

Ionization can neutralize static charges in a matter of seconds[6]. Ionizers create positively and negatively charged ions, which are distributed by fans through the system to be protected. A solution promoted in "Solutions for Static Buildup on Process Rollers"[5] includes conductive graphite in mechanical rollers within the system.

The observation by both the buyer and seller that failures occurred more frequently during the winter months points to ESD as a potential cause of the failures. Heated inside air in the winter has lower relative humidity than inside air from ventilation in spring and fall or chilled air in the summer. Low relative humidity increases the likelihood of electrostatic charge buildup, as intuitively known by getting static shocks after walking across a carpet in winter and touching a metal doorknob.

Industrial systems, such as the equipment, are designed to be robust against ESD using techniques of "Solutions for Static Buildup on Process Rollers"[5] and When Do You Need Ionization?"[6] or others. The position sensors and other components within the system have installation requirements, including the use of shielded cables to guard against static charge "jumping" onto the wires from charged surfaces within the equipment.

3. *Third hypothesis*: Radio frequency interference (RFI) damaged the output stage of the position sensors. The microprocessor and control system for the equipment include components that may emit high-frequency radiation. A design fault or system failure could possibly lead to high-frequency radiation coupling into a wire, such as VSS in **Figure 4** and damaging the junction of the NFET or PFET in a similar way as ESD.

   Typically, such systems are designed for robustness against RFI, but this was a hypothesis to be tested and ruled out.

Given the "zero failure rate" claimed by the seller and the manufacturer of the position sensors, the author planned to investigate only these three hypotheses.

Protocol for Site Visit

The following protocol was requested and accepted:

1. View and photograph the three-phase service, including the transformer mounted on the utility pole, the service drop wires to the service entrance, and electric meter.

2. To observe and photograph while the seller's representative or the buyer's representative:

   a. Demonstrates and operates the systems.

   b. Explains their operation.

   c. Points out their components and their function.

   d. Points out the failing components and explains their failure modes.

3. For the buyer's or the seller's qualified representative to show where and how the power quality test instruments were connected, so that the author may view and photograph.

4. Direct the licensed electrician (subcontracted by the author) to probe for high voltage on neutral wire due to wire damage and the large unbalanced load current it carries when, for example, the forklift charger is operated. This would involve measuring the voltage on the neutral wire near the same location where the power quality probes were attached. Note: An electrical engineer — even a licensed professional forensic engineer like the author — is not necessarily an electrician. Therefore, it is important to delegate certain tasks accordingly.

5. With assistance from the licensed electrician, measure the harmonic content on the three power phases, which may reach high levels while the forklift charger is operated.

6. Evaluate the static electrical charge build-up of

the environment inside the equipment system — that is, measure the strength of static electric field along the product path. This needs to be done with actual product being processed.

7. Evaluate the strength of radio frequency fields within the environment inside the packaging equipment while it is processing product.

Site Visit

Along with the master electrician and his assistant, the author viewed and photographed the three-phase transformers on the utility pole, the ground rod at the foot of the utility pole, and the service-drop cable package — three hot phases and neutral cable — from the transformers to the service entrance. All was well with the electric utility-owned system.

Inside the premises, the electricians removed the cover from the main breaker panel (service disconnect) for the building. This 400A service panel was owned by the buyer.

Figure 5
Panel 1, showing proper configuration of three fuses and neutral-to-ground bonding point.

The bonding point of neutral to ground for the building can be seen to the left of **Figure 5**. All of the neutral return lines within the building should be isolated from ground until they reach this bonding point within Panel 1. One can see that panel cabinet is also bonded to this ground point.

Earth grounding is established by a grounding rod penetrating the foundation into the earth as shown in **Figure 6** (pointed out by the author's foot). This earth-ground is bonded to the node shown in **Figure 5**.

The electricians verified all phase-to-phase and phase-to-neutral voltages. Since earth-ground and neutral are bonded inside Panel 1, ground to neutral is zero volts by construction at this point.

Panel 2 is mounted on the same exterior wall, a few meters from Panel 1. Panel 2, shown in **Figure 7**, limits the available current to 200A. Three hot phases, neutral, and ground wires can be seen. As is proper, neutral and ground are isolated from each other by insulating fittings. This isolation and the bonding between the cabinet of Panel 2 and ground can be seen more readily in **Figure 8**.

Verifying all phase-to-phase and phase-to-neutral

Figure 6
Service ground is established by a steel rod penetrating the foundation into the earth.

voltages within Panel 2, the electrician also confirmed 0V between neutral and ground within Panel 2.

Panel 3 is mounted on an interior wall, about 100 meters from Panel 2. The electrician opened Panel 3, shown in **Figure 9**. Hot phase wires are red, blue, and yellow. To their right is the white connector for neutral.

The close-up of Panel 3 interior in **Figure 10** (on page 28) shows a green screw attached to a bonding clamp on the white (neutral) wire. By convention, this green screw indicates bonding of neutral to ground.

The electricians verified proper voltages between all phases and phases to neutral. Because of the bond, neutral to ground voltage is 0V. Bonding of neutral to ground anywhere other than the main service entrance (Panel 1) violates the *National Electrical Code* (NEC)[7]. The ramifications of this will be discussed later.

Panel 3 is the first panel upstream from the equipment and is shown on the upper right of **Figure 11** (on page 28). Panel 3 supplies power to the two chargers for the

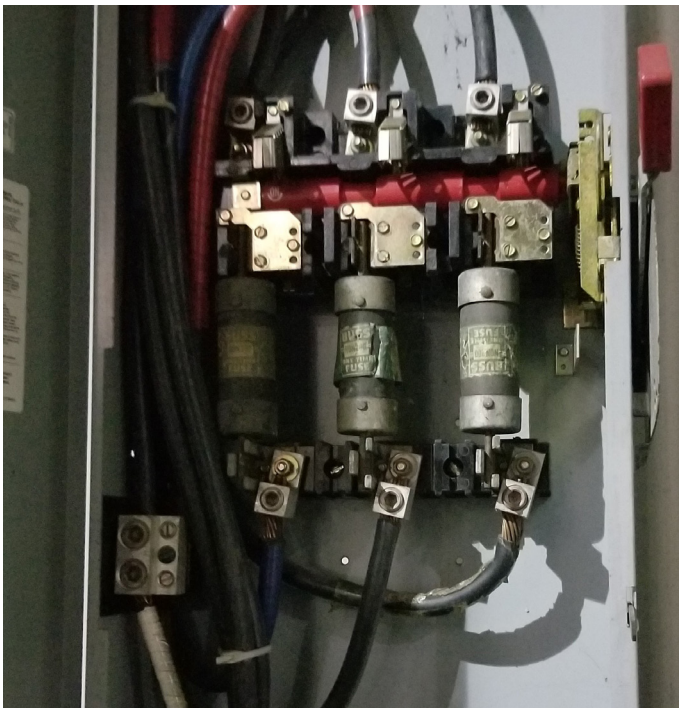

Figure 8
Close-up showing neutral isolated from ground within Panel 2.

Figure 7
Internal view of Panel 2 shows neutral isolated from ground.

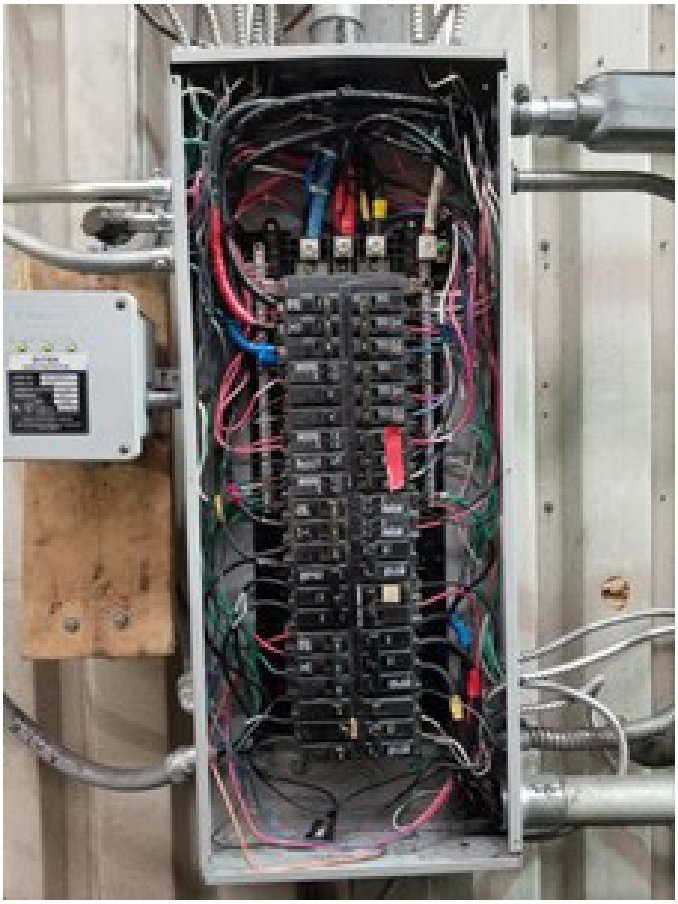

Figure 9
Interior view of Panel 3.

lithium-ion batteries of electric-powered forklifts on the floor beside Panel 3 — and to the subject equipment in a large factory room across the wall from Panel 3.

Continuing on to the subject equipment, **Figure 12** shows one of the position sensors that failed regularly. The green collar attaches the cable to the output stage of the sensor — that is, the push-pull driver shown in **Figure 4**. The green collar also bonds the cable's shielding to the sensor's housing.

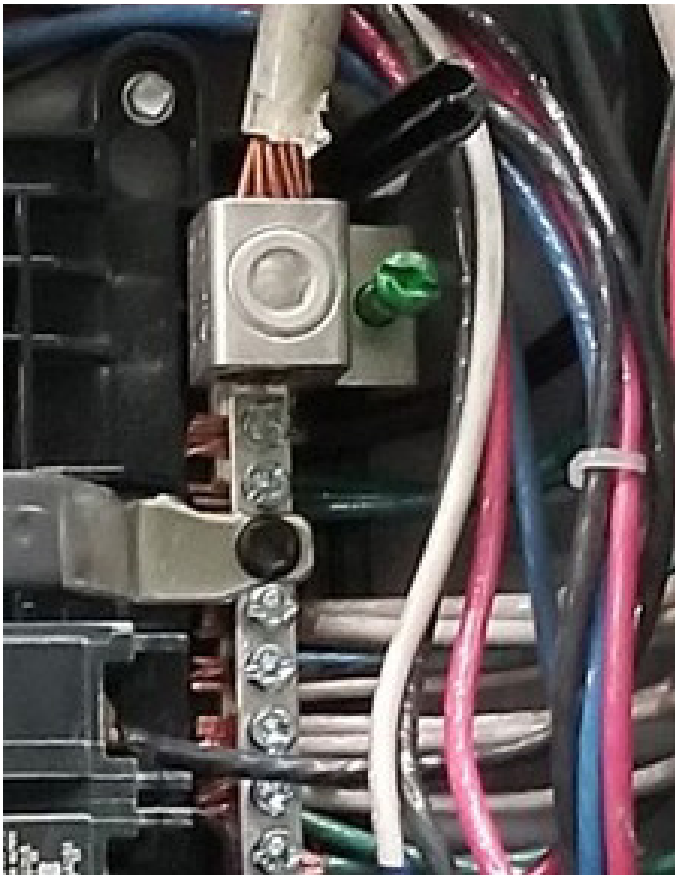

Figure 10
Close-up within Panel 3, showing improper bonding of neutral to ground.

Figure 11
Panel 3 and two forklift battery chargers.

The opposite end of the green cable connector is shown in **Figure 13**, along with the connecting fixture to the microprocessor. Cable and connector include shielding. Outside of connector is connected to shield and makes electrical contact with the encoder housing. Shielded point to point connectivity to grounded metal housings provides protection from ESD and RFI damage. The author observed similar proper grounding and shielding techniques throughout the equipment, making hypotheses

Figure 12
One of the position sensors that regularly failed shows intact cabling and shielding.

Figure 13
Opposite end of the cable of **Figure 10** where it attaches to the microprocessor.

2 and 3 unlikely causes of the repeated failures.

Hypothesis 1 — that equipment failure was due to a fault in the three-phase power distribution — is the most likely of the three hypotheses. The fact that an NEC violation is present adds to that likelihood, and creates an urgent obligation that the buyer be informed of this safety hazard immediately.

Discussion

The unwanted bonding from neutral to ground in Panel 3 was the most important finding and is a safety hazard as well as the most likely cause of the repeated failures. The safety hazard can be explained with these quotations from the NFPA 70, *National Electrical Code Handbook*[7].

250.5 (4) Path for Fault Current:

"The earth shall not be considered as an effective fault-current path."

"The two reasons for grounding are as follows:

1. To limit the voltages caused by lightning or by accidental contact of the supply conductors with conductors of higher voltage

2. To stabilize the voltage under normal operating conditions (which maintains the voltage at one level relative to ground, so that any equipment connected to the system will be subject only to that potential difference)"

...

250.24(a)(5)

(5) Load-Side Grounding Connections.

"A grounded conductor shall not be connected to normally non–current-carrying metal parts of equipment, to equipment grounding conductor(s), or be reconnected to ground on the load side of the service disconnecting means except as otherwise permitted in this article."

...

"Section 250.24(A)(5) prohibits re-grounding of the grounded conductor on the load side of the service disconnecting means. This correlates with the requirement of 250.142(B), which is a general prohibition on the use of the grounded conductor for grounding equipment. ***This prevents parallel paths for neutral current on the load side of the service disconnecting means. Parallel paths could include metal raceways, metal piping systems, metal ductwork, structural steel, and other continuous metal paths that are not intended to be current-carrying conductors under normal conditions."***

(Author's emphasis added)

250.30 (A)

"Installing a system bonding jumper at both the source and the first disconnecting means ***can result in establishing an unintended parallel path for current that would otherwise utilize the grounded conductor. Exposed normally non–current-carrying metal components are often included as part of this parallel path and can present an unintentional safety hazard. This type of installation is prohibited*** *..."*

A plain English explanation is posted as an answer to a frequently asked question[8].

*"**Frequently Asked Question:** Why do the grounds and neutrals need to be separated in a sub-panel? What happens if they aren't?*

Answer: *Though the neutral doesn't have significant voltage, it does carry current. Remember, it's current that kills, not voltage. In a 2-wire circuit, the neutral carries just as much current as the hot conductor. If the neutral and ground are connected in a sub-panel, that current will travel on other paths, such as bare ground wires, equipment enclosures, and metal piping systems, on its way back to the service panel. One problem created by this condition is possible shock hazards, the severity of which depends on the locations of the equipment and the person touching the enclosure or piping system. Another problem is magnetic fields that do not cancel themselves out. Since the return current has multiple paths, the current remaining in the neutral will not counterbalance the*

current in the hot wire. The resulting imbalance creates a magnetic field that can interfere with sensitive electronic equipment. In a metal conduit system, the imbalance will induce current into the conduit, which could cause the conduit to overheat."

NEC Expert Mike Holt, of Mike Holt Enterprises, explains this even more bluntly and directly in his online Code forum[9].

*"At the service panel (**ONLY AT THE SERVICE PANEL - HUGELY IMPORTANT**) the neutral bus bar is bonded to ground. You should see the ground lead and neutral tied to the same bus (the neutral bus bar).*

*However, any sub-panel after the primary service from there **MUST** have an isolated neutral. **DO NOT DO NOT DO NOT bond neutral to ground in a sub-panel**.*

Why is this?

When you tie neutral to earth ground in a sub-panel, you create a potential parallel path for current to return via earth (ground). In the event of a fault, your ground conductor has assumed the role of the return path for current and now everything that you've grounded (sub-panel, appliances, metal fixtures, etc.) to that sub-panel is now hot.

All it takes is a preexisting fault, one rainstorm, or wet feet, whatever... and you touching something energized - and you're doing the 60 cycle shuffle."

Conclusions

From readings and observations during the site visit, the author discarded the second and third hypotheses as unsupportable. Proper grounding and shielding were designed into the equipment. The likelihood of ESD or RFI damaging the output stages of the various sensors used throughout the system was negligible. A summary of case and root causes are shown in **Figure 14**.

	Hypothesis	Findings	Significance
1	Faulty three-phase power distribution	Faulty installation of an electrical sub-panel was found by visual inspection. In the sub-panel powering the equipment and the battery chargers, there was an unexpected and dangerous bonding between the neutral busbar and safety ground	1.This extraneous bond violates National Electric Code 250.5 and others, and creates a safety hazard. 2. In terms of electrical performance, this extraneous bond enables a ground loop which under certain circumstances can cause transient voltages on the neutral line (and VSS within the sensor), large enough to damage the sensor output transistors
2	Electro-Static Discharge damaged the output stage of the position sensors	The author visually inspected the equipment and found no damaged shielded connectors or other obvious damage that would affect ESD susceptibility	Author had reviewed the documentation prior to visiting the site to understand the ESD mitigation intent. Finding all systems in place and intact, author decided ESD damage was a far less likely failure cause than the discovered extraneous ground bond.
3	Radio Frequency Emission damaged the output stage of the position sensors	The author visually inspected the equipment and found no damaged shielded connectors or other obvious damage that would affect Radio Frequency Interference susceptibility	Author had reviewed the documentation prior to visiting the site to understand the RFI prevention intent. Finding all systems in place and intact, author decided RFI damage was a far less likely failure cause than the discovered extraneous ground bond.

Figure 14
Summary of author's findings.

Consider the thousands of installations worldwide and hundreds of installations within the United States. Two machines repeatedly fail. Both are owned by the same customer, operate inside the same building, and are powered from the same improperly wired sub-panel. What is different about this customer and their facility causing the failures? The improper wiring is a likely difference.

The root cause is not due to a single overriding fault, but rather several shortcomings, including the electrical transients that were conducted through the inadvertent ground loop, which combine to the observed failure mode. There is a strong likelihood that fixing the Code violation will make the other contributing causes insignificant.

1. The mistaken bonding of neutral wire to ground at Panel 3, which services the equipment and also the forklift chargers, creates multiple parallel current return paths where there ought to be a single path from all loads within the building facility back to the transformer outside the building.

    a. This dangerous condition can cause injury. Fixing it is not optional: It must be fixed as soon as possible for safety reasons if nothing else.

    b. It is a violation of NEC Section 250.

    c. It can cause voltage fluctuations on the ground and neutral wires within the equipment.

2. Battery chargers next to Panel 3, when used, cause large unbalanced current to flow in the neutral-ground combination that can interfere with the power supplies of the position sensors within the equipment. Removing the illegal bond will allow this unbalanced current to divide and flow properly through the neutral and hot phases without disturbing the ground voltage.

3. Misleading clue #1. Failure Mode Analysis of the position sensors indicated their output stage was burnt out. This pointed to ESD or RFI as a possible cause, especially because failures occur during the heating season when humidity is low and static charge buildup is high. However, the system was designed to be robust against electrostatic discharge.

4. Misleading clue #2. The buyer is the only (known) customer of the seller using the equipment to wrap large all-metal products. If static charge were borderline high, the antenna effect of the ungrounded metal products could be exacerbating the postulated ESD effect. However, the sealer is designed and built to allow processing all-metal products.

Given the danger from this Code violation, the author advised the buyer to fix the violation immediately — before any further investigation of the equipment failures. Once the ground-neutral bond was repaired to Code specifications, it appeared to have fixed the conditions that caused the failures.

References

1. S. Kashyap, “Analyse A Meter,” [Online]. Available: https://analyseameter.com/2020/01/industrial-machines.html. [Accessed 19 May 2021].

2. X. M. Ren, A. B. Rad, P. T. Chan and W. L. Lo, “Identification and Control of Continuous-Time,” IEEE TRANSACTIONS ON INDUSTRIAL ELECTRONICS, vol. 50, no. 3, pp. 478-487, June 2003.

3. L. Liptai and J. Cecil, “Forensic Engineering and the Scientific Method,” Journal of the National Academy of Forensic Engineers, vol. XXVI, no. 1, 2009.

4. eCircuit Center, “Push-Pull Output Stage,” eCircuit Center, 2002. [Online]. Available: http://www.ecircuitcenter.com/Circuits/pushpull/pushpull.htm. [Accessed 3 June 2021].

5. Fluoron, Incorporated. Staff Writer, “Solutions for Static Buildup on Process Rollers,” Fluoron, The Foll Surface and Release Experts, 25 April 2019. [Online]. Available: https://www.fluoron.com/solution-for-static-buildup-on-process-rollers/. [Accessed 3 June 2021].

6. SCS, “When Do You Need Ionization?,” SCS (Static Control Systems), 10 January 2019. [Online]. Available: https://scs-static-control-solutions.blog/2019/01/10/when-do-you-need-ionization/. [Accessed 3 June 2021].

7. National Fire Protection Agency (NFPA), NFPA 70(R): National Electrical Code (R) Handbook, Quincy, MA: NFPA, 2017.

8. Stack Exchange, “Home Improvement,” Stack-Exchange, 30 March 2020. [Online]. Available: https://diy.stackexchange.com/questions/1706/is-it-ok-to-have-mixed-grounds-and-neutrals-on-bars-in-a-breaker-box. [Accessed 4 June 2021].

9. M. Holt, “Topic: Why don't you bond the neutral at a sub panel?,” Mike Holt Enterprises, 12 August 2002. [Online]. Available: https://www.mikeholt.com/forum/Forum1/HTML/003455.html. [Accessed 4 June 2021].

FE Analysis of Modular Woodburning Fireplace Fire with Gas Log Lighter in Determining Fire's Cause

By Jerry R. Tindal, PE (NAFE 642S)

Abstract

A fire originated inside the chase[1] (a vertical enclosure, usually constructed of wood, that houses and conceals a chimney) surrounding a modular fireplace system of a new residence, ultimately spreading and destroying the home. A lawsuit by the homeowner's insurance company was later filed against the general contractor and framing subcontractor, alleging that improper clearances between the fireplace and chase framing caused the fire. The author was retained to perform a forensic engineering analysis of the origin and cause of the fire. An exemplar modular fireplace system and chase were constructed and instrumented, and more than 30 test burns were performed. Additional testing evaluated gas migration from the fireplace log lighter into flexible combustion make-up air ducting and the burning propensity of the ducting. The testing and analysis concluded that the cause of the fire was not improper clearances to the chase framing but improper installation of the combustion air kit facilitating a mediation of the case.

Keywords

Modular fireplace, log lighter, propane, gas migration, combustion air duct, wood burning, chimney, low temperature ignition, smoldering, clearances, fire investigation, methodology, reconstruction, testing, chase, NFPA 921, NFPA 211, UL 127, forensic engineering

Background

The home in question was a newly constructed, two-story, wood-framed structure of approximately 10,000 square feet containing a total of six fireplaces. The incident fireplace was located in the family room and installed in a common chase enclosure next to the exterior covered patio fireplace. **Figure 1** depicts a Google Earth image of the home prior to the fire and the locations of the family room, exterior covered patio, and associated modular fireplaces.

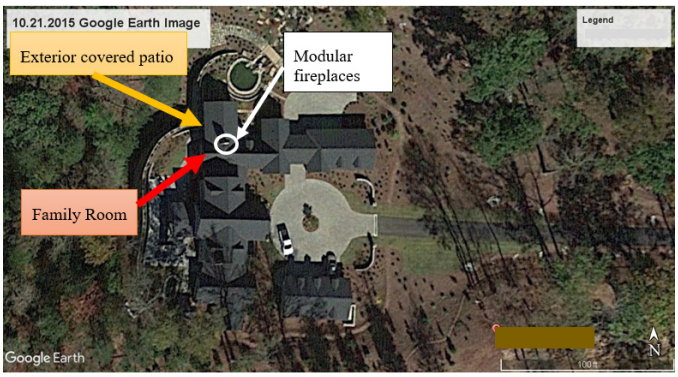

Figure 1
A pre-fire Google Earth image of the residence around the time it was first occupied in October of 2015.

The incident fireplace was identified as a solid woodburning listed masonry modular fireplace system. The firebox incorporated a make-up combustion air kit as well as a propane log lighter kit, which included a recessed pan style burner. Both the make-up combustion air kit and the log lighter kit were specified and approved for use with the fireplace. **Figure 2, Figure 3** (on page 34), and **Figure 4** (on page 34) are excerpts from the installation manual of the fireplace system depicting the style unit.

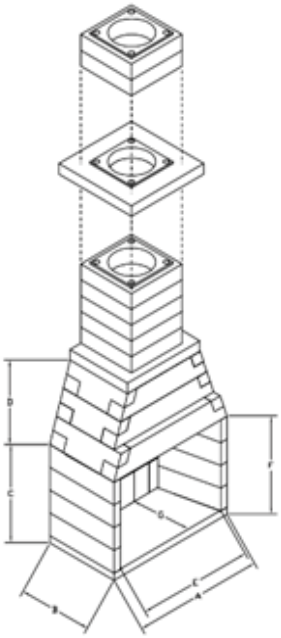

Figure 2
Either masonry or metal chimney kits are available for use with the fireplace system.

Jerry Tindal, PE, 5901 Elwin Buchanan Drive, Sanford, NC 27330, jtindal@safe-labs.com

Figure 5 is an excerpt of the installation instructions for the make-up combustion air kit. **Figure 6** is an image of an exemplar log lighter burner pan and cap that was installed in the incident fireplace.

The homeowner reported that the fireplace had been used approximately 30 times total since they had occupied the home. The homeowner cut, stacked, and seasoned his own firewood. The wood was seasoned for at least 18 months. The fireplace was used with a consistent frequency of once or twice a week during the heating season and used in a consistent manner each time. On the evenings when he would build a fire (around 7:30 p.m.), the homeowner would place three seasoned split oak logs of 3 inches in diameter and 20 to 21 inches long inside the fireplace. He placed newspaper beneath the logs, lit the paper with a grill lighter, and turned on the gas valve to the log lighter. After approximately 10 minutes the firewood would be burning well, and he would turn the log lighter gas valve off. After 60 to 90 minutes, he would add one or two more oak logs of the same size to the fire. At the time he and his wife would go to bed (around 10:30 p.m.), there would be nothing but coals and ashes in the fireplace.

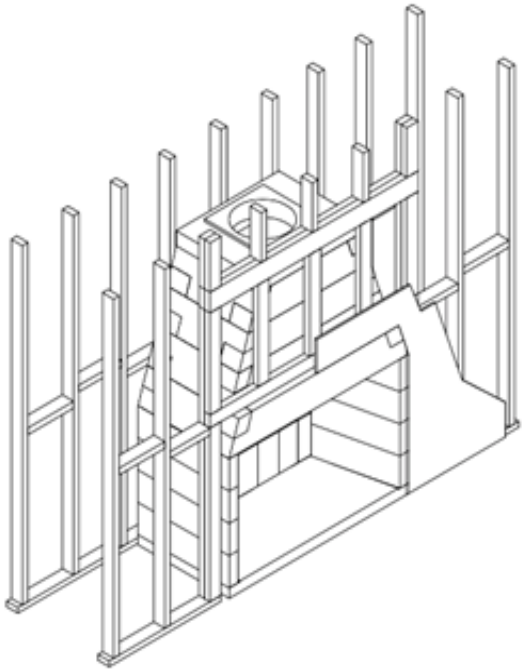

Figure 3
Clearances to combustibles, including wood-framing, are specified in the installation manual as well as on a permanent plate attached to the firebox.

CLEARANCE TO COMBUSTBLES

Unit to side enclosure	1"
Unit to face enclosure	1"
Opening top to combustible mantle	16"
Opening to combustible facewall	12"
Unit to back enclosure	1"
Unit to ceiling joists	1"
Opening to sidewall	28"

Figure 4
Annotated clearances to combustibles table excerpt from the fireplace installation manual (also reflected on the permanent label on the firebox). Note the clearance requirement from the fireplace back and sides to combustibles, including chase enclosure wood wall framing, is 1 inch.

Post-incident, the homeowner reported to the independent fire investigators for his insurance company that he had experienced two or three flash fires[2] with the fireplace

FIREPLACE REQUIREMENTS

1. Install and use the MASON'S CHOICE OUTSIDE AIR KIT only in masonry fireplaces constructed in accordance with the requirements of the standard for chimneys, fireplaces and vents, NFPA 211.
2. In the construction of the air passageway only non-combustible material must be used.
3. DO NOT install in the rear of the firebox because sparks will be blown into the room.

INSTALLATION INSTRUCTIONS

1. Install in the sidewall of the fireplace as far forward as possible, and in the third course of fire brick. (See picture below)
   Caution: DO NOT use combustible material in construction of passageway.
2. Adjust elbow and telescope tube to rear outside wall. Brick around elbow and tube.
3. Caulk back plate of hooded outside vent and push into tube.
4. Caulk (silicone) collar of inside slide door fitting and push into end of elbow.

Standard 3" stainless pipe and elbows may be used to extend air passageway from an inside or basement fireplace.

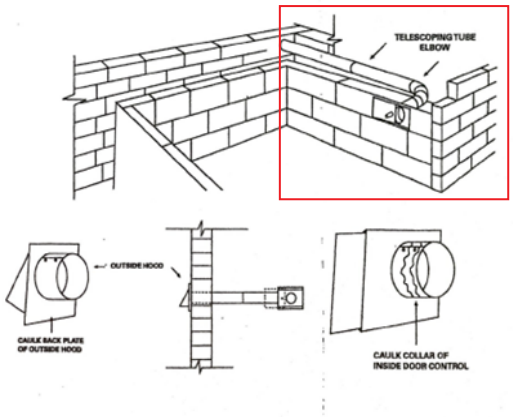

Figure 5
An annotated excerpt from the combustion air kit manufacturer's installation instructions. A steel telescoping horizontal hard duct (tube) is provided with the kit. Note the requirement that the make-up combustion air discharge into the firebox be installed "as far forward as possible and in the third course of firebrick." Note also the multiple instructions not to use combustibles in the construction of the ducting.

Figure 6
An image of an exemplar log lighter burner pan of the style installed in the incident fireplace. The orifice can be removed and a solid plug inserted for purposes of leak checking the gas piping system.

during operation of the gas log lighter. The first flash fire occurred some weeks before the incident in question. The most recent flash fire occurred a few minutes before the home ignited and burned.

On a Sunday evening (approximately 24 hours prior to the home igniting and burning) around 7:30 p.m., the homeowner followed his normal routine of building and maintaining a fire in the fireplace. At the time he and his wife retired to bed at approximately 10:30 p.m., only coals and ashes remained in the firebox. On the following Monday morning, the homeowner went to work, and his wife remained at home all day. The fireplace was not used during the day, and there were no smells of smoke or anything unusual that day. On Monday evening, the homeowner arrived home from work around 6 p.m. He also did not smell any smoke or anything unusual. The homeowner and his wife had dinner in the dining room, which was immediately adjacent to and open to the family room, with the fireplace in clear view. They neither smelled smoke nor observed anything unusual. At around 7:30 p.m., he proceeded to construct his routine fire in the fireplace, except the ashes had not been cleaned out of the fireplace from the Sunday night fire. Shortly after he turned the gas on to light the log lighter, a flash fire occurred, and the resultant overpressure was sufficient to blow ashes out of the firebox and into the family room. According to the homeowner, the flash fire occurred on the left-hand side of the firebox.

After the flash fire dissipated, he continued to allow the log lighter to burn beneath the logs and sat down in the family room to read the newspaper. Approximately 3 to 4 minutes after the flash fire occurred, his wife reported smelling smoke. He then observed smoke, followed shortly thereafter by a fire burning a hole through the front thin wood paneled wall covering of the chase just to the left of (and above) the fireplace. See the annotated pre-fire photograph of the incident unit in **Figure 7**.

Upon discovery of the fire, the homeowner went outside and grabbed a garden hose, pulled it into the home, and began applying water into the wall where he observed the fire. At that time, he also turned off the gas to the log lighter at the log lighter valve. His wife called 911. The fire department arrived and applied water from one of their trucks; however, it ran out of water before the fire was extinguished. There were no nearby fire hydrants and no equipment to pull water from the adjacent lake; therefore, shuttling operations were initiated. The fire spread throughout the concealed spaces/attic, destroying the home.

Following the fire, the insurance company for the homeowner placed the general contractor and several subcontractors on notice of the loss and pending investigation. Two joint scene exams were conducted, artifacts were collected and removed from the scene, and the insurance company for the homeowner ultimately filed a lawsuit against the general contractor and several subcontractors, particularly alleging that the rear chase wall framing clearance to the back of the firebox was improper and caused the fire.

At the time the author became involved in the case, the

Figure 7
Pre-fire photograph of incident fireplace unit. The circle indicates the area where the witness first observed fire burning through the wall.

physical scene was no longer available for examination, other experts had already issued a report and offered opinions, no laboratory examination or testing of the artifacts had been conducted, and basic discovery was still ongoing. The author was retained to perform an engineering investigation and analysis of the incident, including a review of the available investigative documentation, expert reports, expert opinions, and ongoing discovery materials to determine the origin and cause of the fire.

The referenced materials were reviewed, and the author also contemporaneously prepared questions for ongoing discovery depositions of both fact and expert witnesses to obtain additional information concerning the circumstances of the incident and the scene investigation. In addition, the author called for and participated in a laboratory examination of artifacts that were recovered during the scene investigation.

Forensic Engineering Investigation and Findings

Based on a review of the available information, the author concluded that it might have been possible that the framing studs of the rear chase wall were installed with clearances less than the required 1 inch. After researching the subject, no temperature testing data was located for the fireplace being installed and operated with clearances less than 1 inch to wood studs. The plaintiff's experts provided no testing data for tests that either they conducted (or others had conducted); they provided no mathematical modeling or other calculations to estimate the temperatures the wall studs would reach under the conditions the fireplace was actually installed and operated.

Given the relatively large mass of the masonry modular fireplace (the firebox and refractory are approximately 2,000 pounds) and the consistent small, short, and infrequent nature of the fires built in the fireplace by the owner, it seemed unlikely sufficient temperatures would be achieved to either: (1) initiate a direct smoldering fire in the wall studs; or (2) gradually thermally degrade the wood wall studs such that they would be susceptible to the initiation of a smoldering fire via self-heating. The latter (sometimes referred to as long-term low temperature ignition of wood[3,4,5] or LTLTI) was inferred by the plaintiffs prior to expert depositions and then opined in expert deposition testimony. However, since the wall studs were possibly installed with less than the permissible clearance — and no comparable research or testing data was available for the situation — the author determined that testing would be necessary. Additional testing by the author evaluated gas migration from the fireplace log lighter into the flexible combustion make-up air ducting and the burning propensity of the ducting. **Figures 8(a)** through **8(r)** depict exemplars of the fireplace, combustion air kit, and log lighter during construction and testing.

The exterior chase wall behind the fireplace was constructed with manufactured faux stone veneer. During the

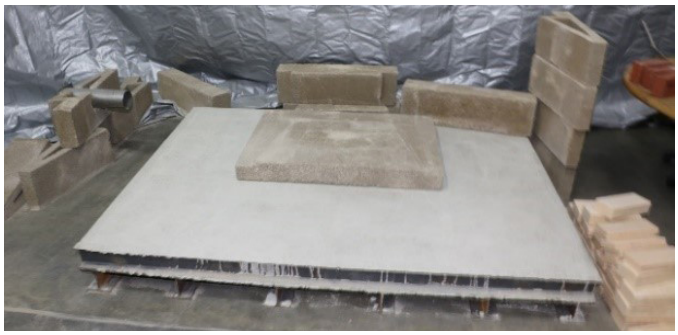

Figure 8a
"Portable" concrete floor assembly.

Figure 8b
Combustion air kit installation and through hole for gas line to log lighter.

Figure 8c
Positioning of log lighter and combustion air kits relative to hearth refractory.

Figure 8d
Firebox construction and wall lining refractory installation.

Figure 8e
Dry-fit hearth refractory and log lighter kit.
Combustion air kit ducting (circled).

Figure 8f
Constructed to match incident installation.
Combustion air kit discharge register door (circled)
near rear of the firebox and flush with the hearth.

Figure 8g
Smoke dome, damper, and masonry
chimney construction in progress.

Figure 8h
Chase walls, hearth extension, and surround construction.

Figure 8i
Chase walls, hearth extension, surround and mantel construction.

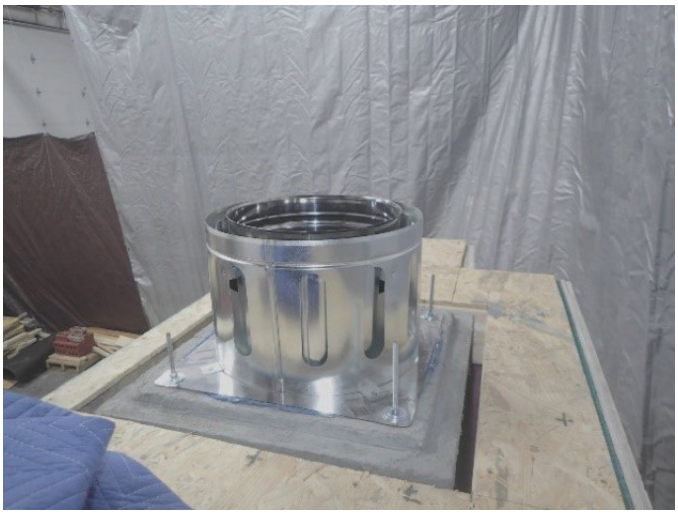

Figure 8j
Transition to metal chimney above the top of the chase enclosure.

Figure 8k
Completed exemplar construction and thermocouple instrumentation.

Figure 8l
Left side of chase with observation windows. Flexible ducting from combustion air kit routed vertically up to elevated exterior intake.

Figure 8m
Thermocouple instrumentation of lower rear chase wall studs. Note the inserted wood wedges to eliminate any clearances.

Figure 8n
Thermocouple instrumentation of upper rear chase wall studs. The smoke dome slopes away from the studs.

Figure 8o
Rear chase wall insulated.

Figure 8p
Rear chase wall covered.

Figure 8q
Log lighter test burn.

Figure 8r
Test burn view. All fires were built against the rear wall of the firebox.

fire incident, the upper portions of the wall, roof, and attic burned and collapsed. The collapse partially displaced the lower portion of the wall relative to the firebox. The fire scene investigators failed to document or even photograph the location of the exterior wall floor plate that was anchored to the slab relative to the back of the firebox. They also failed to document (in detail) the remains of the vertical wall studs behind the firebox (where they contend the fire originated). They failed to reconstruct (see NFPA 921[2] Sections 3.3.76 and 7.8.5.1) the wall and measure the actual clearances that would have been present pre-fire. Determining the location of the exterior wall floor plate (and documenting it) — and the repositioning of exemplar vertical wall studs — would have provided valuable reconstruction information regarding the actual pre-fire clearances between the back of the firebox and the wood studs.

Furthermore, reconstruction would have revealed that the studs could not have been in continuous direct contact with the back of the firebox without the wall being substantially out-of-plumb. During the laboratory assembly of the exemplar fireplace system and chase, it was discovered that the design of the firebox contained a projecting lip of approximately ¼ inch at the juncture between the firebox and the smoke dome installed on top of the firebox. The ¼-inch projecting lip prevented the erection of wood wall studs directly in continuous contact with the rear wall of the firebox without substantially placing the wall studs out of plumb. A plumb wall immediately adjacent to the firebox would have resulted in a minimum of a ¼-inch continuous gap clearance between the back of the firebox and the wood studs. Scene photographs were reviewed, and it was observed that the same (approximately ¼-inch) lip projection existed on the incident fireplace as the one constructed in the lab. Proper scene reconstruction would have identified the projection and corresponding necessary wall off-set. It is extremely unlikely that the wall of the multi-million-dollar home in question was ¾-inch out-of-plumb.

To be conservative, the wall studs in the lab were placed against the bottom of the firebox, creating a wall that was ¾ inches out of plumb and only contacting the firebox at the base plate and the ¼-inch lip. To be ultra conservative, wooden wedges (see **Figures 8 (m)** and **8 (n)**) were installed in the residual clearances between the studs and the back of the firebox where thermocouples were positioned.

The exemplar exterior rear chase wall was insulated with unfaced R-13 fiberglass batt insulation as postulated by the plaintiff experts. The incident exterior chase wall was most probably insulated; however, scene investigators failed to properly document the existence of any insulation in the wall. Their documentation failure resulted in a substantial amount of time-consuming fruitless discovery and deposition questions. The lower portion of the wall near the firebox was intact. Fiberglass batt insulation most often remains at the base of a wall on top of the horizontal floor plate; in this case, an area that was also not properly documented. Furthermore, such insulation acts very effectively to protect the floor plate from the fire.

The incident fireplace was installed immediately adjacent and to the left of another fireplace (patio fireplace). The incident chase was therefore open, except for a second chimney on the right-hand side. To be conservative, the exemplar right-hand chase wall was constructed with a double layer of cement board with fiberglass batt insulation sandwiched between from floor to ceiling. The purpose of the insulated full wall on the right-hand side was to reduce heat transfer through the wall and was conservative relative to the actual installation. A masonry chimney was constructed from the top of the smoke dome up to the top of the 9-foot chase. The top of the chase was capped with plywood leaving a 1-inch clearance gap around the chimney. The actual incident chase was larger in total volume and was open to the concealed attic cavity (overlapping roofs).

A detailed review of the scene investigation photographs provided indicated the remains of a steel wire coil still inside the chase footprint on the left-hand side of the fireplace. The steel wire coil remains resembled the coil remaining after flexible ductwork jacketing is burned away, as can be commonly observed, for example, on dryer vent ducts after a structural fire. No air intake register for the combustion air kit was observed on the remaining lower portion of the exterior wall behind the fireplace. The upper portion of the wall was destroyed. As a result, the author interviewed an additional witness and discovered that the intake register had been installed in the exterior wall near the soffit level approximately 12 feet above grade for aesthetic reasons. As such, the combustion air intake register for the combustion air kit was installed substantially elevated above the air discharge register located within the fireplace. The author's interview also revealed that a "fire-resistant" but combustible, flexible aluminized foil duct (the same type as that used on dryers and sold at local hardware stores) had been installed instead of the rigid metal ducting that came with the approved combustion air kit.

Based on the available specification sheets and purchase receipts used during the construction of the home, the author obtained an exemplar combustion air kit. The kit came with an air intake register, an air discharge register with a sliding door assembly, and a horizontal rigid steel telescoping duct section. In reviewing the installation manual as well as the scene photographs of the actual installation, two primary installation violations were noted as follows:

1. The manufacturer's instructions depicted in **Figure 5** required that only non-combustible materials be used in the construction of the combustion air duct work. The horizontal rigid steel ducting provided by the manufacturer had been replaced with a long vertical run of "fire-resistant" flexible aluminized foil ductwork.

2. The instructions also required that the discharge register be installed as far forward (near the fireplace opening face) as possible and in the third course of fire (refractory) brick (up from the hearth floor). The discharge register was actually installed close to the rear of the fireplace and flush with the hearth floor.

The instructions reference NFPA 211, *Standard for Chimneys, Fireplaces, Vents, and Solid Fuel-Burning Appliances*[6]. Provisions of NFPA 211 reflect the instruction requirements that the ducting be constructed of noncombustible materials. Furthermore, the improper installation of the combustion air kit violated the 2012 *International Residential Code*[7] (IRC), adopted at the time of the construction of the home. Regarding the location of the combustion air intake, the IRC provides, in part:

R1006.2 Exterior Intake

...The exterior air intake shall not be located ... nor shall the air intake be located at an elevation higher than the firebox ....

The *2012 IRC Code Commentary*[8] on this provision provides the following justification:

...The air intake must be lower than the firebox so that the firebox will properly draw in combustion air. Where combustion air openings are located inside the firebox, the air intake opening on the outside of the dwelling cannot be located higher than the firebox. Such an installation could create a chimney effect, drawing the products of combustion up through the combustion air ducts. These ducts are not generally constructed of materials which can withstand the heat and sparks that could be drawn through them....

For the case in question, the installation configuration did in fact result in the *IRC Code Commentary* described chimney effect within the combustion air ducting in every laboratory test performed regardless of the position of the sliding door on the air discharge register located in the fireplace (there is no seal on the loosely fitting discharge register door).

Fire scene investigators failed to collect the remnants of the steel wire ducting coil or the intake and discharge registers. The steel wire ducting coil remains could have been measured and the length of the flexible ducting determined. A measurement of the length of the flexible ducting that was used could have provided information as to how much of the ducting was coiled inside the bottom of the chase, which, in turn, would provide fuel loading information. The flexible ducting came in 10-foot and 20-foot lengths. Therefore, either all of a 20-foot section was used, or it was cut to some length. In addition, fragments of jacketing remaining on the wire coiling could have been analyzed to determine and verify the type of material (including polymeric materials) and the burning properties of the material.

Laboratory testing of the fireplace assembly and individual testing of the flexible ducting indicated that conducted heat, hot gases, sparks, or momentary flames impinging on the polymeric lining material cause melting, degradation, and delamination (separation, shrinkage and curling of the polymer material) from the aluminized jacket. As the polymer lining melts, degrades, separates, and curls, it would increase the exposed surface area (both sides of the curled and degraded polymer material) that would be subject to the next insult and subsequently increase the potential for sustained ignition and continuous burning.

In addition, the scene investigators failed to consider all reasonable fire cause scenarios involving an improper installation. For example, one plausible fire-cause scenario could be a flash fire initiating in the firebox that then propagates into the improperly installed combustible flexible ducting — igniting the ducting. A second plausible fire-cause scenario could involve the migration of gas into the ducting (due to delayed ignition of the log lighter) that

is subsequently ignited and, in turn, ignites the ducting. A third potential fire scenario could involve flames or hot gases from the fire inside the firebox rolling off the bottom of logs, entering the discharge register, and flowing up the vertical run of ducting (chimney effect). Laboratory testing of the incident configuration resulted in flame deflection off the bottom of the logs directly into the opening of the combustion air discharge register. Finally, the flush position of the door opening with the hearth would allow ash, embers, and incompletely burned firewood residual to fall into, or be inadvertently swept (during cleaning) into, the opening, creating a fuel load inside the ducting. Therefore, the combustion air discharge register opening would function as an ash pit.

The wall studs of the chase and combustion air ducting were instrumented as depicted in **Figure 8(m), Figure 8(n), Figure 9** and **Figure 10**. A Keysight Technologies model 34980A Multifunction Switch/Measure Unit data logger[9] was utilized to record temperatures at 1-minute intervals for each thermocouple throughout the duration of each test, including cool down periods after the fire burned completely out. The laboratory ambient temperature was also recorded. Igor Pro 8 scientific graphic and data analysis software by WaveMetrics[10] was used to generate temperature time curves for all thermocouples and for each test. The software can be set up to filter out data curves

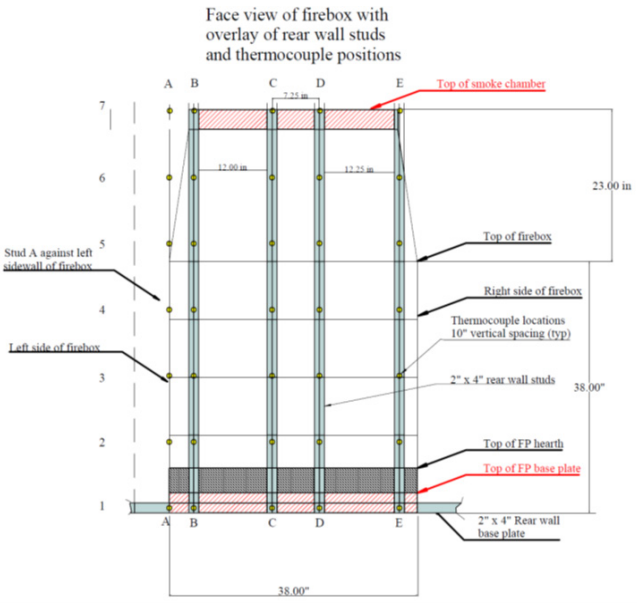

Figure 9
Thermocouple locations on the rear chase wall and interior left side jog wall extension stud. The view is from the front of the firebox looking at the studs behind the firebox. The horizontal lines represent the joints in the masonry firebox and smoke dome construction.

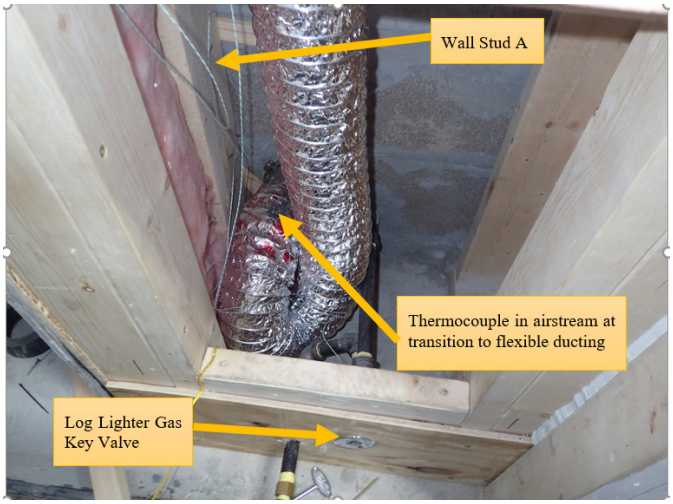

Figure 10
A view into the chase cavity on the left-hand side of the firebox. The rear wall jogged or recessed inward into the chase on the left-hand side. The wall stud, identified as "A," also in **Figure 9**, was placed in direct contact with the firebox and wood wedges inserted in the gaps where thermocouples were located.

below a specified set temperature. For example, any thermocouples with maximum temperatures below 150°F can be automatically filtered out of the displayed curves reducing busyness and improving clarity of the graphs. After initially setting up the program for the first test, the software automatically generates time temperature curves for each subsequent test based on the filters set. Thermal imaging was also performed periodically to depict the overall chase temperatures as well as the combustion air intake register temperatures.

Propane fuel-gas was provided to the home via a two-staged regulator system from a 1,000-gallon underground tank. Gas supply pressure into the home was 11-inches water column. Prior to the laboratory evidence examination, the author procured two exemplar log lighters. The log lighters used a rectangular flush pan-style and cap designed to be recessed and embedded in the hearth refractory. A brass elbow, which screwed into the base of a rectangular steel log lighter pan, contained internal threads into which a steel plug with a number 30 drilled orifice (0.1285-inch diameter opening) was screwed. The exemplar log lighters came from the manufacturer with the steel plug orifices already installed. At 11-inches water column, a number 30 orifice delivers 115,343 Btu/hr.

The plug orifice had been removed from the incident log lighter, likely for leak testing the gas system piping during original construction. The plug orifice, however, was not reinstalled in the incident log lighter (leaving a

0.6670-inch diameter opening). As such, there was no gas flow limiting orifice in the log lighter, creating conditions favorable for large amounts of gas to be released in a short period of time (dependent upon the exact position of the log lighter key valve). See **Figures 11(a)** and **11(b)**, which depict the incident log lighter and the orifice installed in an exemplar log lighter.

As will be discussed later in the paper, ash migration into the perimeter cap openings of the log lighter results in blockage of gas discharge ports and subsequently asymmetric discharge of gas out of the log lighter and therefore an increased likelihood of delayed ignition and a flash fire. So, in addition to the potential for over-firing the fireplace (no orifice), conditions are also favorable for a delayed ignition of gas producing a substantial flash fire and potentially an explosion.

Both the combustion air discharge register and gas log lighter are flush with the hearth and approximately 8 inches apart (see **Figure 8(f)** again); therefore, the potential for propane gas migration into the discharge register is substantial. While the position of the register door at the time of the incident is not clear, the loose-fitting door is not hermetically sealed, and gas will migrate through the door into the ducting (as verified by laboratory testing) when it is either fully closed or fully open or at any position between. Obviously, the more open the door is, the higher the propensity for gas or flames to enter.

Figure 11a
Incident log lighter with no orifice (0.6670-inch opening).

Figure 11b
Exemplar log lighter brass elbow connection
with number 30 (0.1285-inch opening) steel plug orifice.

There were ashes in the base of the firebox from the Sunday evening fire and likely previous fires. The author made several observations concerning ashes and gas log lighters based on studies made in this case as well as studies and testing made in a similar separate case.

1. Ash completely covers the log lighter after a short period of time of operation. One fire in the fireplace will result in the log lighter in this case becoming completely covered.

2. Ash tends to enter and block off portions around the perimeter of the pan style log lighter cap plate where gas would otherwise normally escape and then burn. As a result of this blockage, sometimes no gas discharges around large sections of the perimeter top cap plate while the unblocked portions of the cap plate discharge the full amount of gas (asymmetric discharge of propane gas). See **Figure 8(q)** for symmetric discharge and burning of gas from the log lighter.

3. As an example, no gas may be discharged on the right-hand side of the log lighter (fully blocked) top cap plate gas discharge ports. Therefore, all the gas is discharged on the left-hand side of the top cap plate discharge ports (unblocked). If a piece of paper is lit and placed under the logs on the right-hand side — and the gas is then turned on — there is a delayed ignition resulting in a large flash fire in the firebox. In other words, until the gas discharging on the left-hand side of the firebox migrates and reaches the right-hand side (where the ignition source is), it will accumulate on the left-hand side and inside the immediately adjacent combustion air ducting. Once the gas reaches the ignition source, a substantial flash fire results. See **Figures 12(a)** through **12(j)**, on pages 44 to 45, depicting such a scenario generated during laboratory testing in this case. **Figure 12(c)**

Figure 12a
Ignition of paper on the right-hand side of the fire box. Gas is off.

Figure 12b
After paper ignition gas is ready to be turned on.

Figure 12c
Ash cloud forms on the left-hand side when the gas valve is opened. Note proximity to the register door.

Figure 12d
Flash fire ignites on the right-hand-side and propagates rapidly to the left beneath the firewood.

Figure 12e
Continued flash fire propagation right to left toward register door. Door, circled, partially open.

Figure 12f
Flash fire impingement on the left-hand side of the firebox and door when accumulated gas is ignited.

Figure 12g
Gas accumulated on the left-hand side of the firebox continues burning.

Figure 12h
Asymmetric flames from the log lighter and horizontal deflection to the left side of the firebox and onto the register door. Near flash fire end.

Figure 12i
After the flash fire, flames from the discharging gas impinge on the logs above and toward the left-hand side of the firebox and onto/into the combustion air discharge register door and doorway.

Figure 12j
Ash cleaned out of the log lighter ports to create a more even distribution of gas and flames.

depicts the relatively close proximity of the gas discharging and accumulating at the combustion air kit discharge register prior to being ignited.

3. Ash blockage of the log lighter top cap plate discharge ports can also result in a substantially larger continuous flame on one side of the firebox. Since logs are placed over the log lighter, the natural result is that the large one-sided flame will be substantially deflected horizontally. And in the incident case, the combustion air kit discharge register door is located also below the logs (flush with the hearth and the inlet of the doorway) and is subjected to substantial flame impingement or intrusion when flames are deflected. It should be noted that even without ash blockage, horizontal flame deflection onto and into the doorway occurs because the doorway was not located in accordance with the installation instructions. The condition is exacerbated when ash blockage of the log lighter cap plate occurs.

4. The ash/ember/wood residual cover (depending on the depth, density, and degree of blockage of the log lighter) can facilitate the lateral spread of gas beneath the ash and into the ductwork (similar to the lateral movement of gas in an underground gas leak). The horizontal blockage of the firewood on the grate above also facilitates gas migration toward the combustion air discharge register door.

5. Ash may also form uneven contours as it falls onto the hearth during the operation of the fireplace. As a result, the ash can form "dams" or "trenches" on the hearth that functions to facilitate the lateral spread of "pooling" propane into the combustion air kit discharge register doorway and therefore into the ducting prior to ignition.

For case testing purposes, more than 30 test fires within the exemplar fireplace system were conducted. The fireplace grate was positioned directly against the rear wall of the firebox for all tests to maximize heat and flame impingement on the back wall of the firebox. The combustion air kit inlet door of the firebox was positioned in multiple positions: closed, various states of partial opening, fully open, open/closed during the same test, etc. Although the homeowner indicated he only used oak firewood, well-seasoned (more than 18 months) oak and hickory firewood were utilized in the laboratory testing. In general, hickory is a slightly better firewood[11] than oak (having a greater density and heating value).

Exemplars of the flexible ducting used in the installation of the combustion air kit were obtained, and a simple burn test was performed to evaluate the propensity of the material to burn. A fuel load consisting of a single sheet of loosely balled-up (fist-size) craft paper (approximately 12 inches by 12 inches) was placed into the inlet of the ductwork and ignited via a match. In a horizontal position, the flexible ductwork was resistant to ignition — and did not sustain burning and flame propagation. After the paper was consumed, the fire self-extinguished.

As might be anticipated, the burning characteristics were different in the vertical orientation. A 7- to 8-foot section of ductwork was suspended in a vertical orientation, and the paper fuel load was placed in the base of the ductwork and ignited via match. In the vertical orientation, the flexible ducting easily ignites, burns readily, and propagates flame rapidly. See **Figures 13(a)** through **13(f)**, on page 46, depicting some of the burn testing. Several types of available "fire-resistant" flexible ducting were tested with the same results.

The "fire-resistant" ducting is clearly combustible and will easily sustain burning. In the incident case, the ducting was installed in a vertical orientation in the chase on

the left-hand side of the firebox. The soffit where the ducting terminated is 12 feet above the finished floor. As noted earlier, the ductwork comes packaged in 10- or 20-foot sections. Therefore, a 10-foot section would be too short for the installation in question (requiring a 20-foot section be used). Depending on how much (if any) of the 20-foot section the installer cut off would determine how much of the ducting was coiled up at the base of the chase and what fuel load it represented.

As depicted in **Figures 13(a)** through **13(f)**, very little of the ducting was coiled up at the base in the laboratory exemplar testing; however, sustained burning continues even after the vertical section is consumed, drips, melts and falls to the base. The front interior chase wall from the floor to the ceiling was constructed with thin wood paneling nailed to studs installed in a vertical orientation. The thin wood paneling would be in proximity to (inches from, or directly in contact with) the flexible ducting and would likely be readily ignited by the burning ducting.

During laboratory testing of the full exemplar assembly, elevated air temperatures (briefly exceeding 450°F) inside the flexible ductwork were produced during an

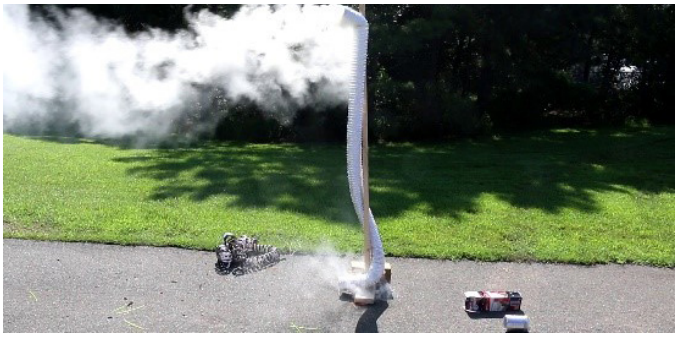

Figure 13a
Immediately after ignition of balled paper in the base.

Figure 13b
Seconds after ignition of balled paper in the base flames burn through and spread rapidly upward.

Figure 13c
Rapid upward flame spread.

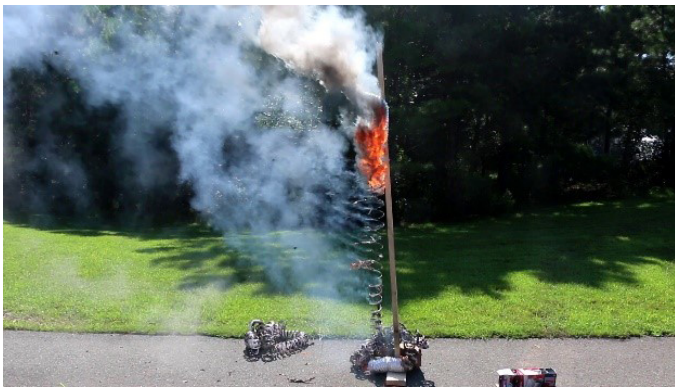

Figure 13d
Rapid upward flame spread.

Figure 13e
Sustained burning at the base.

Figure 13f
Sustained burning at the base.

intentionally generated flash fire event (**Figures 12(a)** through **12(k)**). The elevated temperatures caused concern for potentially igniting the ductwork and the chase assembly in the lab due to flame deflection off the firewood, sparks migrating, and the general chimney effect. Therefore, careful monitoring of the hearth area around the air discharge register was implemented during further testing to intentionally prevent accidental ignition (e.g. coals and ashes were moved, firewood was shifted, etc., to prevent constant exposure to the door and doorway of the discharge register). A dimensional mockup assembly of the firebox, log lighter, and combustion air discharge register was constructed with cement board bounds to observe the effects of gas migration and flash fires generated in the firebox.

For safety reasons, the exemplar log lighter was equipped with the manufacturer's number 30 orifice, and the gas supply was controlled via a flow meter and regulator assembly connected to a 20-pound propane cylinder also equipped with an excess flow valve. Safety candles were positioned in proximity around the assembly and lit to limit the maximum amount of propane that could potentially accumulate prior to ignition. A combustible gas detector was also used to determine the extent of gas migration, particularly into the rigid metal duct stub out. Various positions of the combustion air discharge register door were tested. Flash fires were ignited that propagated into and through the rigid ductwork stub when the door was as little as ½-inch in the open position. Gas migrated through the door in all cases, even in the fully closed position. Removing the orifice and increasing the gas flow into the log lighter would increase gas migration and accumulation prior to ignition. Variations in ash configuration, contouring, damming, and blockages in the ports of the log lighter would likely further enhance gas migration and accumulation prior to ignition.

Figures 14(a) through **14(l)** depict a flash fire generated when gases, ignited on the right-hand side of the fire box, propagated to the left-hand side and then through and out of the rigid steel ducting stub where the flexible ducting would have been attached. Note that the gas flame plume continues to burn [**Figure 14(l)**] after the flash fire subsides on the right-hand side of the firebox due to the blocked ports of the log lighter.

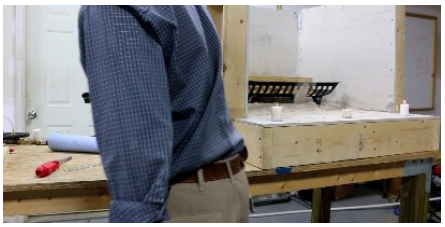

Figure 14a
Test video 6 image capture.

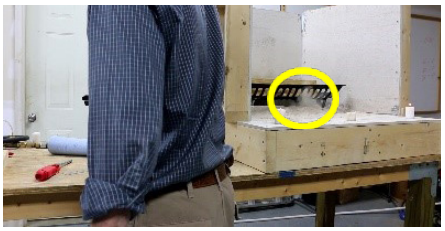

Figure 14b
Ash cloud produced
when gas valve turned on.

Figure 14c
Flash fire initiated at
right-hand side safety candle.

Figure 14d
Flash fire propagates into the firebox.

Figure 14e
Flash fire propagation into the firebox.

Figure 14f
Flash fire propagation right to left.

Figure 14g
Flash fire propagation right to left.

Figure 14h
Pressure wave ahead of the flame front
distorts the candle flame (circled).

Figure 14i
Flash fire propagation through
and out rigid duct work.

Figure 14j
Flash fire continuing out rigid duct work where flexible ducting would be connected.

Figure 14k
Burning continues on the right-hand side after flash fire nears completion.

Figure 14l
Asymmetric burning on the right-hand side continues due to blocked log lighter ports.

Figure 15a
Test video 15 image capture.
Flash fire ignition.

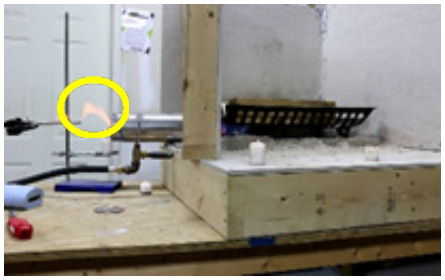

Figure 15b
Flash fire ignition.

Figure 15c
Propagation through ductwork and into the firebox (left to right).

Figures 15(a) through **15(c)** depict an initiating flash fire generated when "trenched" ashes allowed gas to migrate into the rigid ducting and reach the lower flammability limit (LFL) at the point the flexible ducting would have been connected. The combustion air discharge register door was open only approximately ½ inch.

Analysis and Discussion

For all tests performed in the exemplar fireplace and chase system, the weight, diameter, length, and moisture content of each piece of wood was measured, recorded, and tabulated. **Figure 16** provides the data for laboratory test number 4, which was the largest mass of wood burned during a single test (46.7 pounds).

The owner burned (at most) five logs total during each fireplace use measuring 3 inches in diameter and (at most) 21 inches long. Therefore, the maximum cumulative length of wood he burned was 105 inches. Since many normal pieces of firewood are shorter than 21 inches in length, more than five total pieces of wood were burned in some tests to attain a cumulative length closer to 105 inches. In all cases, the minimum diameter of the wood exceeded 3 inches, many times exceeded greater than 3½ inches — and in some cases, were much greater than 3½ inches. Considering five pieces of wood (each 21 inches long and approximately 3 inches minimum in diameter), a baseline test (test number 6) was performed by the author to establish the closest approximation for the incident fireplace use conditions. The baseline test was also used to establish the minimal amount of wood (31.8 pounds) to burn for all subsequent testing. The data for test number 6 is depicted in **Figure 17**. Note that the amount of wood used in test number 4 was approximately 150% of the mass of the amount of wood used in test number 6.

Log Number	Length (inches)	Diameter (inches)	Moisture Content (%)	Weight (lbm)
1	19	> 3.5	11.3	12.7
2	21	> 3.5	11.0	9.8
3	22.75	> 3.5	11.2	9.4
4	21.5	> 3.5	11.6	7.4
5	19	> 3.5	11.5	7.4
Total	**103.25**			**46.7**

Figure 16
Wood burned during laboratory test number 4.
Largest amount burned during a single test.

The moisture content for all firewood in all tests was substantially uniform (approximately 10% to 12%). Therefore, as expected, the total weight of wood burned for each test fire was the driving factor for temperatures achieved in the firebox walls. **Figures 18** and **19** depict the time-temperature curves for tests 4 and 6, respectively.

The maximum temperature reached during test 4 on the exterior wall of the firebox in contact with the wood was approximately 193°F, occurring 6 hours after the initiation of the test. The software was set to depict the graphs of all thermocouple points that exceeded 150°F. Temperatures briefly exceeded 450°F in the combustion air ducting during the flash fire illustrated in **Figure 12**; however, the temperature point was removed to maintain graph scale and clarity. For the most part, flames and embers were intentionally kept away from the combustion air door, but occasionally burning wood fell near the door and temperatures in the duct work elevated.

The combustion air door was opened further in test 6 and resulted in substantial temperature fluctuations in the ducting throughout the firewood burning, depending on where hot coals, or burning wood landed as they fell. In most cases, the test attendee tried to keep coals, sparks, and flames from becoming diverted into the duct opening or onto the door to prevent accidental ignition of the flexible ducting. Care was also taken not to inadvertently sweep ashes and unburned charred pieces of wood into the doorway when the fireplace was cleaned out, although such occurrences would be realistic. Maximum observed temperatures in the exterior firebox wall in contact with the wood studs remained below 160°F throughout the test. The temperatures of test 6 most likely conservatively reflect the temperatures experienced during the actual use conditions of the fireplace. Air temperatures in the flexible ducting were substantially higher than those of the exterior wall of the firebox.

During all laboratory tests, the combustion air ducting operated in reverse, allowing hot gases to flow into the ducting. Substantially elevated temperatures within the ducting occurred: (1) during a generated flash fire event; (2) during normal operation of the fireplace when hot embers dropped and piled against the doorway when the door was closed or in the doorway when it was open; or (3) when flames rolled off of the bottom of the logs and onto the door (when closed) or into the doorway (when open).

The incident fireplace was only utilized once or twice a week. During testing, it was observed that 24 hours after the initiation of the fire that the masonry firebox mass (exterior wall) was still at approximately 105°F to 110°F.

Log Number	Length (inches)	Diameter (inches)	Moisture Content (%)	Weight (lbm)
1	17.5	> 3.0	10.9	5.2
2	18	> 3.0	10.6	5.0
3	18.5	> 3.0	11.5	6.1
4	18	> 3.0	11.3	5.2
5	17.5	> 3.0	9.0	3.8
6	20.375	> 3.0	10.9	6.5
Total	**109.875**			**31.8**

Figure 17
Wood burned during laboratory test number 6.
Smallest amount burned during a single test.

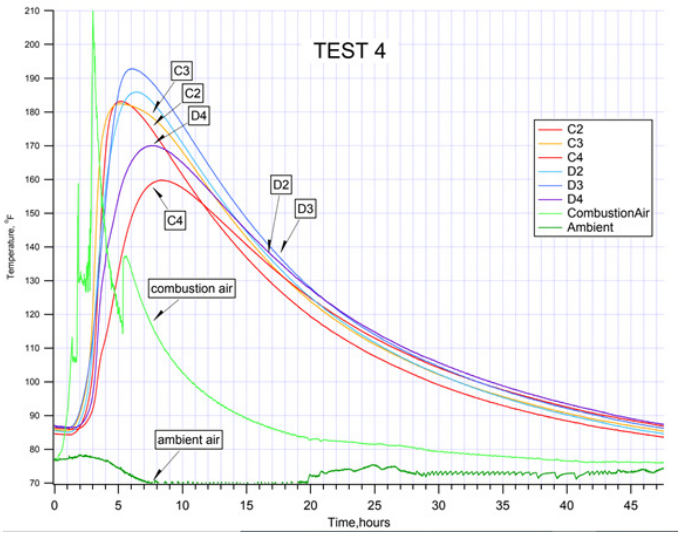

Figure 18
Time-temperature curves for test 4. The combustion air duct door was partially open during the testing.

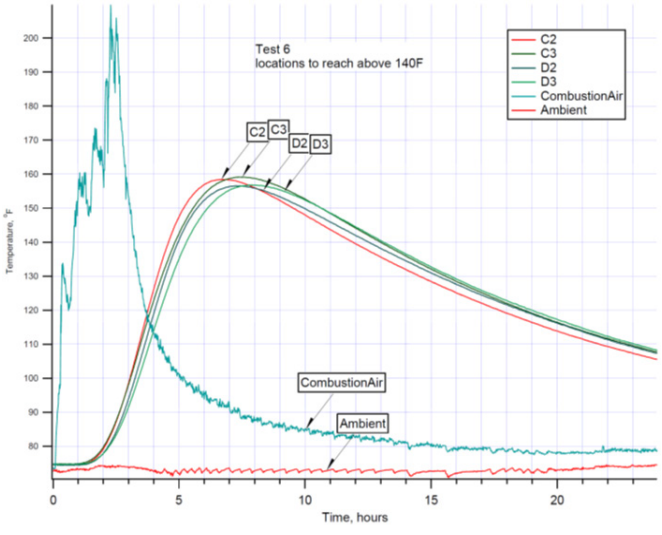

Figure 19
Time-temperature curves for test 6, baseline test most approximating use conditions of the fireplace. The combustion air duct door was partially open during testing. Maximum temperatures of the firebox wall remained below 160°F.

Therefore, to develop conservative results, multiple series of tests were run "back-to-back" (i.e., assuming a fire of similar size and duration was burned in the fireplace consecutively every 24 hours) — sometimes two to three days in a row. **Figure 20** depicts testing results from one set of back-to-back testing over a three-day period. Even with the back-to-back testing, maximum temperatures did not exceed 222°F. In these tests, it was observed that the heat transfer to other portions within the large masonry fireplace mass begin to increase (i.e., more thermocouple points begin to appear on the graphs) as the heat is more uniformly distributed within the firebox masonry.

Figure 21 provides the summary data for the wood burned in the consecutive testing depicted in **Figure 20**.

After a total of 32 burn tests were performed, the rear chase wall was opened, and the wood studs and wood wedges examined. There was no discoloration of the studs or wedges, no charring, no cracking or other detectable physical changes to the wood.

As previously noted, the firebox and refractory are of substantial masonry mass (approximately 2,000 pounds), and, as such, would have a large thermal capacity available. Small fires of relatively short duration combined with the large thermal capacity of the firebox and refractory, the normal expected system heat losses to the environment, and relatively new condition of the unit brings into question the likelihood of sufficient heat transfer occurring into the studs to either significantly thermally deteriorate them or otherwise directly ignite them. The observed temperatures and exposure times were insufficient to generate any substantial or even detectable thermal degradation of the wood leading to LTLTI much less direct smoldering ignition. As noted in *Kirk's Fire Investigation*[4], 8th Edition page 260 [underlined emphasis added]:

> *...the investigator must be careful of blaming "pyrophoric carbon" for any fire in the vicinity of a flue or hot water pipe merely because no other cause can be identified....*
>
> *...The time has to be long enough (weeks, months, or years, depending on the intensity of the applied heat); .....*
>
> *...Because of the time required for the production of charcoal, low-temperature ignition of wood can generally be eliminated as a cause of fires in very new buildings.*

The maximum exposure temperatures achieved during testing for the extreme conditions considered in the subject case were 222°F. The baseline testing temperatures did not exceed 160°F. While temperatures during some of the testing did exceed the Underwriter's Laboratories (UL) 127[4,12] threshold of approximately 170°F for relatively short periods of time, both the temperature and exposure times (including cumulative times) were comparatively substantially small when considering LTLTI. For example, empirical data from well documented restaurant fires combined with engineering laboratory testing and analysis of those fires provides[3]:

> *.... it was concluded for the conditions studied that ignition of wood occurred under exposure temperatures of as low as 256 °F when exposed to 12 to 16 hours per day in as little as 623 days or approximately 21 months....*

In other words, it took nearly two years of daily temperatures of 256°F or greater with exposure times of 12 to

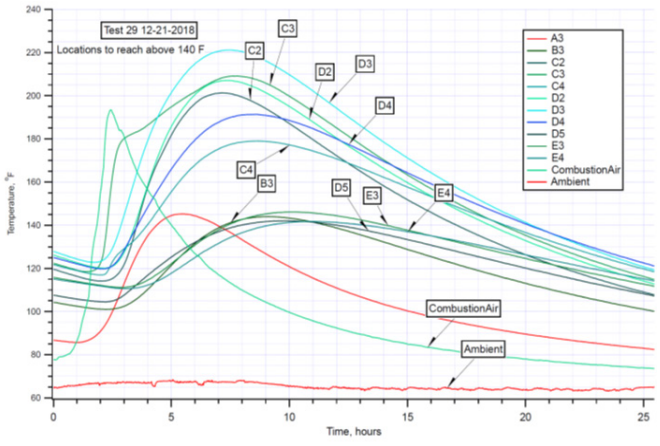

Figure 20
Results of back-to-back testing over three consecutive days. Note that the incident fireplace was only used once or twice each week (the home had five other fireplaces).

Test Number	Total Wood Burned (lbm)	Total Length (inches)
27	36.10	108
28	36.80	106.25
29	41.80	123.25

Figure 21
Summary data for wood burned in consecutive testing depicted in **Figure 20**.

16 hours per day to initiate an LTLTI fire in the wood studs. In addition, for the referenced study, there were metal fasteners exposed to a heat source that penetrated the wood. There were no such fasteners in the present case. Finally, the temperatures achieved in the present case are substantially insufficient to cause direct smoldering ignition.

Following is a summary of opinions that were offered by the author along with the supportive testing and research data summarized in this paper. The forensic engineering analysis facilitated the mediation of the case.

1. The origin of the fire was inside the base of the flexible combustion air ducting on the left-hand side of the firebox, not in the wood studs of the chase framing behind the firebox.

2. The flexible combustion air ducting was combustible and in a vertical orientation ignites, burns readily, and propagates flames rapidly.

3. The combustible flexible ducting installation violated the manufacturer's installation instructions, the *International Residential Code* (IRC) and NFPA 211.

4. Hot gases, sparks, ash, embers, and/or flames flowing via a chimney effect from the fire inside the firebox into the flexible ducting during normal operation of the fireplace would act to melt, thermally degrade, and delaminate the plastic polymer lining inside the ducting making it susceptible to ignition during further insult.

5. The flush mounted discharge register door opening of the combustion air ducting was only inches from the propane gas log lighter and subject to gas migrating and accumulation inside the ducting during delayed ignition incidents. Contoured ash accumulations and ash blockage of the log lighter ports would facilitate gas migration and asymmetric burning inside the fireplace.

6. The missing stainless-steel plug orifice created conditions favorable for quick relatively large releases of propane gas increasing the likelihood of gas migration and flash fires or explosions during delayed ignitions.

7. The most likely source of ignition of the thermally degraded combustible flexible ducting was heat from the flash fire or heat from flames diverted horizontally into the ducting due to blocked log lighter ports.

8. The most likely cause of the fire was the improper material selection and installation of the combustion air kit and combustible flexible ductwork.

9. Assuming there was zero clearance between the stud wall and back of the firebox (which is unlikely) there was insufficient time and temperature exposure to the wood stud walls to generate a smoldering fire either via direct ignition or self-heating via LTLTI.

10. Wood wall studs installed less than the specified clearances of the manufacturer do however present a fire hazard via smoldering ignition or LTLTI under the right conditions.

Conclusions

Determining the correct cause of a fire and contributing factors to the cause of the fire is critical to the prevention of future fires. To that end, investigators and forensic engineers must employ proper procedures and reliable methodologies in their analysis. If no, or insufficient, research and testing data exists for the scenario being considered, engineering testing or modeling should be performed to fully evaluate the scenario. One of the purposes of publishing this paper is to make some such testing data readily available for use in the fire investigative and forensic engineering industry.

In this paper forensic engineering research, testing, and analysis were implemented to evaluate the true cause of the fire. The presence of a possible or real fire code violation (e.g., clearances to combustibles) should not be automatically assumed to be the cause of the fire without complete and proper analysis. The conditions under which systems (e.g., fireplaces) are used and operated are important to understand as part of the analysis. In addition, the identification and comprehensive evaluation of all fire code violations and installation errors are critical to performing a competent investigation that will allow an accurate determination of the cause of the fire.

References:

1. Hearth Fireplace Specialist Training Manual, Hearth Education Foundation Arlington, VA, USA, 2000.

2. Guide for Fire and Explosion Investigations, NFPA 921, 2017.

3. J. Tindal and J. Warren, “Forensic engineering analysis of low temperature ignition of wood,” Journal of the National Academy of Forensic Engineers, vol. 26 no. 1, pp. 85-103, June 2009.

4. D.J. Icove and G.A. Haynes, Kirk’s Fire Investigation, 8th ed. New York, NY, USA: Pearson, 2018.

5. C. Lautenberg, S. Sexton, and D. Rich, “Understanding long term low temperature ignition of wood,” in 7th Proc. of the International Symposium on Fire Investigation Science and Technology, Hyattsville, MD, USA, 2014 pp. 361-373.

6. Standard for Chimneys, Fireplaces, Vents, and Solid Fuel-Burning Appliances, NFPA 211, 2013.

7. International Residential Code, ICC, Country Club Hills, IL, 2012.

8. International Residential Code Commentary, ICC, Country Club Hills, IL, 2012.

9. Keysight 34980A Multifunction Switch/Measure Unit Mainframe User’s Guide, Keysight Technologies, Penang, Malaysia, 2019.

10. Igor Pro 8 Scientific Graphic and Data Analysis. (2018). WaveMetrics. Accessed May 4, 2021. [Online]. Available:https://www.wavemetrics.com/products/igorpro.

11. D. Marcouiller, and S. Anderson, “Firewood: How to obtain, measure, season and burn,” Oklahoma Cooperative Extension Service Fact Sheet F-9440. [Online]. Available: https://tinyurl.com/y2dpow5g. Accessed 10/28/2019.

12. Standard for Factory-Built Fireplaces Northbrook, IL: Underwriters Laboratories; 2015.

Forensic Issues that Arise from Recirculating Hot Water Systems

By Stephen R. Jenkins, CPEng (NAFE 11)

Abstract

There has been a significant increase in the failure of pipes used for recirculating hot water systems installed in hospitals, apartment blocks, and hotels in recent years. The rise has occurred as these systems have increased in popularity, and thermostatic mixing valves have made the higher operating temperatures in recirculating systems safe. A common theme tends to be the continuous flow of water above 65°C (150°F) at velocities that have been found acceptable for non-continuous flow. Failures have been experienced in pipes made from both copper and polypropylene random copolymer. Explanations have been slow to emerge and are still subject to debate, particularly as to the initiating causes of pin-hole corrosion (one of the more common modes of failure). Since it is not possible to view the initiation of the pin hole, proof of the cause of the initiation is still unknown. There are indications from consistent correlations between operating conditions and the onset of pin-holing corrosion that are used by authorities as the basis of modifications to design and installation standards to minimize occurrence. This paper will cover some of the background, myths, and current thinking on the causes of the problem in both copper and polypropylene from the point of view of a forensic engineer trying to make sense of uncertain science and the complications of a problem that is trans-disciplinary in nature.

Keywords

Recirculating hot water, pin-hole corrosion, erosion corrosion, installation faults, polypropylene cracking, copper pipes, forensic engineering

Introduction

The widespread use of copper pipes began in the mid-1800s — formed from copper sheets with longitudinal lap joints and screw thread connections. Around 1900, pipes began to be drawn or extruded but were still either joined by fine screw threads or push fit joints, incorporating O-ring seals. In 1936, the first British standard was published, allowing capillary brazing for joints[1]. Since then, the use of copper pipes has been normal practice and is covered by a range of engineering standards.

Copper piping has long been the favored material selection for plumbing systems for domestic water, having been used for water piping successfully from the days of early civilizations to the present day. Copper pipes to drain water from the ceremonial areas in the pyramids of Abusir around 2750 BC in Egypt were discovered by archeologists in 1994 (these were still functional). Copper began to be used as a roofing and water proofing material in around 650 BC. Copper pipes have been in regular use in the Western world for more than 100 years as evidenced by standards for manufacture and use[1,2,3].

However, copper has not been without occasional problems — generally appearing as accelerated corrosion, resulting in leaks or blue water staining on sanitary fittings. These problems have tended to arise in concentrated areas, or, at particular times, followed by research on the problem that has identified and generally resolved the immediate problem — often without finding more general solutions or the actual root cause. For example, an area of a community may experience an outbreak of pin-hole corrosion, which (after investigation) is found to be related in time to the introduction of a water softening system with an associated change in the chemical ions present in the water, but the mechanism of failure may not be clear[4].

In parallel with the use of copper, alternative piping systems based on plastics have developed and generally been successful for cold water applications. The extension

Stephen Jenkins, CPEng, P.O. Box 1591, Wellington, New Zealand, 6140, +64 21 325998, stephen.jenkins@aurecongroup.com

of service conditions for plastic piping into hot water systems have often not been successful with some systems having a short commercial life before being withdrawn (author's observation).

With the rise of reliable and economic point-of-use thermostatic mixing valves, recirculating hot water systems have become popular in large facilities (such as large hospitals or apartment blocks) where peak usage patterns and the length of the reticulation system make the use of higher temperatures a practical engineering solution to maintaining satisfactory water temperatures for users as well as microbiological hygiene, in some instances. In parallel with the growth of this engineering solution, there has been a significant increase in pin-hole corrosion in copper pipes and unexpected failures in random polypropylene random copolymer used in hot water recirculating systems[5].

Most hot water used for personal hygiene (e.g., showers and basins) is used at between 38°C and 43°C (100 to 110°F). Tests by the author indicate users prefer the lower end of this range. To reduce storage volumes, it is held at higher temperatures and reticulated generally in the 60°C to 65°C (140 to150°F) range. This is also the temperature where legionella cannot colonize the water reticulation — just below the temperature copper is prone to develop failures. Unfortunately, where high peak demand occurs, a simple solution is to raise the water storage temperature. In the author's experience, temperatures of 75°C to 80°C (167 to 176°F) are not unknown in hotels and other buildings with high peak demands.

This paper is based on the author's experience in trying to understand the reasons for persistent pin-holing. The investigation included the collection of data and examination of samples from a large building over the course of five years — where he was leading a team of experts, metallurgists, and tradespersons.

The Use of Copper

Copper is a soft and reasonably reactive material. When used in water reticulation systems, it typically develops a protective coating either through the formation of copper oxide or copper carbonate films or a layer of minerals precipitated from the water being carried by the pipe. In essence, the copper becomes the mechanical support for a contact surface that is not metallic copper (**Figure 1**).

This both protects the copper and preserves the chemical quality of the water. However, there are circumstances

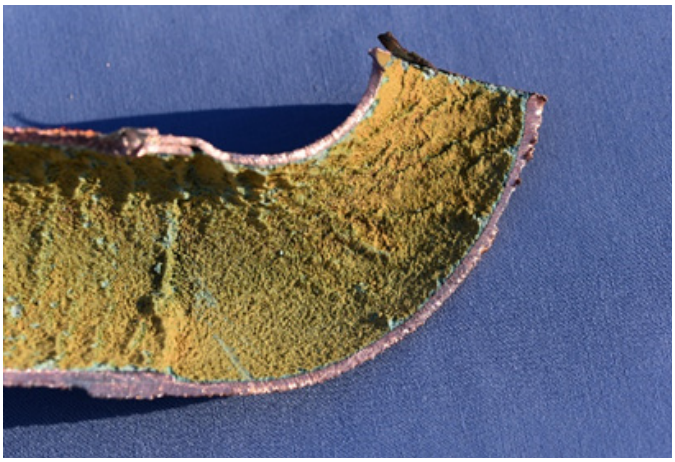

Figure 1
Copper pipe after 30 years of service with an internal coating.

where the formation of these films is imperfect, and reactions between the water and the copper pipe can create problems that fall into reasonably well-recognized classes. These classes of problems include: blue water, where dissolved copper gives the water a characteristic blue tinge and often results in blue stains on sanitary fittings; pinhole pitting in relatively short time frames of two to five years; microbially induced corrosion; erosion corrosion; and leaks generated by deposits of flux or debris on the inside pipe surface.

There is a wide range of research in published literature, much of which concentrates on trying to relate the chemical characteristics of the water carried by the pipe and the type of failure observed that inevitably leads to much confusion and contradiction amongst reports of research with words like "suggested," "proposed," and "likely" common[4,6].

There is no doubt that water chemistry (particularly the pH and softness/hardness of the water) plays a part in the problem. However, the author's review of some of the published research and investigations carried out over the last 20 or 30 years emphasizes the fact that water is an amazingly versatile compound with a wide range of characteristics and a high ability to absorb small amounts of other materials. This has led to many papers identifying a unique aspect of water chemistry apparently associated with a particular problem, often superseded by other research proposing an entirely different chemical cause for a similar problem.

This, coupled with what appears to be quite complex chemical and electrochemical behavior of copper and the variable conditions of temperature and velocity in the

pipes, makes the problem a transdisciplinary issue that does not lend itself to a single path to resolution[7,8,9].

Characterizing Copper Corrosion

Because there are distinctly different circumstances associated with corrosion of copper pipe, types of corrosion have been described and classified by industry associations such as the Water Services Association of Australia[10,11]:

- Type I pitting (largely eliminated by better manufacturing processes), which occurs in cold water reticulation systems.
- Type II pitting (the current problem), which occurs in hot water systems, often soft waters with a pH of around seven.
- Type III pitting initially associated with stagnation particularly early in the life of the pipe.
- Microbially induced corrosion generally arising from the development of a biological film in cold or warm soft waters able to support biological activity.
- Erosion corrosion from high-velocity water, particularly in hot water systems or because of cavitation at any temperature.
- Flux induced corrosion or poor workmanship during construction or repairs.
- Concentration or differential aeration cell corrosion arising from debris and deposits in the pipes often because of inadequate flushing after construction or an accumulation of solids delivered in the supplied water.

Although these characterizations are still commonly referred to in discussions of copper pipe corrosion, research and experience have modified the classifications.

Type I pitting is rarely (if ever) seen in current installations. This is because the root cause was identified as being a thin carbon film left on the inside of the pipe during the manufacturing process as a result of oxidation of drawing lubricants[12,13] (**Figure 2**). This film was generally imperfect, and accelerated electrochemical pitting took place at breaks in the film. This happened in cold water, and initial perforations typically appeared after about two years. Tests were devised, and manufacturing processes were adjusted some 20 years ago to eliminate the formation of this film. It is unlikely that any installed pipe networks with this problem remain in service (as they would have failed many years ago).

Type II and Type III pitting (**Figure 3**) are now recognized as similar processes with a high probability that both originate or are associated with periods of stagnation during construction or use, although other processes are suggested in the literature[14,15]. Installation standards now recognize this problem and recommend procedures to avoid it.

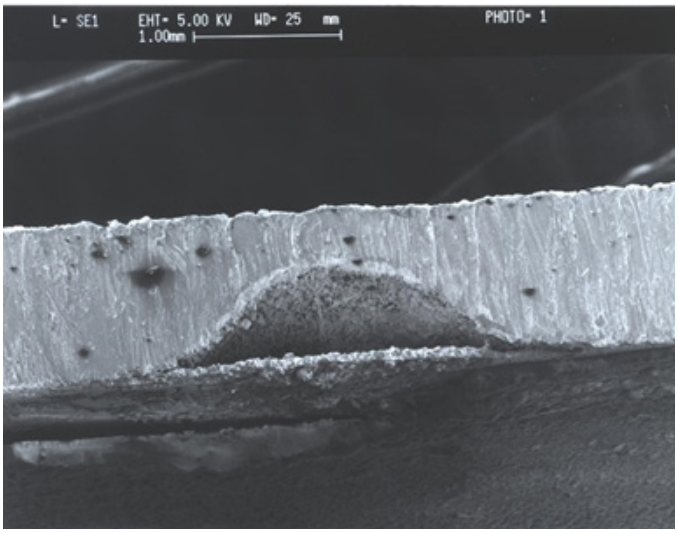

Figure 2
Scanning electron micrograph of a Type 1 pit.

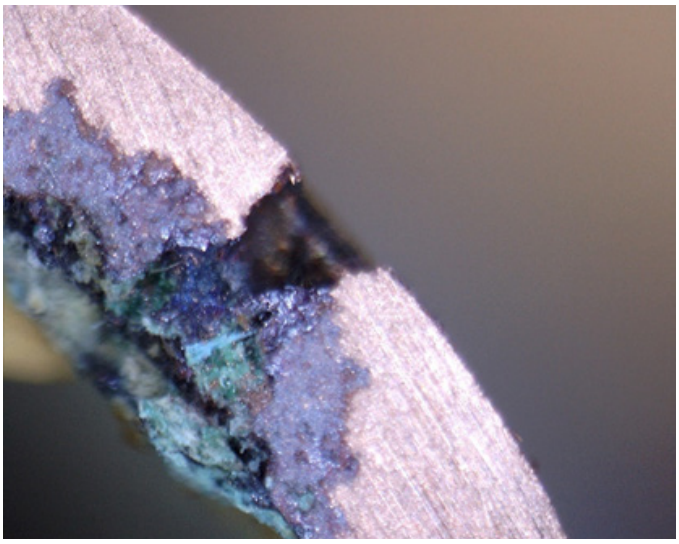

Figure 3
Polished section through a Type II pit from a system that was subject to stagnation.

Pits caused by debris on the bottom of the pipe can be easily identified by the inclusion of large debris in the corrosion cap (**Figure 4**). It should be noted that a Type II corrosion cap can contain finely divided copper released by the corrosion process. This type of corrosion, which involves differential access to oxygen caused by the presence of the debris, is not limited to copper pipe.

Research into the Causes and Characteristics of Copper Corrosion

In an analysis of some 48 published water analyses from a range of literature, the author found references to 61 compounds and elements and five characterization tests with little consistency in the conclusions drawn relating to the proposed causative chemical for any particular type of failure.

Comparison across the published water analyses show cause being allocated to a particular element. Chlorine, silica, iron, and manganese have all been identified as having an effect coupled with pH and temperature in particular circumstances, but there is contradictory evidence in other research reviewed by the author. For example, where an element is claimed to be causative in one investigation, it is present in other investigations where cause is allocated to different elements present in the analytical results. Therefore, conclusions drawn from a single water analysis are likely to be unreliable.

Temperature and pH are common factors in the speed and intensity of observed corrosion. This is an area where, as forensic engineers, we need to be both cautious and skeptical. Senior metallurgists who have spent a lifetime working with copper corrosion in water pipes advise that while many proposed causes have been eliminated, there is still some uncertainty as to the actual processes that initiate corrosion in copper pipe[9]. Many technical papers use terms such as "provides insight" or "indicating," suggesting caution in accepting the conclusions of a single research paper. Much of the knowledge is based on correlating suspected issues with known results. So, for example, pin-hole corrosion is frequently experienced where copper pipes are left stagnant for long periods, typically greater than eight weeks[11]. pH seems to have an effect in a certain range. Temperatures above 65°C appear to accelerate the process.

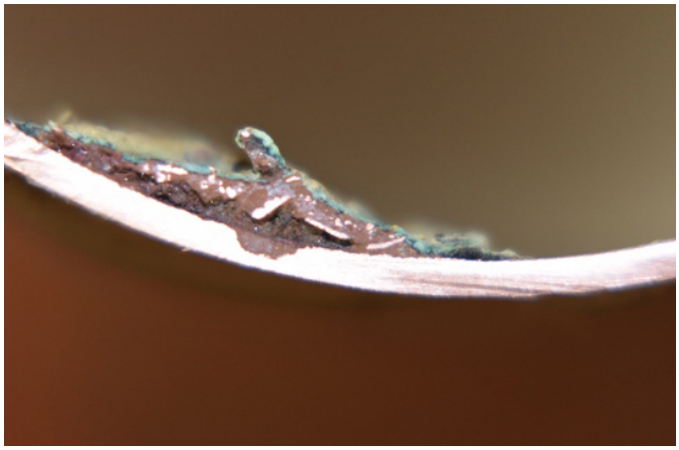

Figure 4
Pit caused by an accumulation of debris at the bottom pf the pipe.

It is often maintained that the corrosion relates to, or is initiated by, a "bad batch" of pipe or a particular manufacturer. This tends to be reinforced for lay persons by the fact that these problems are either localized in a community on a single water supply or occur in a large installation. The extent of the problem can often be traced to a consistent construction method where there are a limited number of tradesmen in a local community or a large installation where all pipes have been subject to similar treatment. Occasionally, the water chemistry is the cause of widespread but similar issues, particularly where a new water supply is introduced from a source with different characteristics (i.e., hard, soft, surface, deep well, artesian.)

Despite extensive testing, no repeatable research has managed to establish a difference in performance between copper pipes from different manufacturers that have good quality assurance and comply with manufacturing standards (as most do) or between different batches from the same manufacturer[1].

It is also often suggested that electrical currents arising from the use of copper pipe networks for electrical earthing promotes or accelerates corrosion processes[1]. Again, there is no repeatable research that demonstrates or proves stray currents or impressed voltages have a discernible effect on pin-hole corrosion rates. Indeed, research concludes there is no effect on rates or origination of corrosion from this cause.

When copper pipes are recovered and opened after periods of service, they often exhibit characteristic linear blue-green deposits (**Figure 5**), which, to an observer, suggest a logical connection between linear surface defects arising from the extrusion or drawing process and pin-hole leaks or corrosion. However, no research has found a definite correlation, although there is still some unproven suspicion that there is a connection between them.

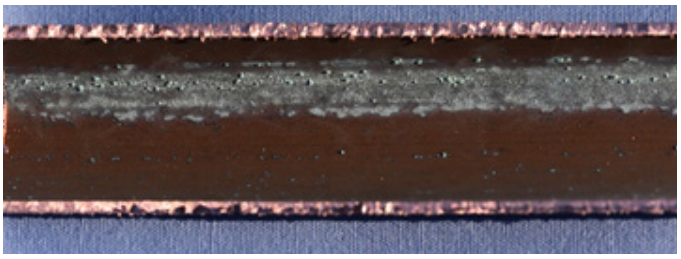

Figure 5
Normal linear markings inside copper pipes removed from service at around 10 years.

What is generally agreed by research metallurgists is that pitting corrosion is an electrochemical process that is initiated by small sites associated with defects in the normally protective oxide or carbonate coatings that form on the inside of the pipe. The cause of these defects — and their relationship to the initiation of pitting — is still a subject for research.

Microbially Induced Corrosion (MIC)

For many years, it was thought that microbes could not exist in a copper-rich environment; therefore, microbially induced corrosion could not be a cause of problems in copper pipe. Experience and research have shown that microbes are often present in cold water systems reticulated in copper pipe[16,17]. They certainly contribute to (and may be the primary the cause of) blue water, and appear to possibly play a part in the initiation of pitting corrosion. One of the problems of establishing a firm connection is that pitting corrosion is clearly an electrochemical process and is only detected when pipe wall penetrations occur. No one sees the start of the process.

In most operating hot water systems, microbial activity is not present because temperatures are too high — and legionella does not survive temperatures greater than 50°C (122°F)[18,19]. In cold water systems, if microbes are detected in corrosion pits, it is not clear whether they have been there from the start, or simply found a convenient place to live — sheltered from the water flow and possible disinfectants.

When the ability of microbes to survive in copper piping systems was firmly established, it was, for a while, regarded by many as the answer to copper corrosion problems — and certainly was raised as a defense in litigation. It now appears to be better understood as a potential contributor rather than an unavoidable natural root cause.

Problems in Recirculating Hot Water Systems

Currently in New Zealand, Australia, and Europe, the failure of piping systems in recirculating hot water systems has become a regularly reported problem. It's also the subject of wide discussion in the building design profession because the issue is creating problems in hospitals, hotels, and apartment buildings. (This geographical concentration is most likely to be because these countries have common engineering design standards. The problem is likely to arise elsewhere in the world where recirculating hot water systems are becoming common — there are no particularly local characteristics to either the design or the failure process.)

Typically, systems in large facilities that fail begin to experience pin-hole corrosion after four to five years in their hot water system if they have used copper pipe, or they experience splits in polypropylene random copolymer pipe apparently appropriately rated for the operating temperatures. Both failures appear to be continuing after the initial appearance with pin-holing, in particular showing little sign of reducing over time if no corrective action is taken. Some mitigations (such as precise temperature control below 65°C) can slow the process. However, metallurgists tell us that once pinholes have started, the only thing that can be controlled is the speed with which they penetrate the pipe wall.

One common factor in both these types of failure is a water temperature above 65°C, but the nature of the failure obviously is different in different materials. Some failures as observed in polypropylene random copolymer are related to stress or joints that appear to have been moved during fabrication while the joint is still hot and occur in both hot and cold services (**Figure 6**, on page 58).

In terms of the failures investigated by the author in polypropylene random copolymer systems, the problem appears to be a combination of temperature and pressure, particularly in high-rise buildings as the failures tend to occur at a level where the static pressure is high, and the recirculating water has not lost much temperature.

Figure 6
Typical failures in PPr piping in hot and cold systems. Left: internal surfacing cracking; center: cracking from point stress; right: cracking from poorly formed joints.

Examination of the rating tables supplied by pipe manufacturers suggest that the life of polypropylene random copolymer at the combinations of temperatures and pressures that are being seen is relatively short.

One of the suggested causes is that a mixture of polypropylene random copolymer and copper in a hot water system results in dissolved copper attacking the plasticizers in polypropylene random copolymer. Manufacturers claim this is a cause, and recommend that polypropylene random copolymer should not be used in a system with any copper piping or fixtures[20].

Causes Proposed for Copper Pipe Corrosion

There is no doubt when the fundamentals of reactions between copper and water are examined scientifically that there is a region where a combination of temperature around 65°C and pH around 7.0 result in a change in the processes that are taking place[21,22]. However, there is not a full understanding of what these processes are and how they can be controlled, apart from moving either the temperature or the pH out of the critical region.

Temperature is obviously the easiest parameter to control. Unanticipated consequences are likely if dosing to adjust pH is undertaken, given the fact that many of the systems fed by the reticulation in health or industrial installations are likely to be tuned to the current water chemistry.

In copper recirculating hot water systems, we are seeing both pitting and erosion. The rate at which these processes are damaging the copper pipes appears to be closely related to the combination of temperature and velocity in the pipes. Since 2000, engineering standards around the world have been steadily reducing design velocities for hot water in recirculating systems from the original standard based on non-recirculating systems of 3 m/s (10 ft/s) to figures as low as 0.5 m/s (less than 2 ft/s). There are also strong recommendations that temperatures should not exceed 65°C (150°F) and should preferably be in the order of 60°C (140°F). These are reinforced by recommendations in health facility specifications to maintain the temperatures in recirculating hot water systems between 60°C (140°F) in the flow lines and 50°C (122°F) in the return lines for control of legionella species[23].

Standards also require that during construction and commissioning copper pipe systems should not be allowed to stand with stagnant water for extended periods (AS4809 recommends no more than eight weeks)[11]. The standard requires either routine flushing on a regular basis or draining and drying the piping systems. This creates a practical problem as normal construction sequencing generally leaves pressurized water in the pipes between the first and second plumbing fix to ensure any pipe damage during the fitting of wall linings is detected. (First fix is installing concealed pipework before the wall linings are installed. Second fix is connection of the fittings and fixtures.) This can be overcome by testing with air (taking care to test in steps to avoid burst incidents) and leaving a low residual pressure that can be monitored for sudden drops that will indicate pipe damage has occurred.

The recommendations are essentially practical, based

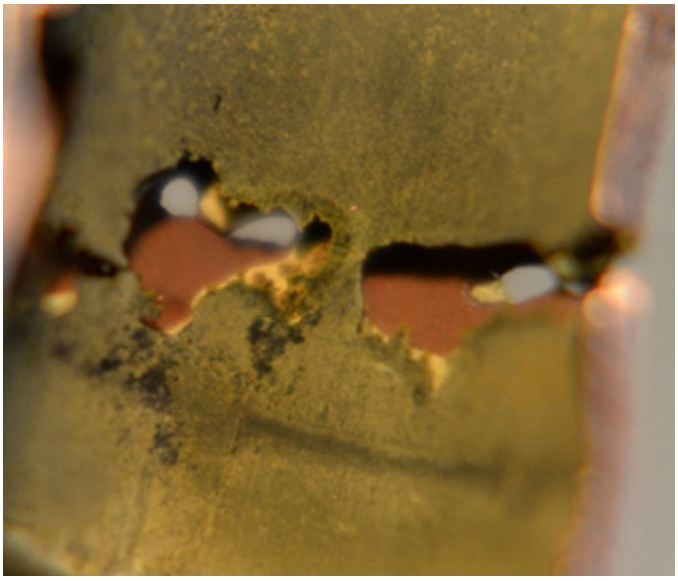

Figure 7
Erosion penetrations at poorly formed joints.

on observation and experience, although some consistent opinion (rather than hard research) on the cause is beginning to emerge.

Observations to date are:

- Systems that are not subject to periods of stagnation and are put into service soon after construction do not have pin-hole corrosion problems.
- Similar systems that have had periods of stagnation exceeding eight weeks, particularly during construction, are often subject to pin-hole corrosion.
- The rate of pin-hole corrosion appears to be reduced if water temperature is reduced.
- Erosion corrosion is observed less frequently in areas of reticulation systems where velocities and temperatures are lower.

It is suggested, but not proven, that during early stagnation the formation of protective oxide or carbonate layers can be disrupted by naturally occurring microbes in the water. This creates defects in the protective layer, which become sites that allow aggressive high temperature water to initiate pin-hole corrosion processes when the microbe colonies die. This suggests a connection between microbial-induced corrosion as an initiator with the electrochemistry of pin-hole corrosion as the driving mechanism.

Hot water above 65°C is an aggressive material with a high capacity to damage copper through erosion, particularly as a result of cavitation, which can be originated by poor joints (**Figure 7**) or partially closed valves used for flow control (**Figure 8**). It can also erode apparently smooth surfaces most likely starting at a small surface imperfection[3] (**Figure 9**, on page 60).

Recognizing Different Corrosion Types

There are many references, some of which are quoted in this article, that assert blue water is a result of microbial colonization and can generally be controlled by either shock dosing with chlorine disinfectant followed by

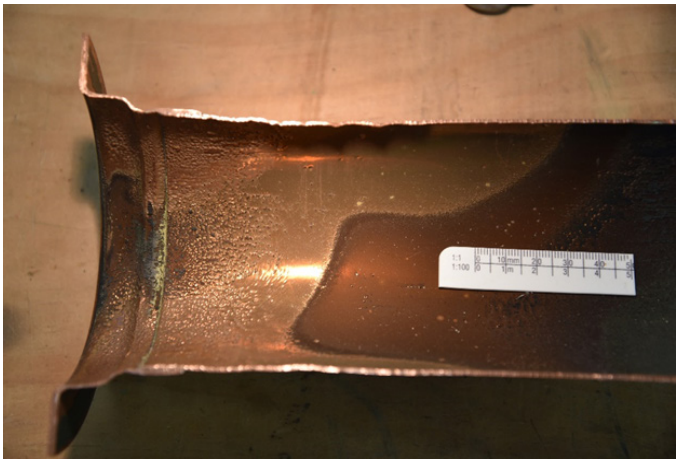

Figure 8
Copper pipe removed from service showing erosion and surface polishing where a butterfly valve was used to throttle flow rates. Flow left to right.

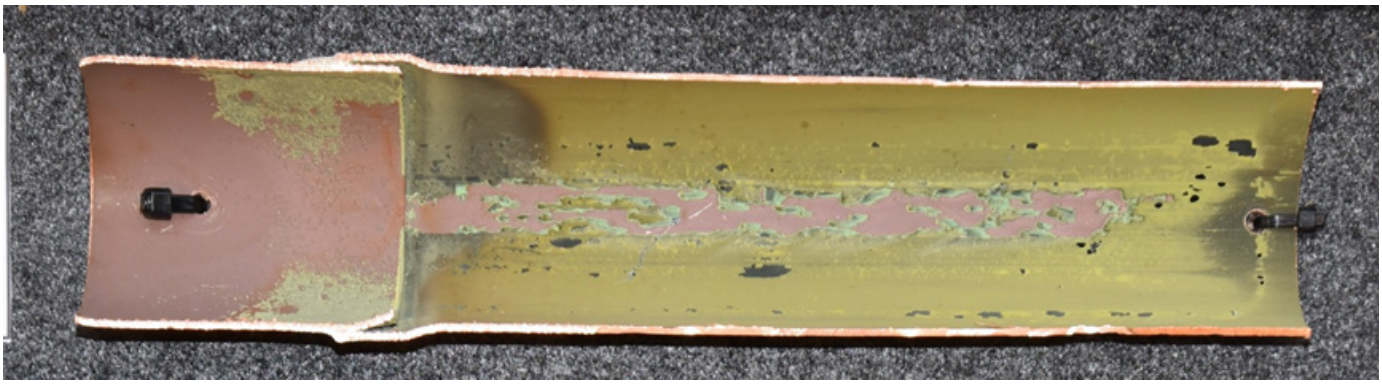

Figure 9
Left-hand end general material removal from surface with gross erosion extending from a burr measured at 0.1 mm high at the joint coupled with a poorly formed joint. Flow left to right. (Bend in joint at bottom was caused when the section was cut.)

subsequent normal levels of chlorination or by flushing the system with hot water typically at 60°C (140°F)[10,11,16,17]. Care must be taken to ensure that temperature-sensitive elements are not present and people are prevented from using the fixtures if hot water treatment is the chosen alternative.

Tests can be performed, if necessary, to prove microbial colonization. These typically involve recovering pipe samples aseptically and providing them to specialists who will use staining followed by microscopic examination[17]. Gross colonization can often be recognized as a slimy surface on the inside of the pipe.

Pin-hole corrosion in hot water systems can be recognized from the outside of the pipe, as it will either weep or spray from a relatively regular small hole. The leak rate may be low enough that initially the water will evaporate from the hot pipe surface before it flows away, leaving a mass of corrosion, adhered insulation material, and mineral deposits on the outer pipe surface. Examined internally, it will have a mound of corrosion product often with a comet tail extending downstream of the deposit (**Figure 10**).

In cold water systems (Type 1 corrosion), the external appearance of the pin-hole will be the same (although with less mineral and adhered materials). But internally the corrosion site will more likely appear flat or slightly depressed with raised corrosion material around the edge. Type 1 corrosion does not occur in hot pipes and is unlikely to be observed in current cold systems. Erosion leaks tend to be irregular in shape woprihen examined from the outside of the pipe and will often appear in groups or in a circumferential pattern around an artifact, such as a brazed joint (**Figure 7**).

Gross erosion is identified by large areas of material removal often with small peaks surrounded by a bright

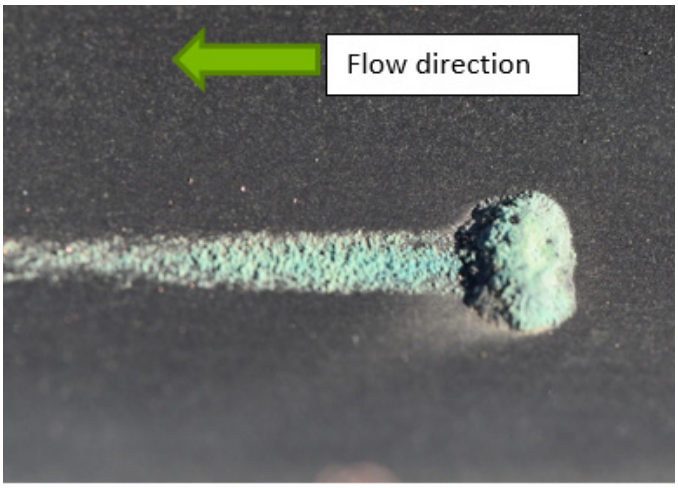

Figure 10
Typical active pin-hole leak and internal corrosion tubercule.

Figure 11
Gross material erosion. Flow from left to right cut from a section of pipe about 3 meters (10 feet) long.

horseshoe shape (**Figure 11**). The direction of flow can be identified using the mnemonic that horses walk upstream. It may be difficult to find an origination for this kind of erosion, which can extend for significant distances along the inside surface of the pipe.

Rough internal surfaces (**Figures 8** and **9**) or highly polished areas are both indications of surface material loss as a result of local cavitation or high-velocity flow fields.

When carrying out investigations into leaks in copper pipes, the location of the leak (top, bottom, or side), the direction of the flow, and the orientation of the pipe are important to record as they provide clues as to the cause. Pitting proposed to be caused by stagnation typically is observed at the top of the pipe and can be present on vertical sections of the reticulation — pitting caused by debris is almost always on the bottom of the pipe, and erosion can be at any orientation.

Conclusions

The current apparently sudden increase in pin-hole corrosion in hot water systems using copper pipes appears to be closely correlated to the appearance of high temperature recirculating hot water systems.

Although much has been written about the relationship between corrosion in copper pipes, and the composition and stability of the water flowing in them, it appears that temperatures above 150°F (65°C), velocity in the region of 6 to 10 ft/sec (2 to 3 meters per second), and possibly a water pH of around 7.0 appear to be the critical factors — probably coupled with periods of stagnation during construction or commissioning. The problem appears to be controllable by ensuring that the new design criteria appearing in standards for temperature and velocity are adopted, and stagnation during construction is avoided. Tests have not found any root cause associated with the manufacture or the material of copper pipe.

Other failures occurring in systems using polypropylene random copolymer pipe appear to be related to the ability of the material to withstand combinations of temperature and pressure that occur in the recirculating system. Polypropylene random copolymer manufacturers do not recommend the use of this material in association with copper in hot water systems[20]. Polypropylene random copolymer pipes have an entirely satisfactory service history at cold temperatures, but many designers are justifiably reluctant to use them for hot water reticulation based on industry experience, although manufacturers claim the product has been improved.

References

1. D. M. Nicholas, “Corrosion of Copper in Australasian Drinking Waters: A Historical Review,” Corrosion and Prevention, no. Paper 21, p. 14, 2014.

2. C. A. Copper Development Association, “Copper Through the Ages.” [Online]. Available: https://copperalliance.org.uk/about-copper/copper-history/copper-through-the-ages/#:~:text=The%20Sumerians%20and%20Chaldeans%20Copper%20first%20came%20into,others%20somewhere%20between%205000%20and%206000%20years%20ago.

3. Copper Tube Handbook Industry Standard Guide for the Design and Installation of Copper Piping Systems, Handbook A4015-02/16, C. D. A. I. C. Alliance, New York, 2016.

4. Z. Jia, C. Du, D. Zhang, and X. Li, “Analysis of Copper Pitting Failure in Drinking Water Distribution System,” Journal of Failure Analysis and Prevention, vol. 11, no. 2, pp. 152-157, 2011/04/01 2011, doi: 10.1007/s11668-010-9415-y.

5. S. R. Jenkins, “Personal observations and commissioned investigations,” ed, 2016 -2020.

6. D. A. Lytle and M. R. Schock, “An Investigation of Copper Pitting Corrosion and Pinhole Leaks,” presented at the World Environmental and Water Resources Congress 2007: Restoring Our Natural Habitat, Tampa, Florida, 2007. [Online]. Available: https://ascelibrary.org/doi/

abs/10.1061/40927(243)592.

7. D. A. Lytle and M. R. Schock, "Pitting corrosion of copper in waters with high pH and low alkalinity," Journal AWWA, vol. 100, no. 3, pp. 115-129, 2008, doi: https://doi.org/10.1002/j.1551-8833.2008.tb09586.x.

8. B. D. Custalow, "Influences of Water Chemistry and Flow Conditions on Non-Uniform Corrosion in Copper Tube," Master of Science, Environmental Engineering, Virginia Polytechnic Institute and State University, Blacksburg, VA, 2009. [Online]. Available: https://vtechworks.lib.vt.edu/handle/10919/34388

9. J. C. Rushing, "Advancing the understanding of water distribution system corrosion: Effects of chlorine and aluminium on copper pitting, temperature gradients on copper corrosion, and silica on iron release." Master of Science in Environmental Engineering, Virginia Polytechnic Institute and State University, Blacksburg, 2002. [Online]. Available: https://vtechworks.lib.vt.edu/bitstream/handle/10919/34235/RushingETD.pdf?sequence=1&isAllowed=y.

10. Corrosion of Copper Pipe in Australian Drinking Waters, Technical W. S. A. o. Australia, June 2015.

11. Copper pipe and fittings-Installation and commissioning, A. Standards, Sydney, 2003.

12. H. S. Campbell, "PITTING CORROSION IN COPPER WATER PIPES CAUSED BY FILMS OF CARBONACEOUS MATERIAL PRODUCED DURING MANUFACTURE," J. Inst. Metals, vol. 77, p. 14, 1950.

13. G. J. Schafer, "CORROSION OF COPPER AND COPPER ALLOYS IN NEW ZEALAND POTABLE WATERS," New Zealand Journal of Science, vol. Dec 1962, p. 10, 20 August 1962 1962. [Online]. Available: file:///D:/Corrosion%20of%20Copper%20and%20Copper%20Alloys%20in%20New%20Zealand%20Potable%20Waters.pdf.

14. W. S. Holden, Ed. Water Treatment and Examination. London: J. & A. Churchill, 1970, p. 513.

15. R. J. Oliphant, "A Review of Current Knowledge CAUSES OF COPPER CORROSION IN PLUMBING SYSTEMS," Foundation for Water Research, Marlow, September 2010 2010.

16. J. T. Walker, D. Wagner, W. Fischer, and C. W. Keevil, "Rapid detection of biofilm on corroded copper pipes," Biofouling, vol. 8, no. 1, pp. 55-63, 1994/04/01 1994, doi: 10.1080/08927019409378260.

17. P. J. Bremer, B. J. Webster, and D. B. Wells, "Biocorrosion of Copper in Potable Water," AWWA, p. 10, August 2001 2001.

18. N. A. o. S. E. a. Medical, Management of Legionella in Water Systems. Washington, DC: The National Acadamies Press, 2020.

19. B. J. Webster, S. E. Werner, D. B. Wells, and P. J. Bremer, "Microbiologically Influenced Corrosion of Copper in Potable Water Systems—pH Effects," Corrosion, vol. 56, no. 9, pp. 942-950, 2000, doi: 10.5006/1.3280598.

20. OPNA, "COPPER IONS AFFECT ON PP-R," ed: Pestan North America, 2021.

21. B. Beverskog and I. Piugdomenech, "Revised Pourbaix Diagrams for Copper at 5-150ºC," Swedish Nuclear Power Inspectorate (SKi), SKi Report 95:73, October 1995 1995. Accessed: 27/5/2016.

22. J. D. Gates, "Erosion-Corrosion of Copper Pipes in Hot Water Reticulation Systems - Case Studies and Wider Implications," The University of Queensland, St Lucia, 7 July 2014 2014. Accessed: 30/5/2016.

23. Scottish Health Technical Memorandum 04-01: Water safety for healthcare premises Part A: Design, installation and testing, N. N. S. Scotland, 2014.

Electrocutions and Downed Powerlines: a Forensic Electrical Engineering Analysis of Causes, Reasons, and Effects

By Helmut G. Brosz, PEng (NAFE 1029C)

Abstract

In October of 1999, four individuals were walking a dog after a storm. The group of three males and one female came upon a large puddle, which covered most of a T intersection on their intended route. The female walked around the puddle as her two sons entered the puddle barefoot. Two of the male individuals were electrocuted. The surviving male entered the puddle to help and was immediately electrocuted. The dog followed them into the pool and was electrocuted. The female turned around to see her two sons and friend lying face down in the puddle. She entered the puddle to help them and ultimately was electrocuted by the same 480VAC downed and energized streetlight powerline in the pool. The facts discussed in this paper include vegetation management, short-circuit electrical protection, the conductivity of water and soil, human response to electrical current, sag, and tension of power lines.

Keywords

Electrocution, downed power lines, vegetation management, electrical protection, conductor damage, forensic electrical engineering

Introduction

In October of 1999, after a storm reportedly produced winds of approximately 70 mph, a mother took her two sons, their friend, and the family dog out for a walk in the dark. The individuals approached a giant puddle covering the T intersection on the road. The two brothers decided to walk through the pool barefoot, their mother went around the puddle with shoes on, and their friend entered the puddle after taking off his running shoes (followed by the dog). Upon noticing the brothers, the friend, and the dog lying in the puddle unconscious, the mother turned around and entered the puddle as well. All were electrocuted by an energized 480-Volt (V) downed streetlight conductor found lying in approximately 4 inches of water. The heads of the three deceased males were located about 1 foot from the underwater streetlight conductor. The female's feet and head were approximately 25 feet from the other side of the conductor (**Figure 1**).

No witnesses observed the electrocutions. The electric utility responded to a phone call, and took down two pieces of 265 feet #4 AWG (American Wire Gauge) AAAC (All Aluminum Alloy Conductor) 480VAC (Volts Alternating Current) streetlight circuit between two poles. One-piece that remained energized in the water was a 126-foot length from the west pole where the conductor was broken. A second 139-foot piece from the east pole was de-energized. The entire 480V streetlight circuit, consisting of 52 streetlights, was supplied by a single-phase 25kVA (Kilovolt Ampere) rated pole-top oil-filled transformer from a 3-phase 13,200/7,600VAC overhead distribution circuit running east-west along the

Figure 1
Location of victims observed in the puddle of water after electrocution.

Helmut G. Brosz, PEng, Forensic Sciences International Group, 64 Bullock Dr. Markham, ON, L3P3P2, (844) 554.4666, hbrosz@forensicsig.org

north side of the street. A neutral conductor (3/0AWG AAAC) was underbuilt. The #4 AWG AAAC streetlight conductor was mounted 1 foot below the neutral at each concrete pole (**Figure 2**).

The pole-mounted transformer was located only two spans to the west of the electrocution location. The streetlighting transformer 7,600VAC primary was protected with a 4K current-rated fuse after the fact. With this information, it was established in deposition to have been a 6K fuse, never operating during any time of the electrocution event. The electric utility de-energized the transformer, took down the streetlight control box, and stored it. The original 6K transformer fuse was not presented as evidence as it could not be located.

The 265-foot neutral and streetlight span, which crossed the intersection from west to east, was found to be in contact with a Ficus tree, among other trees and bushes displayed in **Figure 3**.

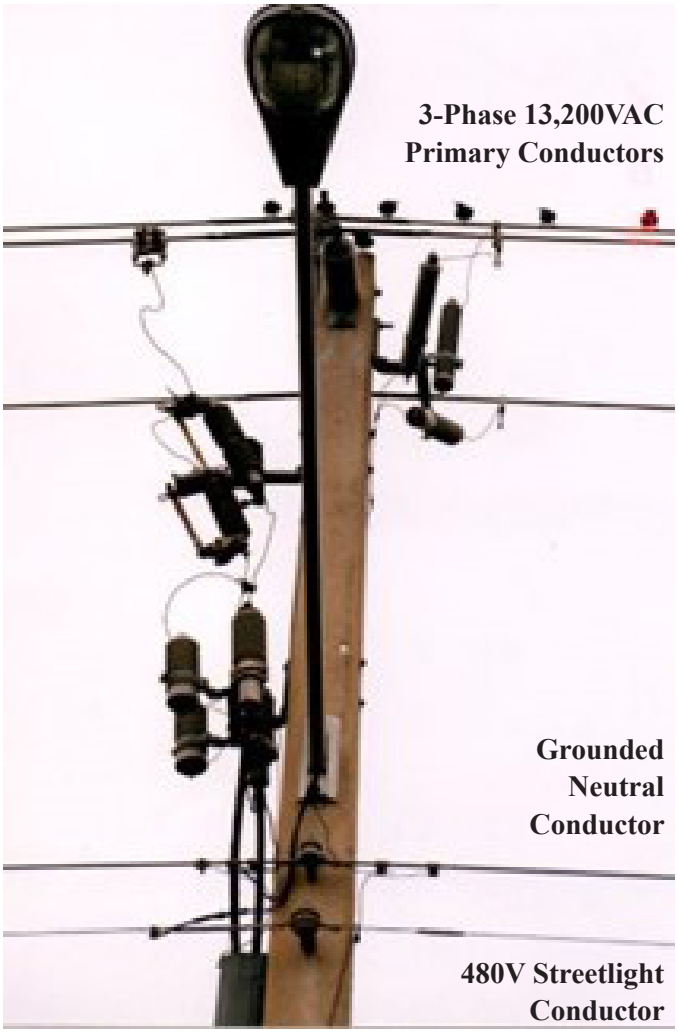

Figure 2
Streetlight conductor configuration.

Figure 3
Neutral conductor in the Ficus tree after the incident.

The utility trimmed the Ficus tree after the incident occurred. The cut marks were later marked on a survey drawing (**Figure 4** and **5**). The #4 AWG AAAC was found severed from its attachment point at the west pole 126 feet and 139 feet from its attachment point on the east pole. The 126-foot energized section of the conductor hung from its 22-foot vertical attachment point on the west pole, laying in the puddle spanning the entire width of the road. The 139-foot de-energized section of the conductor was suspended in the air by vegetation. The scope of work included reporting the causes, reasons, and effects of the streetlight conductor falling.

The cause of death of the victims was determined to be electrocution. No electrical burn marks were identified; this is consistent with electrocutions conducted in water.

Preliminary examination identified that — from ground level — there was an anomaly or damage to the still in-service neutral conductor at the 126-foot location six years after the incident occurred (**Figure 6**). Furthermore, two tape marks were observed wrapped around the neutral conductor on either side of the anomaly (**Figure 7**).

The evidence requested for analysis and documentation included:

1. The neutral conductor was examined while connected in place between the two concrete poles

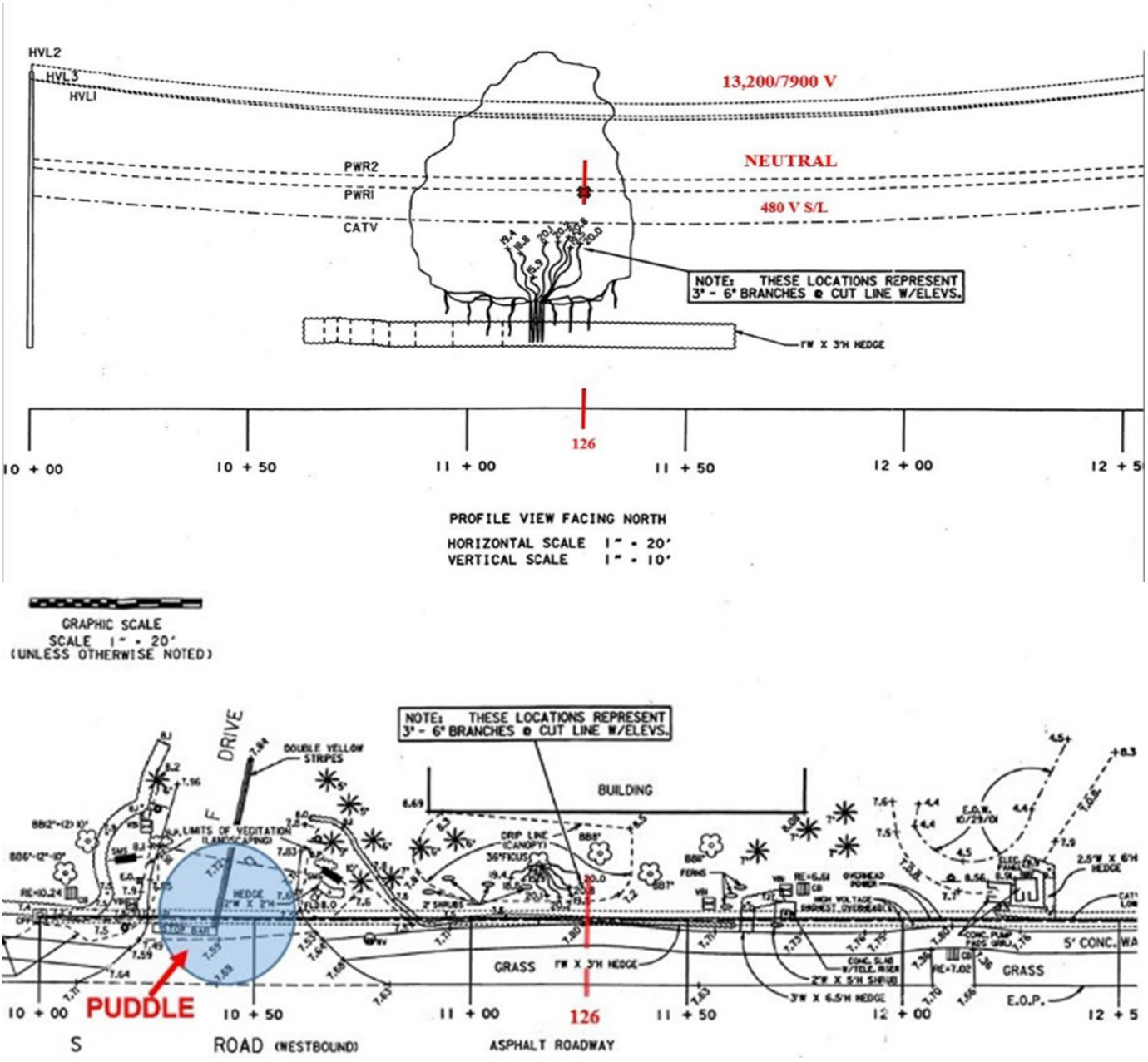

Figure 4 and **Figure 5**
Survey of scene.

Figure 6
Neutral conductor defect.

Figure 7
Two pieces of tape on 3/0 neutral conductor.

Figure 8
Forensic Engineer and Professor Helmut Brosz at the bucket truck to inspect the conductors close-up.

using a bucket truck (**Figure 8**).

2. The utility took the neutral conductor and presented for examination and documentation (**Figure 9**).

3. Examination of the trimmed branches on the tree. The diameter of the Ficus tree cuts at the location of the severed streetlight conductor.

4. To examine all sections of downed #4 streetlight conductors in conjunction with the neutral conductor (**Figure 10**).

A survey of the scene to locate the precise positions of poles, conductors, tree branches, neutral conductor defect, and 126-foot conductor break was conducted to present a diagram. This is done between the concrete poles (**Figures 4** and **5**).

A rope copy was made of the 265 feet of streetlight and neutral conductor, including all anomalies (i.e., arc marks, vegetation contact, corrosion on a ballroom floor to facilitate the preservation of the evidence (**Figure 9** and **11**).

Figure 9
Severed streetlight conductor.

Figure 10
Examination of conductor.

Tests and Examinations

All sections (per inch) of neutral, 3/0 AWG, AAAC and #4 AWG, AAAC conductor were examined visually

Figure 11
Rope copy of conductor with vegetation contact markings.

and with microscopy (**Figure 9** and **10**)

Preliminary Analysis

When a scenario of an electrocution associated with a downed power line is presented, potential factors that may have caused the line to come down and remain energized should be considered, such as:

Wind forces impacting powerline

a. The applicable N.E.S.C. (National Electrical Safety Code) requires overhead distribution lines at this location to be designed to withstand average wind speed of 150 mph (67 mps) at 33 feet (10 m) height). In this area, the winds were reported not to exceed 70 mph in weather records. The rated breaking strength of the #4 conductor is 1,760 pounds. The weight of the 265-foot span of #4 AWG AAAC conductor is 12 pounds (based on 45.4 pounds per 1,000 feet).

b. The possibility of galloping (high-amplitude, low-frequency oscillations of overhead powerlines due to wind) of the conductor occurring was considered and excluded from investigation. This is due to the conductor being supported at various locations by vegetation. Its vibrational amplitude would be limited by intermittent contact with adjacent vegetation.

Short Circuits

a. Close visual and optical examination of the neutral and streetlight conductor revealed a short circuit occurred between the two at the 126-foot location and at other locations. The seven strands (7 x 0.0843 inches) of the #4 AWG streetlight conductor were melted and severed (**Figure 9**). The larger neutral conductor was only one of its seven 0.1672-inch strands severed (**Figure 6**).

b. On the severed conductor, evidence of long-term contact with vegetation (**Figure 11**) resulted in a form of corrosion. The survey was conducted six years after the event and tree trimming.

c. New shoots emanating from the Ficus tree trimming cuts were observed. The diameter of the cuts ranged from 3 to 6 inches, corroborating the extent of branches in contact and in the vicinity of the open conductor. Production of documents revealed trimming had not occurred for at least six years prior to the electrocution. The tree trimming cycle of three years (as set out in the utility standards) was missed at this location (**Figure 12**). Furthermore, the tree trimming cycle does not take into consideration the growth rate of the various vegetation species. A Ficus tree can grow up to 6 feet per year.

d. The primary cause factor for the short-circuit event was due to the lack of vegetation maintenance. The vegetation was not appropriately managed in maintaining a 6-foot clearance between powerlines and trees. According to the utility standards, appropriate vegetation management requires to maintain a clearance of 6 feet between power lines and trees[5]. This distance was not met and was a large factor in causing the short-circuit event.

e. Short circuits caused by conductive flying objects were ruled out due to the lack of flying conductive objects found, seen, or reported. Furthermore, the momentary contact would not be long enough to produce the damage observed.

f. Sustained contact with branches alone at 480VAC would not draw sufficient current to produce the arcing damage observed — only corrosion evidence is attributed.

Lightning damage to conductor

Lightning was reported during the storm. The neutral and streetlight conductor were protected directly from above by the 3-phase, 7,200V circuit and did not trip. This is according to utility and resident reports. Therefore, possible damage to the #4 conductor due to lightning was excluded from the investigation. A Lightning Detection Network search revealed no lightning within the area of the electrocution site. Additionally, the hypothesis of

Figure 12
Ficus branches below neutral 3/0 and #4 streetlight conductor (removed) following the incident and prior to trimming.

conductor damage due to lightning is not consistent with the actual arcing damages observed.

Electrical protection

a. The 480V electrical circuit begins at the 25kVA transformer having a rated secondary current of 52 amps (A). The 52 connected streetlights draw a calculated current of 0.833A each for a total of 52 x 0.833A= 43.318A. The ampacity of #4 AWG AAAC is approximately 60A. The circuit did not exhibit any visual signs of melting or annealing. The 6K-rated fuse on the primary side of the transformer allows a long-time current flow of approximately 180A at 480VAC before operating, according to its 6K time current curve[6]. Since the fuse did not operate, a current flow was maintained. Current overload due to normal lighting load on the secondary side of the transformer did not exist.

b. Winds caused the branch/ branches of the Ficus tree to lift the #4 AWG AAAC streetlight conductor intermittently up into contact with the neutral conductor. Every time the branch made contact, a short circuit of variable duration would occur. The fault current flowed along the #4 conductor to the point of contact with the 3/0 neutral at the 126 feet mark, flowing back along the neutral to the transformer. The cumulative short circuits lasted long enough to melt the seven strands of the #4 AWG AAAC and one strand of the seven larger #3/0 streetlight conductor[1]. This caused the west section of the #4 conductor to fall into the puddle and remain energized.

c. When the still-energized west section of the #4 conductor fell into the puddle, the current path extended from the conductor through water, through the ground back to the grounding rod (**Figure 13**) at the base of the concrete transformer pole. From there, the current flowed up the solid copper #6 AWG bare conductor to the neutral of the streetlight transformer. The impedance of the circuit was high enough (and the current low enough) so as to prevent the transformer 6K fuse from operating on a 480V and less than a 225A fault.

Effect of current on the human body

a. The brothers entered the puddle and approached the unseen conductor lying in about 3 to 4 inches of water. The voltage between their feet, also known as "step potential," was of an approximate magnitude to exceed 85VAC. The impedance between wet foot to foot based on the I.E.C. Standard 479-1-1994 (**Figure 14**) is indicated to be 100% of the wet hand to foot impedance of 850 ohms (for 50% of population) at about 500V (**Figure 15**).

Figure 13
Ground rod at the base of the transformer pole.

Loss of muscle control occurs at approximately 10 milliamps of current, causing the individual to fall. In this case, the brothers fell forward. In both male's cases, the current entered the body and traveled through the heart, with the majority of current exiting through the feet. With the mother falling backward, the current entered the feet and exited from the head. In all cases, electrocution occurred.

b. Electrocution occurs if a current greater than approximately 50mA passes through the heart for

Touch voltage V	Values for the total body impedances Z_T (Ω) that are not exceeded for		
	5 % of the population	50 % of the population	95 % of the population
25	1175	2 175	4 100
50	1100	2 000	3 675
75	1025	1 825	3 275
100	975	1 675	2 950
125	900	1 550	2 675
150	850	1 400	2 350
175	825	1 325	2 175
200	800	1 275	2 050
225	775	1 225	1 900
400	700	950	1 275
500	625	850	1 150
700	575	775	1 050
1 000	575	775	1 050
Asymptotic value =internal impedance	575	775	1 050

NOTE 1 Some measurements indicate that the total body impedance for the current path hand to foot is somewhat lower than for a current path hand to hand (10 % to 30 %).

NOTE 2 For living persons the values of Z_T correspond to a duration of current flow of about 0,1 s. For longer durations Z_T values may decrease (about 10 % to 20 %) and after complete rupture of the skin Z_T approaches the internal body impedance Z_i.

NOTE 3 For the standard value of the voltage 230 V (network-system 3N – 230/400 V) it may be assumed that the values of the total body impedance are the same as for a touch voltage of 225 V.

NOTE 4 Values of Z_T are rounded to 25 Ω.

Figure 14
Total body impedances Z_T for a current path hand to hand a.c. 50/60 Hz, for large surface areas of contact in water-wet conditions.

around 1 second or more. This causes ventricular fibrillation, leading to death[3]. The deceased individuals spent a prolonged amount of time, exceeding 1 second, with the current flowing through their hearts.

Conclusion

The lack of clearance between the streetlight conductor and the Ficus tree allowed the tree branches to lift the streetlight conductor into the grounded neutral when wind occurred. The responsibility of maintaining the vegetation to conductor clearance rests with the utility as per the NESC and Public Service Commission. Persistent wind (over time) resulted in repetitive short circuits severing the streetlight conductor, causing it to break and fall into the puddle.

It continued to remain energized, in part, due to the impedance presented by the return-current path. The deceased's legs muscles were subjected to currents that caused loss of muscle control. Thus, the individuals collapsed and were electrocuted in the puddle with lethal currents flowing from head to foot. Cause of death was determined to be electrocution, according to the coroner's report. The utility did not give a reason as to why trimming was not done. In conclusion, to prevent further electrocutions from occurring, it is crucial to maintain tree trimming standards in preventing vegetation contact with powerlines.

The author wishes to thank his colleague Steve Paniri, P.Eng., for his assistance in this forensic analysis.

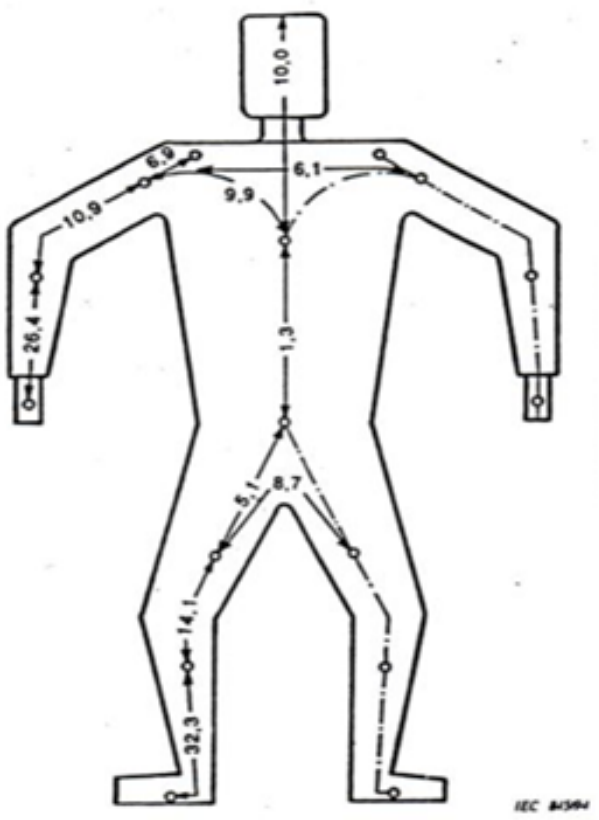

Figure 15
Total body impedance for a current path hand to hand.

References

1. "TransPowr AAAC Bare Overhead Conductor (US)," Prysmian Group. https://na.prysmiangroup.com/product-center/utilities-and-power-grids?&page=1&business_unit=6284&search_product_center=AWAC+Bare+Overhead+Conductor+(US)*&fixed_sidebar=6295&content_type=products (accessed Sept. 14, 2021).

2. Extreme Wind Loading, National Electrical Safety Code Handbook 250C, Sept 2021, [Online]. Available: +https://onlinelibrary.wiley.com/doi/pdf/10.1002/9781118098974.fmatter.

3. "Effects of current on human beings and livestock," Int. Electrotechnical Comm., Geneva, Switzerland, Rep. TS 60479-1, 2005-7.

4. K. Malmedal and P.K. Sen, "Structural loading calculations of wood transmission structures," NEI Electric Power Engineering, Arvada Colorado, U.S.A, 2003. [Online]. Available: https://www.neiengineering.com/wp-content/uploads/2021/08/Structural-Loading-Calculations-Of-Wood-Transmission-Structures.pdf.

5. F. den Ouden, M.P.R.M. Santos Silva, E.J. Veneklass, "Determinants of growth rate in Ficus benjamina L. compared to related faster-growing woody and herbaceous species," Department of Plant Ecology and Evolutionary Biology, Utrecht, The Netherlands, 2002. [Online]. Available: https://www.sciencedirect.com/science/article/abs/pii/S0304423801003156.

6. Total Clearing Time Current Characteristic Curves, Kearny Type K Fuse Links - Eaton, Nov 2021 [Online]. Available: https://www.eaton.com/content/dam/eaton/products/medium-voltage-power-distribution-control-systems/cooper-power-series-historical-literature/lipe/kearney-k-fuse-links-time-current-curves-k-31000ab.pdf.